Master of Science Thesis

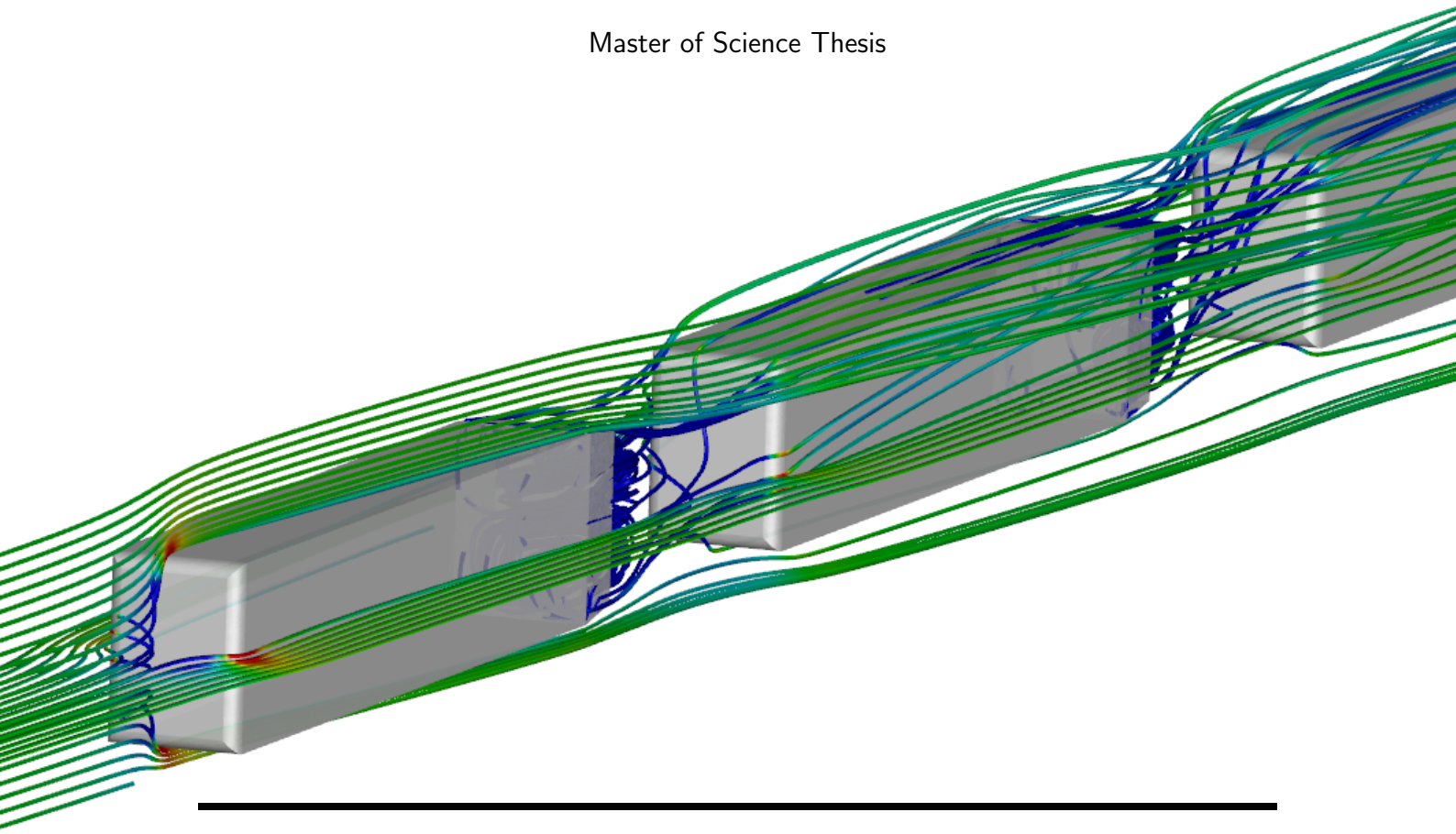

Aerodynamic analysis of a platoon of bluff bodies subjected to cross wind

A numerical investigation on the effect of drag reduction devices

Thomas Gheyssens

January 28, 2016

Aerodynamics

TU Delft

Faculty of Aerospace Engineering

Delft University of Technology

Aerodynamic analysis of a platoon of bluff bodies subjected to cross wind

A numerical investigation on the effect of drag reduction devices

Master of Science Thesis

For obtaining the degree of Master of Science in Aerospace Engineering
at Delft University of Technology

Thomas Gheyssens

January 28, 2016

Faculty of Aerospace Engineering · Delft University of Technology

Delft University of Technology

DELFT UNIVERSITY OF TECHNOLOGY
DEPARTMENT OF AERODYNAMICS

The undersigned hereby certify that they have read and recommend to the Faculty of Aerospace Engineering for acceptance the thesis entitled **"Aerodynamic analysis of a platoon of bluff bodies subjected to cross wind"** by **Thomas Gheyssens** in fulfillment of the requirements for the degree of **Master of Science**.

Dated: January 28, 2016

Supervisors:

Dr. Richard Dwight

Dr. Ir. Gandert Van Raemdonck

Prof. Dr. Stefan Hickel

Dr. Daniele Ragni

Preface

Already at the start of my studies in Delft in 2010, my main interest was the aerodynamics of aircraft, cars, buildings and even athletes. The wake of a certain bluff body has always been intriguing and in this thesis I could study the interaction of this wake with other vehicles in a platoon of bluff bodies. The work done during this thesis study fully satisfied my interests in the aerodynamics of road vehicles. This thesis is the result of several months of work and it is the final product of my MSc degree in Aerospace Engineering.

Acting as my daily supervisor, Gandert Van Raemdonck had a certain enthusiasm that was very catching. After every meeting, I was really motivated to finish this thesis with good results. His guidance to point out the right direction to go with this thesis is highly appreciated. I'd like to thank him for his inspiration and motivation. I'd also like to thank Richard Dwight, who was my supervisor from within the university, for making sure the thesis was fitting inside the framework of an MSc thesis. I appreciate the interest in my thesis as well as the time spend on reading and grading it.

Furthermore, I'd also like to thank all my colleague students and friends, who were always there to discuss some serious matter or to joke around during the coffee breaks. They even made the souterrain 'gezellig'. I wish all of them best of luck with the remainder of their studies in Delft.

A special thanks goes to my parents for supporting in all sorts of ways during the five and a half years of studying and living in Delft. It doesn't need to be said that without their support, I would've never finished this study. Finally, I'd like to thank my girlfriend, who never stopped believing in the good outcome of all my exams and my thesis.

Thomas Gheyssens
Delft, The Netherlands
January 28, 2016

Summary

Due to the awareness of climate change, more sustainable and efficient ways of transport are needed. The most polluting road transport mode in the European Union are the long-haul tractor-trailer combinations. This study will investigate the aerodynamic characteristics of three vehicles in a platoon subjected to cross wind conditions. The effect of front- and rear drag reduction devices is investigated numerically. The frontal edge radius is considered the front drag reduction device while the rear drag reduction device is represented by a boat tail.

ANSYS Fluent® was used to solve the RANS equations that were closed with the SST $k-\omega$ turbulence model. The GETS model was used to analyse the aerodynamic characteristics of a simplified heavy-duty vehicle. The geometry was meshed and a mesh sensitivity study showed the asymptotic behaviour of the drag as a function of mesh size.

It was shown that the frontal edge radius influences the flow behaviour largely. For the radii of 0.54 m and 0.27 m, a large thrust force on the frontal edges decreased the drag of the front part of the vehicle significantly such that the drag contribution of the front part was lower than 15% of the total drag while the pressure drag at the rear delivered around 70% of the drag. Halving the frontal edge radius to 0.135 m, caused the drag contributions of the front and rear part of the vehicle to be about 45% of the total drag. Adding an inward deflected tail increased drag drastically by increasing the base pressure. Adding a cross wind component to the incoming flow increased the drag and gave a side force.

The inter-vehicle distance had a large influence on the drag of the individual vehicles. At a very short distance, the lead vehicle experienced a very large drag reduction because of the presence of the high pressure region in front of the middle vehicle. This lead to a large reduction in pressure drag. When the distance is increased, the drag goes asymptotically to the value in isolation. The trailing vehicle showed opposite behaviour. The drag of the trailing vehicle was increased when the inter-vehicle distance decreased due to the fact that the streamlines were deflected inward after the middle vehicle and they experienced a deceleration due to the concave trajectory of the flow arriving at the frontal surfaces of the trailing vehicle. This lead to a decreased thrust force on the frontal edges of the trailing vehicle. For the lowest inter-vehicle distance, the trailing vehicle was positioned inside the near-wake of the middle vehicle and the drag decreased again. The middle vehicle experienced a combination of the effects on the lead and trailing vehicle, its drag remains fairly constant except for the closest distance where the negative effect on the frontal part started to decrease. These trends are

similar for all platoons, the amount of drag increase or decrease however was determined by the geometric variables and the cross wind condition.

The drag reductions of the different vehicles in the platoon were mainly determined by the frontal edge radius. The relative drag reductions on the lead vehicle were higher when the frontal edge radius was larger, since then the pressure drag at the rear represents a larger portion of the total drag. The drag decrease in drag counts however only slightly changed. For the large radii, the trailing vehicle experienced a drag that increased up to a value above that in isolation when the inter-vehicle distance was decreased. A trailing vehicle with the smallest frontal edge radius, 0.135 m, experienced a drag reduction. The combined effects of the lead and trailing vehicle caused the drag reductions of the middle vehicle to increase for a lower frontal edge radius.

The drag reductions decreased when tails were added or deflected inwards. A tail on a specific vehicle mainly influences the vehicle driving behind the tail. Deflecting a tail decreased the drag reductions caused by the slower incoming flow field, i.e. the lower dynamic pressure experience by the following vehicles. Deflecting a tail on the lead vehicle inward has the same effect on the middle vehicle as increasing the inter-vehicle distance, it decreases the influence of the lead vehicle's wake on the middle vehicle. For a frontal edge radius of 0.27 m, the total drag reduction of a following vehicle was decreased when the tail was deflected from 0° to 6°, but it was increased when deflecting the tail from 6° to 12°. Decreasing the frontal edge radius to 0.135 m gave different results. The total drag of the following vehicle was increased when the tails of the vehicle in front were deflected more inward.

Overall, the drag reductions obtained in a platoon were not much affected by the applied cross wind conditions. It is shown that the lead vehicle of a platoon redirects the flow such that the middle and trailing vehicle experience a significantly lower side force. The side force of the lead vehicle itself is not changed significantly. When inward deflected tails are applied to the lead and middle vehicle, the side force reduction on the following vehicles is diminished but still significant.

The final results showed that the platoon with the worst performing vehicles in isolation, the 'nnn' configuration with $R = 0.135$ m, experienced the largest drag reduction, namely 29%, corresponding to 1223 drag counts. If this is extrapolated to a vehicle with an initial drag coefficient as high as a real heavy-duty vehicle, this could lead to a fuel saving of 2.48 L/100km. Considering the absolute drag coefficients, the platoon with the best performing vehicles was still the optimal platoon with the lowest drag coefficient, namely the 't12t12t12' platoon with the largest frontal edge radius. This aerodynamic analysis investigated the effect of the drag reduction devices in a platoon of bluff bodies subjected to cross wind conditions. It was shown that the frontal edge radius can determine whether the following vehicles experience a drag reduction or a drag increase. Tails reduced the drag of the individual vehicles but did also decrease the drag reductions experienced in the platoon. The drag reductions were still present under cross wind conditions. Considering the set-up of platoon formations, vehicles with the most streamlined front should be placed as lead vehicle. Vehicles with large tail angles should be used as trailing vehicle.

Table of Contents

Preface v

Summary vii

Nomenclature xiii

1 Introduction 1

1.1 Background . . . 1

1.2 Bluff body aerodynamics . . . 3

1.2.1 Basic bluff body . . . 3

1.2.2 Effect of cross winds . . . 4

1.2.3 Effect of drag reduction devices . . . 5

1.3 Platoon aerodynamics . . . 7

1.4 Present study . . . 10

2 Numerical Set-up 11

2.1 Simulation set-up . . . 11

2.1.1 Turbulence modelling . . . 11

2.1.2 Wall treatment . . . 12

2.1.3 Boundary and operating conditions . . . 14

2.1.4 Solver settings . . . 15
2.2 GETS model . . . 16
2.3 Grid generation . . . 17
2.4 Mesh sensitivity . . . 19
2.5 Tested configurations . . . 22
2.6 Limitations . . . 23

3 Analysis and Validation of the GETS model 25

3.1 Basic configuration . . . 25
3.2 Effect of frontal edge radius . . . 28
3.3 Effect of tails . . . 32
3.4 Effect of yaw angle . . . 36
3.5 Validation of computational results . . . 42
3.6 Summary of the isolated GETS results . . . 45

4 Analysis of the Platoon Configurations 47

4.1 Platoon configuration 'nnn' . . . 47
4.1.1 Effect of inter-vehicle distance . . . 47
4.1.2 Effect of frontal edge radius . . . 56
4.1.3 Effect of yaw angle . . . 59
4.1.4 Absolute drag values . . . 67
4.1.5 Summary of the 'nnn' configuration . . . 69
4.2 Platoon configuration 'nnt12' . . . 70
4.2.1 Effect of inter-vehicle distance . . . 70
4.2.2 Effect of frontal edge radius . . . 73
4.2.3 Effect of yaw angle . . . 75
4.2.4 Absolute drag values . . . 77
4.2.5 Summary of the 'nnt12' configuration . . . 77

4.3 Platoon configurations 'ttt' 79
4.3.1 Effect of inter-vehicle distance 79
4.3.2 Effect of frontal edge radius 85
4.3.3 Effect of yaw angle 91
4.3.4 Absolute drag values 95
4.3.5 Summary of the 'ttt' configurations 98

5 Platoon Comparison **99**
5.1 Leading vehicle 99
5.2 Trailing vehicle 101
5.3 Middle vehicle 103
5.4 Platoon average 105
5.5 Optimal platoon 107

6 Conclusion & Recommendations **109**
6.1 Conclusions 109
6.2 Recommendations 112

Bibliography **115**

A Absolute drag values of all vehicles **119**

Nomenclature

Abbreviations

CFD	Computational Fluid Dynamics
DES	Detached Eddy Simulation
DNS	Direct Numerical Simulation
GETS	Generalised European Transport System
LES	Large Eddy Simulation
LV	Lead vehicle
MV	Middle vehicle
nnn	Platoon configuration with all no-tailed vehicles
nnt12	Platoon configuration where the trailing vehicle is equipped with a tail of 12°
PIV	Particle Image Velocimetry
RANS	Reynolds Averaged Navier Stokes
SAE	Society of Automotive Engineers
t0t0t12	Platoon configuration where the first two vehicles have a tail of 0° and the trailing vehicle is equipped with a tail of 12°
t12t12t12	Platoon configuration where all vehicles have a tail of 12°
t6t6t12	Platoon configuration where the first two vehicles have a tail of 6° and the trailing vehicle is equipped with a tail of 12°
TV	Trailing vehicle

Greek Symbols

Δ	Increase of a certain parameter	
ω	Turbulent dissipation rate	[1/s]
τ	Wall shear stress	[Pa]

Roman Symbols

δ	Boundary layer thickness	[m]
$\hat{n}$	Unit normal to the surface	[−]
$\overline{u}$	Mean velocity	[m/s]
$\vec{F}_p$	Pressure force vector	[N]
A	frontal area	[m]
C_D	Drag coefficient	[−]
C_f	Friction coefficient	[−]
C_L	Lift coefficient	[−]
C_p	Pressure coefficient	[−]
C_p	Pressure coefficient	[−]
C_S	Side force coefficient	[−]
D	Dimensionless inter-vehicle distance	[−]
D	Drag force	[N]
G	inter-vehicle spacing	[m]
k	Turbulent kinetic energy	[m^2/s^2]
L	Lift force	[N]
N	Number of surfaces	[−]
p	Static pressure	[Pa]
p_{total}	Total pressure	[Pa]
R	Frontal edge radius of the model	[m]
Re	Reynolds number	[−]
Re_x	Reynolds number based on the length	[−]
Re_x	Reynolds number based on the position along the length of the boundary layer	[−]
Re_τ	Reynolds number based on the friction velocity	[−]

S	Side force	[N]
S_w	Side force	[N]
t	Time	[s]
u'	Turbulent velocity fluctuation	[m/s]
u^*	Friction velocity	[m/s]
x	Coordinate in the longitudinal direction	[m]
Y	Yaw angle	[°]
y	Coordinate in the lateral direction	
y^+	Dimensionless wall coordinate	[−]
$y_{\frac{1}{2}}$	Half height of the first cell on the surface	[m]
z	Coordinate in the height direction	
D_w	Wind-axis drag force	[N]

Subscripts

LV	Of the lead vehicle
MV	Of the middle vehicle
$Y = 0°$	For a yaw angle of 0°
$Y = 3°$	For a yaw angle of 3°
avg	Average value
domain	Of the domain
i	In isolation
model	Of the model
p	In a platoon formation
ref	Reference value
upp	Upper

Chapter 1

Introduction

This introduction states the importance and motivation for the current research on truck aerodynamics. A brief background will first be given. Afterwards a more technical background, based on a literature study, is given. This will introduce the reader to the aerodynamics of single bluff bodies and the aerodynamics of vehicle platoons.

1.1 Background

In the last years, there has been an increasing awareness of climate change, as demonstrated in the climate conference in Paris recently [1]. Besides this, oil production in most of the oil producing countries has already peaked. In the coming years it will become more and more difficult to produce high-quality and cheap oil [2]. These two facts provide the drive to come up with more sustainable and efficient ways of transport. The most polluting road transport mode in the European Union are the long-haul tractor-trailer combinations. These heavy-duty vehicles are responsible for 30% of the on-road CO_2 emissions [3]. Only limited attention is paid to the aerodynamic design of those vehicles, compared to aircraft or formula one cars. This leads to vehicles that are not very streamlined. However, more and more studies are performed on the aerodynamics of these vehicles to make them more fuel efficient, like studies from Pankajakshan or Sreenivas on the effects of drag reduction devices or cross winds on the drag force [4, 5]. The importance of an aerodynamic design can be seen in Figure 1.1. At a velocity of 90 km/h, the aerodynamic drag is about 50% of the rolling resistance.

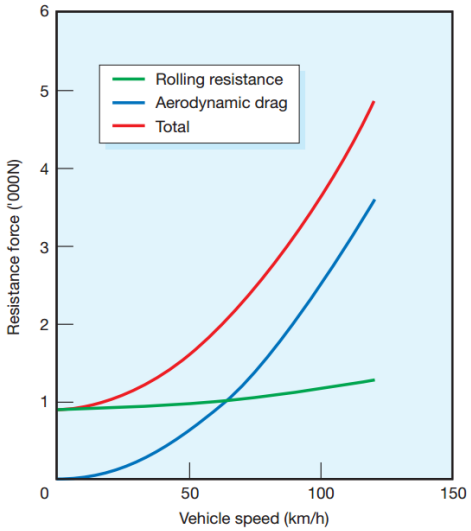

Figure 1.1: Different resistance forces as a function of velocity for a 10-tonne rigid vehicle [6].

Besides optimising the aerodynamic shape of a single vehicle, several studies investigate the effect of a platoon on the drag of different vehicles. A platoon is a group of two or more vehicles that line up, while driving, to save fuel. The following vehicles drive in the wake of the vehicle in front and could experience a decrease in drag. Track tests indicated that the fuel consumption reduction can be as high as 21% for the trail truck and 7% for the lead truck with a 10 m spacing and a velocity of 80 km/h. With increasing truck mass or decreasing truck velocity, the proportion of aerodynamic resistance decreases, and with it the fuel consumption reduction [7]. Tsugawa et al. [8] used three fully-automated trucks, driving at 80 km/h with a 10 m gap, to investigate the fuel consumption reduction of a platoon. The lead truck savings were $7.5\% - 10\%$, those of the middle truck were $17.5\% - 18\%$ and the trailing truck saved $14\% - 16\%$. The savings in energy consumption for the entire platoon were 14%. At a close spacing, the lead vehicle experiences a lower drag force than the trailing vehicle. The reversal between the lead and trailing vehicle as 'most benefiting' vehicle occurred at a vehicle length of 0.43 [9].

Currently, platooning is becoming more and more known. For example, in 2016, the European Truck Platooning Challenge will take place. This will involve various brands of automated trucks driving in platoons on public roads from several European cities to the Netherlands. The aim of this Challenge is to stimulate the implementation of platooning [10]. An illustration of two platoon formations is shown in Figure 1.2.

(a) A 4-vehicle platoon (b) A 2-vehicle platoon

Figure 1.2: Example of trucks riding in platoon formations [11, 12].

1.2 Bluff body aerodynamics

The aerodynamics of heavy-duty vehicles has already been studied extensively. These vehicles are aerodynamically characterised as bluff bodies, i.e. bodies where the largest part of the drag consists of pressure drag and where the friction drag is much less significant. The aerodynamics of basic bluff bodies can be influenced largely by adding, for instance, drag reduction devices.

1.2.1 Basic bluff body

Basic bluff bodies experience a very large pressure drag compared to the friction drag due to the blunt shape of the front and rear part. The flow around these bodies is also characterised by the presence of large regions of separated flow, like the wake. A study on the distribution of the aerodynamic drag for a tractor-trailer vehicle showed that the front face and the trailer base of the vehicle have the same drag contribution as can be seen in Figure 1.3. The other two important areas that create the most drag are the gap between the tractor and trailer and the undercarriage of the vehicle. A 2D sketch of the flow around two simplified heavy-duty vehicles can be seen in Figure 1.4

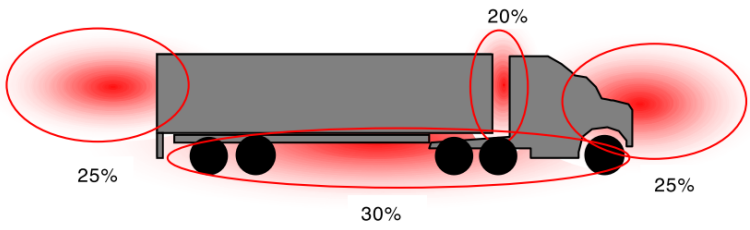

Figure 1.3: Distribution of the aerodynamic drag for a heavy vehicle tractor-trailer truck [13].

The aerodynamic properties of such a vehicle are largely influenced by the flow around the front part. As can be seen in Figure 1.4, the flow can either separate when not much attention is paid to the streamlining of the front faces. By increasing the radius of several frontal facing edges and attaching extra surfaces, the flow is able to follow the geometry without separating.

This is a very effective way of reducing the drag of the front part of the vehicle.

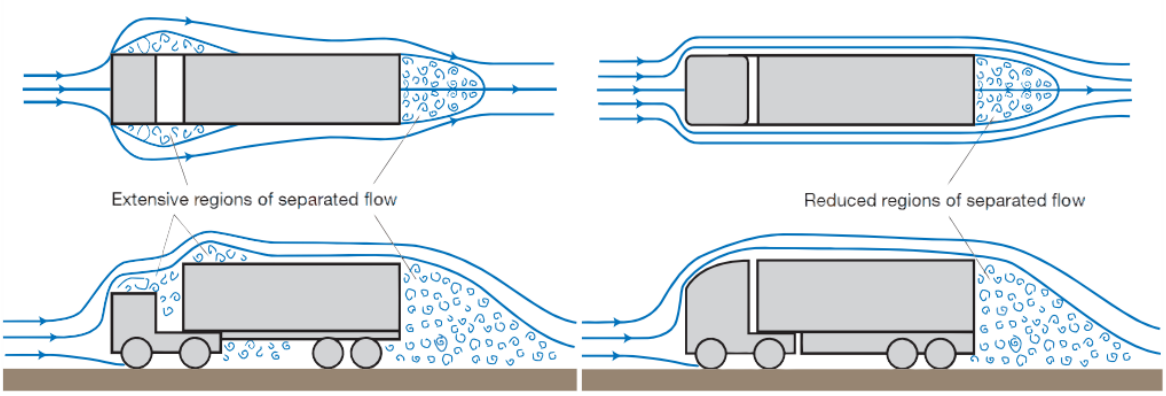

Figure 1.4: Airflow around a more (right) and less (left) streamlined heavy-duty vehicle [6].

One of the most complex aspects of the flow around a bluff body is the wake behind the body and its relation to the front part of the body. This wake is highly unsteady, shear layers develop on the periphery of the vehicle and roll up into a vortex ring which is advected downstream [14]. The wake of bluff bodies accounts for the largest contribution of drag when more simplified models are used, i.e. without gap, undercarriage. This pressure drag at the rear can be decreased either by using drag reduction devices or by driving in a platoon formation with a following vehicle. These methods will be elaborated on further.

1.2.2 Effect of cross winds

In reality, road vehicles do not operate often in conditions where the flow is perfectly aligned with the vehicle's axis. When a cross wind velocity is added, the freestream velocity, experienced by the vehicle, is rotated with a certain yaw angle. Due to the high driving velocity, road vehicles experience yaw angles between $-10°$ and $10°$ for 88% of the time [15].

Large Eddy Simulations (LES) of the flow field around a full-scale heavy duty truck showed that the drag coefficient increases with increasing yaw angles. As the yaw angle increases, the separation on the windward side was mitigated and the flow became fully attached at a yaw angle of $10°$. On the leeward side, the separation was enhanced for increasing yaw angles [16].

For relatively small yaw angles, i.e. below $10°$, the drag of a bluff body increases with increasing (constant) cross wind [5]. This is however not always the case, Cooper [17] gathered results of wind tunnel studies with different geometries. In these studies it was shown that the drag of the more streamlined geometries was less sensitive to increasing yaw angles. Some geometries even showed a drag decrease due to cross wind. This increase or decrease of the drag can be explained with the use of Figure 1.5. The increase in body-axis drag with yaw angle depends on the increase rate of the wind-axis drag force, D_w, and the increase rate of the bracketed term containing the yaw angle and the side force to drag force ratio, $\left(\frac{S_w}{D_w}\right)$.

Because of the geometry of road vehicles, i.e. a larger length than width, the wind-axis drag force always increases with increasing yaw angle. If the vehicle is very streamlined and has a high side force to drag force ratio, $\left(\frac{S_w}{D_w}\right)$, the drag becomes less sensitive to an increase in yaw angle or can even be reduced [18].

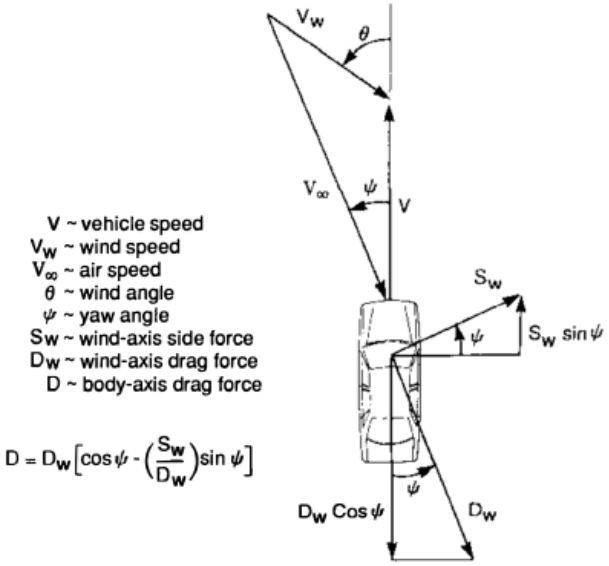

Figure 1.5: Body-axis drag at a non-zero yaw angle [18].

1.2.3 Effect of drag reduction devices

Drag reduction devices have shown great potential in decreasing the drag of a bluff body. One of the most basic drag reduction methods is increasing the radius of the frontal edges. It is clear that the model with the largest leading edge radius experiences the lowest drag [19]. This was also already illustrated in Figure 1.4.

Tails or flaps at the base of a trailer try to increase the base pressure by allowing the flow to follow the shape of the body more easily. An example of base flaps or tails on a heavy-duty vehicle can be seen in Figure 1.6.

Figure 1.6: Example of base flaps applied on a heavy-duty vehicle [20].

The effect of base flaps on a truck geometry has been studied. The base flaps consisted of four panels inclined at an angle of 15° with a length of one-quarter of the trailer width. The results showed that the wind-averaged drag reduction was 15%. The effectiveness of the base flap did not depend particularly to the crosswind direction, though it performed slightly better without cross wind [4]. The study of McCallen et al. also showed that base flaps decrease the drag coefficient significantly and that their effect is not sensitive to yaw angles [21]. This can be seen in Figure 1.7.

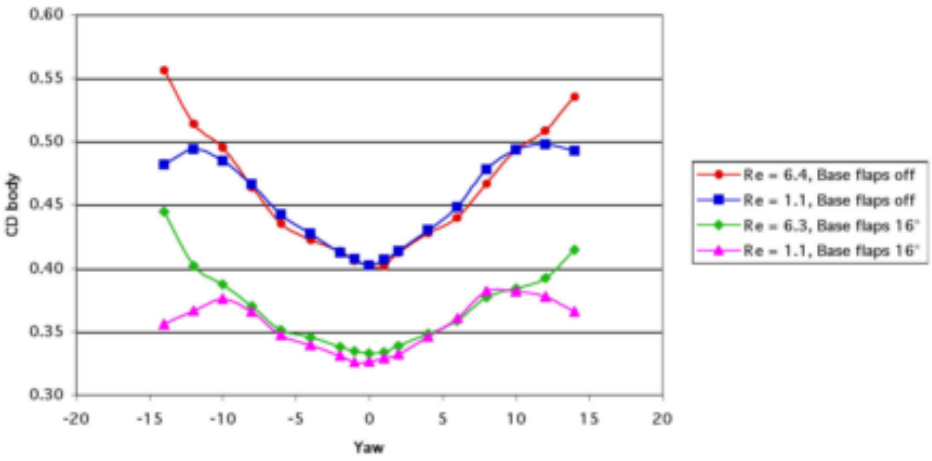

Figure 1.7: Drag coefficient versus yaw angle with and without base flaps for $Re = 1.1$ million and 6 million [21].

Van Raemdonck [15] performed experiments on boat tails, both numerical, in the wind tunnel and on a full scale prototype. Wind tunnel experiments on the Generalised European Transport System (GETS) model showed that an open boat tail with a slant angle of 12° reduced the drag by an amount of just over 30%. This drag decrease can even be improved to 40%, when longer boat tails are applied. Due to the longer tails, a higher pressure recovery is achieved. It is also shown that the efficiency of longer tails increases with increasing yaw angle. For the more realistic standard semi-trailer model, the slant angle of 15° performed best at increasing the base pressure, but the slant angle of 10° showed the largest decrease in drag coefficient.

1.3 Platoon aerodynamics

The principle of platooning is that the following vehicle drives in the wake of the vehicle in front. This way, the low pressure in the wake increases while the high pressure in the stagnation region of the following vehicle decreases. Both vehicles thus benefit from the platoon. An example of a numerical simulation on a platoon of vehicles can be seen in Figure 1.8.

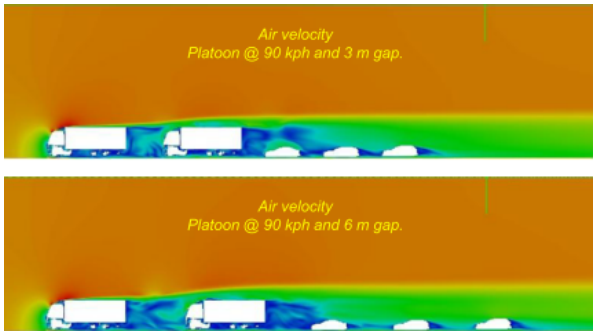

Figure 1.8: Aerodynamic representation of the vehicles at 3 m and 6 m gaps [22].

Unlike for heavy duty vehicles, it is shown for generic passenger vehicle models, e.g. the Ahmed model with a slanted rear, that the drag of the trailing model increases for a decreasing spacing and decreases again from an inter-vehicle distance of about 0.3 vehicle length, while the drag force on the leading model always decreases. The drag coefficient of the trailing vehicle was also larger than that of the vehicle in isolation. Still a net platoon drag reduction was achieved [23]. The trailing vehicle's drag increase was due to the significant flow impingement on its front by the flow leaving the lead car's rear slant [24]. Wind tunnel experiments performed on a platoon of two Ahmed bodies showed that the rear vehicle experiences drag reductions for spacing between one and four vehicle lengths. Between 0.1 and 1 however, the drag goes up significantly, even above the drag of the isolated model [25].

By testing 1/8 scale models of the GM Lumina Van in the wind tunnel, the PATH project showed that for a 2-vehicle platoon, at spacing greater than one vehicle length, the lead vehicle is almost unaware of the presence of the trailing vehicle. This trailing vehicle however, already experiences a decrease in drag. Lowering the spacing below one vehicle length decreases the drag of both vehicles drastically. For a spacing below 0.5 vehicle length, the drag of the trailing vehicle increases abruptly and becomes larger than the lead vehicle drag. Adding vehicles to the platoon increases the complexity of the vehicles behaviour. The interior vehicles experience the lowest drag. These results can be seen in Figure 1.9.

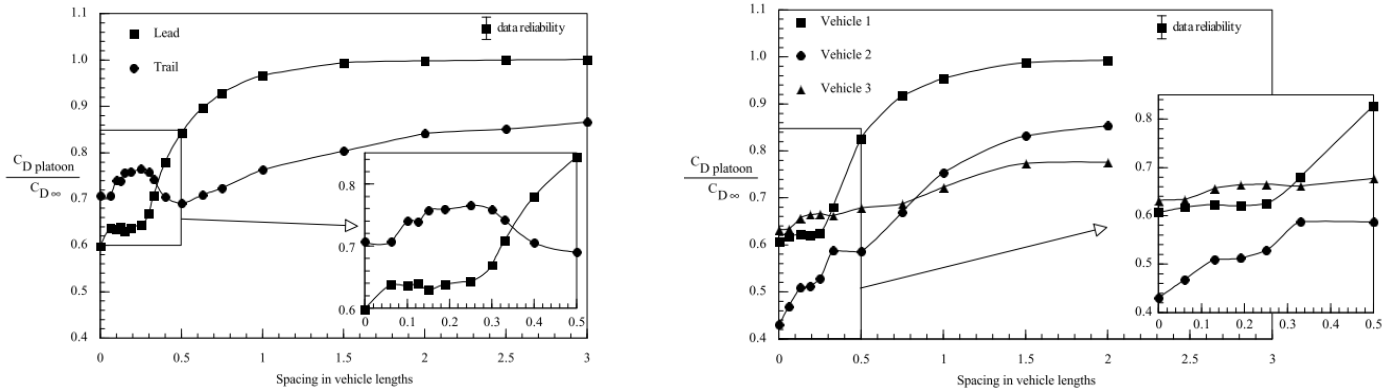

(a) 2-vehicle platoon

(b) 3-vehicle platoon

Figure 1.9: Resulting drag coefficients for different platoons [26].

Using Computational Fluid Dynamics (CFD) based on the time accurate Lattice-Boltzmann Method, Smith et al. showed that while the drag of the lead truck always decreases with decreasing spacing, the drag of the trailing truck started to rise again for the shortest spacing. The reason for this is that besides reducing the stagnation pressure on the trailing vehicle, the wake of the leading vehicle also reduces the suction pressure on the curved frontal surfaces of the trailing vehicle. This was observed for yaw angles of zero and six degrees. These findings correspond to trucks like the Peterbilt Model 386. It must be noted that most trucks in Europe do no resemble this geometry. The measured mass flow through the heat exchangers of the trailing vehicle showed that with decreasing spacing, the mass flow also decreases. In real life situations this could lead to the necessity of an operating fan which could lower the fuel savings [27].

Hammache and Browand [19] tested a tandem of both rounded and blunt trucks. Using these two different bluff body shapes, four different platoon configurations could be tested in the wind tunnel. In the region of $0 - 1$ gap width, there is a strong interaction. For larger gap widths there was a low interaction region. Their results are plotted in Figure 1.10. Every configuration contributes to lower drag coefficients compared to an isolated value. In the strong interaction region, the relative drag coefficient of the rear body starts at a value of 20% (blunt) or 40% (rounded) of the isolation value. When enlarging the spacing, a steep increase in drag coefficient is noticed for the trailing body.

It was observed that applying a rounded edge on the leading body always reduces the drag on that body as well as on the total platoon. Rounding the front of the rear body however, increases the relative drag coefficient of the rear body and of the total platoon due to the loss in suction force on the leading edges. The most beneficial configuration is thus a rounded body followed by a blunt body. The highest relative drag coefficient occurs for the platoon with a blunt front body and a rounded rear body. The blunt-blunt and the rounded-rounded configurations behave alike in the strong interaction region, but in the low interaction region, the rounded-rounded configuration has a higher relative drag coefficient and it even becomes higher than for the blunt-rounded configuration after a spacing of 2.5 vehicle length. In all the

configurations except for the rounded-rounded configuration, the trailing vehicle experienced significantly lower drag forces. For the rounded-rounded configuration, the drag of the trailing body was lower than that of the front body, but it was the other way around in the low interaction region. It must be noted that the non-dimensional gap width, $G/\sqrt{A}$, where G is the spacing and A the frontal area of the model, was normalised using the squared frontal area instead of the vehicle length [19]. A remark has to be made that these results should not be interpreted as absolute drag values. The drag coefficient is normalised using the drag coefficient in isolation, which is higher for the blunt body than for the rounded geometry. This can cause the rounded body to experience a higher relative drag coefficient.

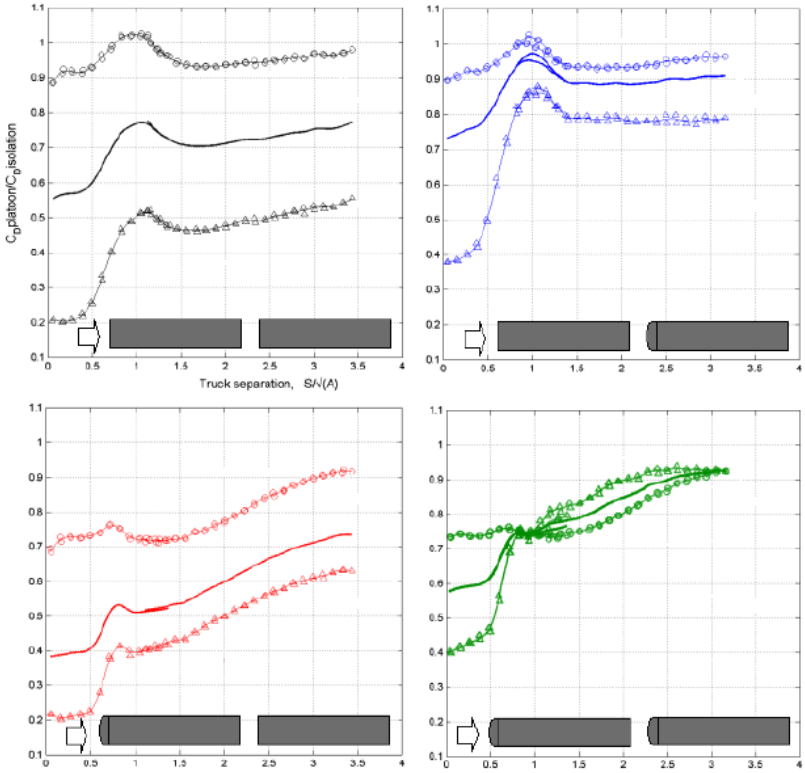

Figure 1.10: Relative drag coefficient for four platoon configurations as a function of the separation between the models. △-symbols resemble the trailing vehicle, ○-symbols the lead vehicle and the bold line resembles the average platoon drag [19].

Doppenberg studied the effect of different drag reduction devices on the performance of a platoon based on time averaged numerical simulations. A three-vehicle platoon is considered with bodies both with and without a tail and for a spacing of 1.5 m, 4.5 m and 16.5 m. Bodies with a tail benefit from the increased base pressure but the following body experiences an increased drag force due to the inwards deflected streamlines, resulting in a higher stagnation pressure at the front body. The results showed that only the last vehicle needs to have a boat tail in order to reduce the platoon drag at short spacing. For this configuration, the flow was able to follow the platoon contours the best. When the spacing was large, the best solution was obtained when all the vehicles had a boat tail since this is also the best option when the vehicles would drive in isolation [28].

The effect of cross wind conditions on a platoon has been studied by Marcu and Browand. The drag reductions gained by platooning are still present under side wind conditions. At a spacing of 0.1 vehicle lengths, the average platoon drag coefficient is approximately 61% of that of a yawed vehicle in isolation. The platoon drag coefficient for a zero yaw condition was only 58% of the value in isolation (zero yaw). Without taking into account the extra rolling resistance due to side winds, the savings in a platoon decrease under cross wind conditions. On the lead vehicle, the largest side force and yawing moment was observed. It appeared that the platoon redirects the air flow into its axial direction such that the trailing vehicles experience less side forces and yawing moments due to cross wind. The side force and yawing moments on the lead vehicle are practically insensitive to the presence of trailing vehicles. The axial force on the lead vehicle is insensitive to the presence of the third vehicle. It is the nearest upstream neighbour that influences the vehicle the most [29].

It can be concluded from the literature study that not a lot of studies investigate the effect of cross wind conditions and/or drag reduction devices on a platoon. Besides, some studies report a drag increase of the trailing vehicle due to the platoon, others report a drag decrease. None of the papers clearly makes a distinction between these two cases or explains why this discrepancy exists between several studies.

1.4 Present study

The objective of this study is to investigate the effects of drag reduction devices on a platoon of bluff bodies in cross wind conditions. The aim is to have quantitative indications of platoon performance while also having an understanding of the flow phenomena that cause this. This leads to following research question:

What is the effect of drag reduction devices on a platoon of bluff bodies subjected to cross wind conditions?

To answer this question, this study performs a numerical analysis on the flow around three GETS models. These models are highly simplified truck models with the dimensions of a European tractor-trailer combination [30]. The drag reduction devices will be represented by the varying frontal edge radius and the addition of a boat tail. Chapter 2 gives all the details on the set-up of the simulation and the generation of the mesh around the GETS model. Simulations of vehicles in isolation as well as in platoon formation are performed. The variables that are changed during the simulations are the inter-vehicle distance, the cross wind, the frontal edge radius and the tail configuration of the vehicles. In Chapter 3, the results of the vehicles in isolation are given, as well as the effects of all variables on a single vehicle. These results are compared to data from wind tunnel experiments in order to validate the computational results and are used as a baseline result when studying the effect of a platoon configuration. The analysis of the different platoon configurations can be seen in Chapter 4. After the complete analysis, the performance of the different platoon configurations is compared for every vehicle and some thoughts on the optimal platoon configuration are given in Chapter 5. Finally conclusions are drawn and some recommendations are stated in Chapter 6.

Chapter 2

Numerical Set-up

Simulating the flow around a certain object can be done by solving the Navier-Stokes equations. For this study, these are solved numerically using the ANSYS Fluent software. In this chapter, the set-up of this numerical simulation is described. First, the settings of the solver are going to be examined, this can be found in section 2.1. For every numerical study a model is needed and a mesh needs to be generated around the model. The model and the meshing strategy are explained in section 2.2 and 2.3. A mesh sensitivity analysis is shown in section 2.4 in order to investigate the dependency of the results on the mesh refinement. section 2.5 presents the different configurations that are simulated. At last, the limitations to this study are shown in section 2.6.

2.1 Simulation set-up

2.1.1 Turbulence modelling

A Direct Numerical Simulation (DNS) fully solves the Navier-Stokes equations. However, to capture the smallest turbulent scales at a Reynolds number as high as for road vehicles, combined with a large domain, would lead to computational costs that exceed the capability of the most powerful computers. Therefore, the turbulence, or part of it, should be modelled. In ANSYS Fluent® , three possible methods exist to do so, namely:

- Large Eddy Simulation, LES
- Detached Eddy Simulation, DES
- Reynolds Averaged Navier Stokes, RANS simulation

While LES resolves the large eddies and models the smaller ones, the RANS equations are time-averaged and thus only solve the mean flow and model the effects of the turbulence on the mean flow. DES is a mix that uses LES combined with RANS in the proximity of walls. However, for simulations with large mesh sizes, LES and DES are too computationally expensive in the framework of this thesis. Therefore the RANS equations will be solved. These equations look as follows:

$$\frac{\partial \overline{u}_i}{\partial x_i} = 0 \tag{2.1}$$

$$\rho\left(\frac{\partial \overline{u}_i}{\partial t} + \overline{u}_j \frac{\partial \overline{u}_i}{\partial x_j}\right) = -\frac{\partial}{\partial x_j}\left[\overline{p}\delta_{ij} - \mu\left(\frac{\partial \overline{u}_i}{\partial x_j} + \frac{\partial \overline{u}_j}{\partial x_i}\right) + \rho\overline{u_i' u_j'}\right] \tag{2.2}$$

The first two terms in the square brackets are the mean molecular stress terms, while the third term is the Reynolds stress term, i.e. the turbulent stress. The turbulence stress terms need to be modelled in order to create a closed system of equations.

To model these terms, several turbulence models are available in Fluent® like the $k-\epsilon$, $k-\omega$ and the Reynolds Stress Model (RSM). While the standard $k-\omega$ model outperforms the $k-\epsilon$ for cases where a severe pressure gradient or separation occurs, it is too sensitive to the turbulence properties from the free-stream inlet. Therefore these two models have been combined in the Shear Stress Transport (SST) $k-\omega$ model. While the models discussed above are two-equation models, the RSM is a seven-equation model and requires large computing costs. While the other models use an isotropic eddy viscosity, this model solves all components of the turbulent transport. However due to identical problems with the $k-\epsilon$ modelling, it performs the same as the $k-\epsilon$ for some problems. It was observed that the Menter $k-\omega$ SST model performed the best when compared to four other two equation models [31]. Therefore the SST $k-\omega$ model is chosen to close the RANS equations in this study.

2.1.2 Wall treatment

The flow close to the wall can be divided in an outer layer and an inner layer. In the inner layer, a distinction is made between the viscous sublayer and the buffer layer. The overlap region between the inner and outer layer is contained in the log-law region. The location of these layers can be described by use of the dimensionless wall coordinate, y^+. This coordinate can be described by following equations [32, 33].

$$C_f = \frac{0.455}{ln^2(0.06Re_x)} \tag{2.3}$$

$$\tau = \frac{1}{2}C_f \rho U^2 \tag{2.4}$$

$$u^* = \sqrt{\frac{\tau}{\rho}} \tag{2.5}$$

$$y_{\frac{1}{2}} = y^+ \cdot \frac{\nu}{u^*} \tag{2.6}$$

Where C_f is the friction coefficient at the surface, τ the wall shear stress and Re_x the Reynolds number based on the length along a surface. u^* is called the friction velocity and $y_{\frac{1}{2}}$ is half the height of the first cell. Now the three different layers can be put in perspective to y^+. The different layers are sketched in Figure 2.1.

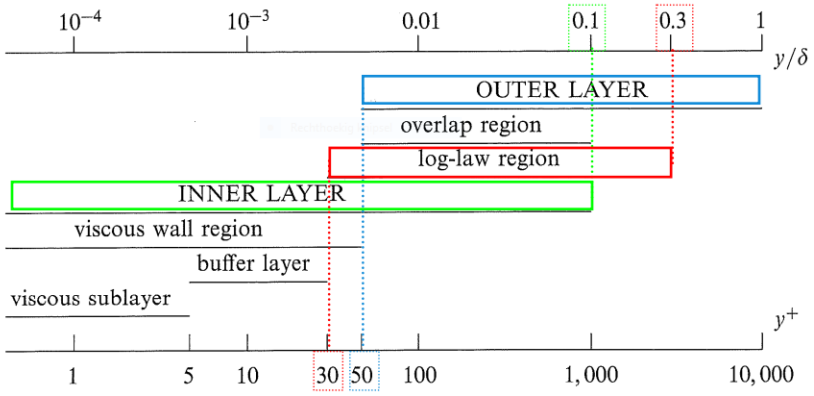

Figure 2.1: A sketch showing the various wall regions and layers defined in terms of $y^+ = y/\delta_\mu$ and y/δ, for turbulent channel flow at high Reynolds number ($Re_\tau = 10^4$) [32].

- Viscous sublayer: $y^+ < 5$
- Buffer layer: $5 < y^+ < 30$
- Log-law region: $y^+ > 30$

ANSYS Fluent® has the option to resolve the entire boundary layer using the near wall model or it can use wall functions to model the flow in the layers/region mentioned above. The difference between these two methods is illustrated in the sketch in Figure 2.2. One can imagine that a very fine grid is needed to use the near wall model, $y^+ < 5$ is definitely needed. In order to use the wall functions, y^+ should be between 30 and 300 [34]. Wall functions perform well for high Reynolds number flows where the turbulent boundary layer is fully developed. However, since the y^+ value is based on the friction, this value will not be larger than 30 on the entire model surface (e.g. on the stagnation surface). In these regions it is not beneficial to use the wall functions. Therefore Fluent® has the Enhanced Wall Treatment function that uses wall functions if the y^+ is within the valid range and uses the near wall treatment when y^+ is small enough. This procedure is automatically selected when the $k - \omega$ model is used.

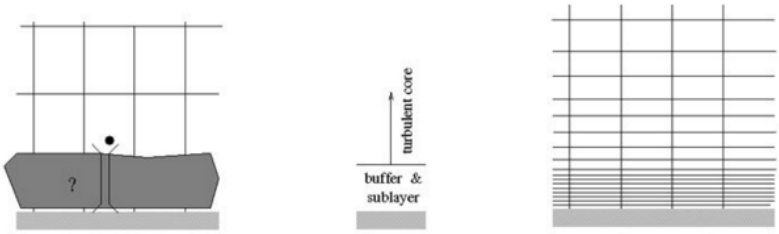

Figure 2.2: Left: mesh used when wall functions are applied in the region close to the wall. Right: mesh to resolve the entire boundary layer.

2.1.3 Boundary and operating conditions

The boundary conditions of the domain vary with the yaw angle applied to the incoming flow. They can be seen in Table 2.1.

Table 2.1: Boundary conditions for varying cross wind conditions.

Surface	**Boundary condition**	
	No cross wind	Cross wind
Front	Velocity inlet	
Right boundary	Symmetry	Velocity inlet
Left boundary	Symmetry	Outflow
Back	Outflow	
Top	Symmetry	
Bottom	Moving wall	
GETS model	Wall	

For the mesh sensitivity study, where the model is scaled like in wind tunnel tests by Van Raemdonck [15], the turbulence intensity was set to 1%, similar to the value in the wind tunnel. For the full scale simulations, the turbulence intensity was set to 5%, this value was found in extensive road tests by McAuliffe et al. [35].

The difference between the simulations with and without cross wind lies in the boundary conditions on the side and the inlet. To simulate the cross wind, a lateral velocity component is added to the inlet. This creates yaw angle between the models axis and the incoming flow. The yaw angle that is simulated in this study is 3°, based on road measurements [15]. When a yaw angle is applied, both the side on the left and the outlet act as an outflow boundary. Depending on the domain length and the yaw angle, the mass flow that enters the domain across the inlet and the right side is calculated. Weightings are set for the side outlet and the back outlet such that the same amount of mass flow that comes in from the side inlet also goes out through the side outlet. The same applies for the front inlet and the back outlet. This assumes that the flow reaches freestream conditions when it leaves the domain. This method has already been applied successfully [36], it is much more time efficient than rotating the model in the domain and re-meshing the entire domain. The moving wall condition at the bottom represents the driving velocity. Since only cross winds are considered (no longitudinal gusts/wind), the moving wall always has the same velocity in x-direction as the freestream velocity. It never has a velocity component in any other direction.

The operating conditions of the simulation are a density of 1.225 kg/m^3 and an operating pressure of zero. The latter is done, since Fluent® always subtracts the real static pressure with the operating pressure in order to plot the static pressure. Thus by setting the operating pressure to zero, the static pressure given by Fluent is equal to the real static pressure. The operating conditions can be seen in Table 2.2.

Table 2.2: Operating conditions.

	Mesh sensitivity study	**Full scale simulations**
Model scale [-]	1:15	1:1
Driving velocity [m/s]	60	25
Density [kg/m^3]	1.225	1.225
Reynolds number* [-]	8.2×10^5	5.1×10^6
Yaw angles [°]	0	0-3

*this Reynolds number is based on the square root of the frontal area,$\sqrt{A}$.

All the computed forces on the models will be normalised using the freestream velocity, density and the frontal area of the model as can be seen in Equation 2.7. Where D, S and L are respectively the drag force, the side force and the lift force on the model. For the lift coefficient, instead of the frontal area, the upper surface area is used.

$$\begin{aligned} C_D &= \frac{D}{\frac{1}{2}\rho U^2 A} \\ C_S &= \frac{S}{\frac{1}{2}\rho U^2 A} \\ C_L &= \frac{L}{\frac{1}{2}\rho U^2 A_{upp}} \end{aligned} \tag{2.7}$$

2.1.4 Solver settings

The pressure-based coupled solver is used in Fluent® since this yields superior performance to the segregated solver. This is also recommended by SAE International guidelines [34]. The density-based solver is not used since this is mostly applicable for high speed compressible flow, combustion, etc... The gradients of the solution variables at the cell centres are determined using the Green-Gauss Node-Based approach [37]. This approach minimises false diffusion and is thus recommended for tetrahedral meshes. Both the momentum, turbulent kinetic energy, specific dissipation rate and pressure are discretised with the default scheme (1^{st} order / standard) for 150 iterations. After these initial iterations, the pressure is discretised with a second order scheme. The other variables use a second order upwind scheme for the spatial discretisation [34]. The required limits for the convergence residuals are also adapted in order to have a fully converged flow. The criteria are set to 10^{-5} for the continuity and velocity residuals and to $1e-04$ for the turbulent kinetic energy (k) and the turbulent dissipation rate (ω). The flow field is initialised using the flow parameters from the velocity inlet.

2.2 GETS model

Heavy-duty vehicles have a complex geometry. Besides the gap between the cab and the trailer, there is also a complex shaped under-body, rotating wheels, side mirrors, mud flaps etc. To mesh such a geometry requires a very time consuming process and would lead to high computational costs. Furthermore, this study focuses only on the general flow behaviour around a platoon of bluff bodies. There is thus no need to capture the details of a real truck geometry. A model with a simplified geometry is used, i.e. the GETS model [30]. Using this model, only the primary effects will be measured without interference of secondary effects due to the details of the more complex geometry. An example of the model can be seen in Figure 2.3. The dimensions are given in Table 2.3.

Figure 2.3: Geometry of the used GETS model.

Table 2.3: Dimensions of the GETS model.

Dimension	Symbol	Value
Length [m]	l_m	16.5
Width [m]	w_m	2.6
Height [m]	h_m	3.5
Front edge radius [m]	r_m	0.54*
Tail length [m]	l_t	1.5
Tail angle [°]	α_t	12*
Ride height [m]	$h_{r,m}$	0.5

*these values are varied during this study.

During the modelling, all the surfaces of the model are categorised to one of the following parts: front, sides, back (and tail if applicable as displayed in Figure 2.3). This way, the forces working on the model can be split into the forces working on every part and the origin of the forces can be traced. The vehicle parts can be seen in Figure 2.4. Note that the sides also include the top and bottom surface. The pressure force on a body is calculated by subtracting the pressure on the front part by the one on the rear part multiplied by the frontal area. When the surfaces are split up, Fluent® calculates the pressure part of the individual surfaces by relating them to the reference pressure as shown in Equation 2.8. $\vec{F}_p$ is the force vector, p the static pressure, p_{ref} the reference pressure and A the area of the surfaces. N is the number of surfaces and $\hat{n}$ is the unit normal to the surface.

$$\vec{F}_p = \sum_{i=1}^{N} (p - p_{ref})\, A \cdot \hat{n} \tag{2.8}$$

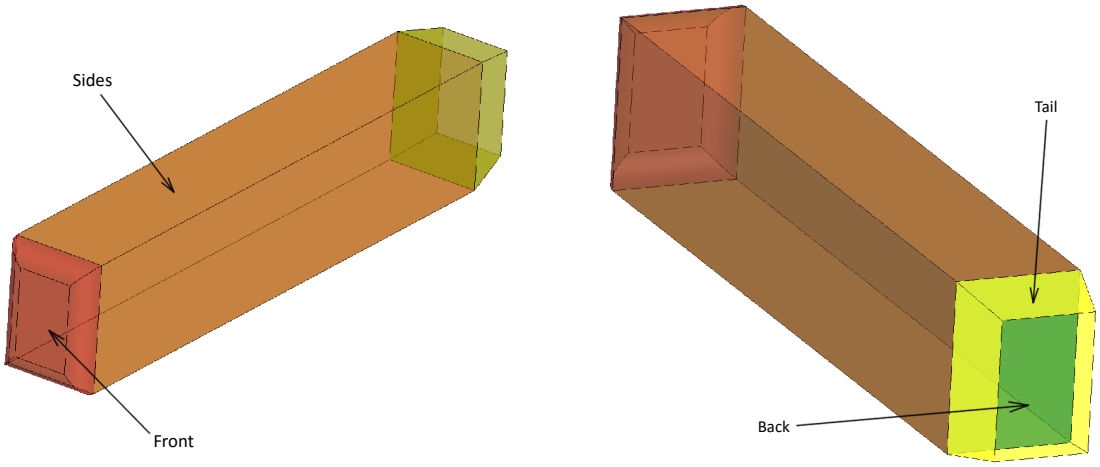

(a) Front and sides (b) Back and tail

Figure 2.4: The different vehicle parts of the GETS model.

2.3 Grid generation

To mesh the GETS model, the ANSYS ICEM CFD meshing software is used. The dimensions of the domain are shown in Figure 2.5. Using these dimensions the blockage ratio is sufficiently small as seen in Equation 2.9 [38].

$$\text{Blockage Ratio} = \frac{A_{model}}{A_{domain}} = 1.34\% \tag{2.9}$$

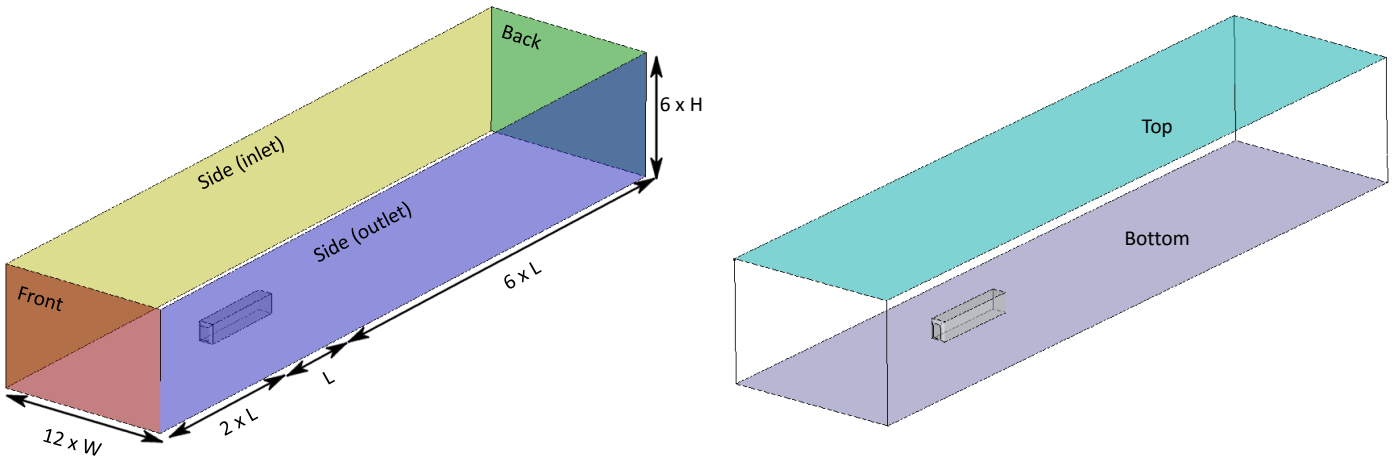

(a) Vertical surface boundaries

(b) Horizontal surface boundaries

Figure 2.5: Domain size and boundaries.

To capture the relevant flow phenomena and still keep the amount of cells reasonable, the mesh is only refined in certain areas. To accomplish this, two density boxes are used in the domain. One contains the immediate surroundings of the GETS model and its wake, while the other surrounds a larger area around the model (and other models in the case of a platoon). The dimensions of these density boxes can be seen in Figure 2.6.

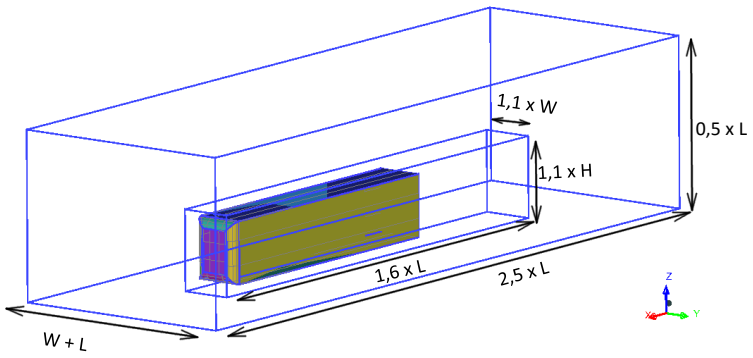

Figure 2.6: Dimensions of the mesh density boxes around the GETS model.

After generating a tetrahedral mesh, a layer of prism elements is needed in order to capture the flow phenomena in the boundary layer of the GETS model. These prisms are placed on every surface of the model, except for the back side. The height of the boundary layer and the height of the first cell are computed separately for the 1/15 scaled model and the full scale model. The height of the boundary layer can be estimated using flat plat theory, according

to Prandtl [33], it is estimated by following equation.

$$\delta = \frac{0.16}{Re_x^{1/7}} \cdot x \tag{2.10}$$

where Re_x is the Reynolds number based on the length (of the boundary layer). The height of the first cell can be estimated with Equations (2.3)–(2.6) [33]. y^+ is set to 100 since the boundary layer will be modelled with wall functions instead of computing the entire boundary layer.

2.4 Mesh sensitivity

When using CFD, the results of a simulation depend on the number of cells up unto a certain amount of cells. To determine this dependency, a mesh sensitivity study is performed with the 1/15 scale GETS model. The mesh in the density boxes is refined step by step in order to generate eleven meshes. The properties of the meshes and their differences can be seen in Table 2.4.

Table 2.4: Mesh sensitivity parameters.

	Cell size wake box [mm]	**Cell size surrounding box [mm]**	**First prism layer height [mm]**T	**Cell count**
Mesh 1	15	30	1.3	1 073 688
Mesh 2	10	20	1.3	2 683 167
Mesh 3	8	16	1.3	4 561 296
Mesh 4	7	14	1.3	6 713 015
Mesh 5	6	14	1.3	7 659 382
Mesh 6	6	12	1.3	10 296 562
Mesh 7	5	12	1.3	12 009 483
Mesh 8	5	11	1.3	14 091 460
Mesh 9	5	10	1.3	17 096 999
Mesh 10	4	12	1.3	15 466 359
Mesh 11	4	11	1.3	17 525 658

As can be seen, from mesh 7 to 8 and 9, only the outer box is refined twice. Afterwards for mesh 10-11, the same is done for a smaller refinement of the wake box. This is done in order to check the mesh sensitivity for each box. A comparison between the first and the fifth mesh can be seen in Figure 2.7.

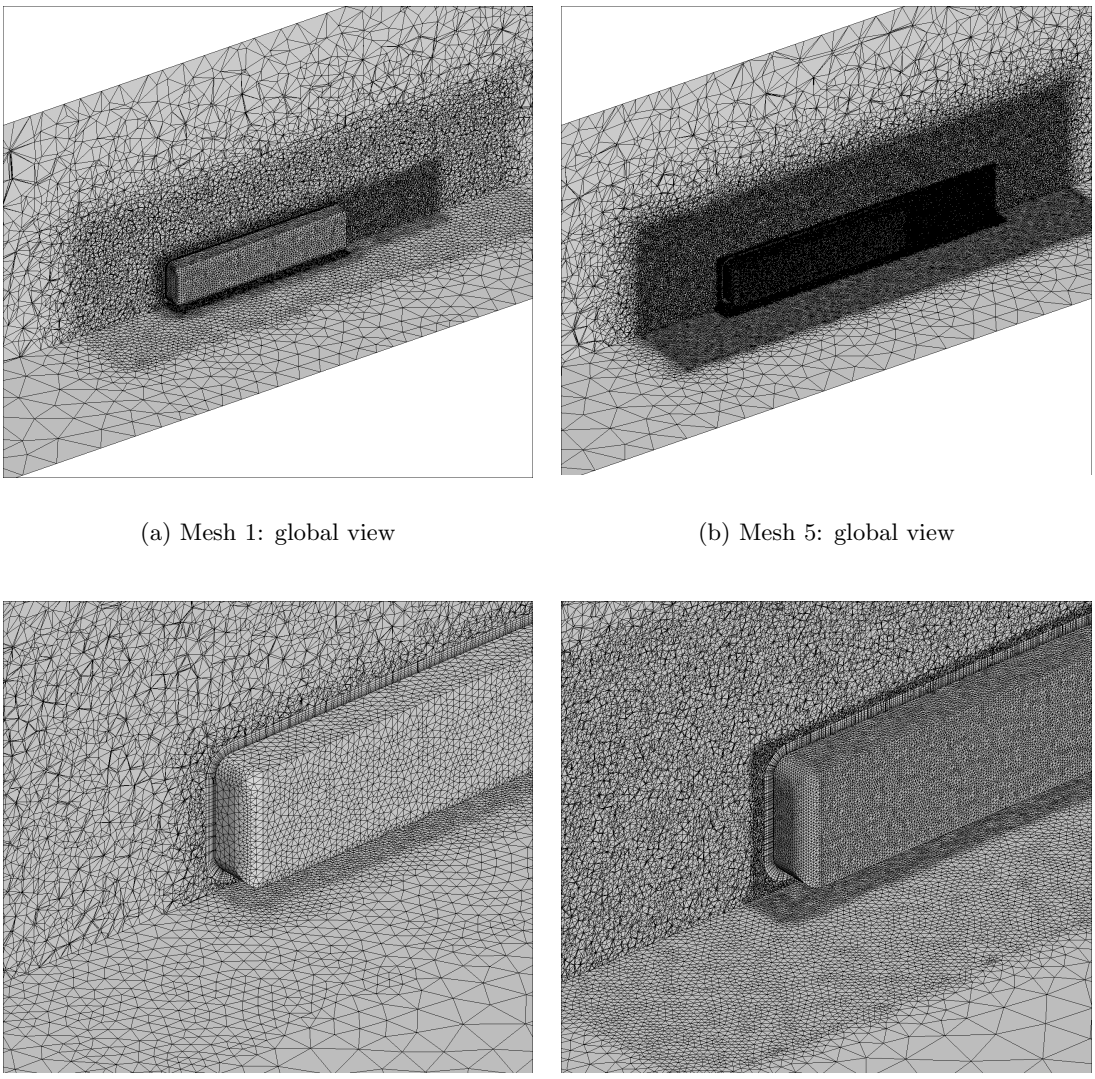

(a) Mesh 1: global view

(b) Mesh 5: global view

(c) Mesh 1: close-up

(d) Mesh 5: close-up

Figure 2.7: Comparison of two different grids.

First the convergence of every simulation is checked, this is done by plotting the evolution of the drag coefficient during the simulation in Figure 2.8(b). For every simulation, the value of the drag coefficient was sufficiently levelled out.

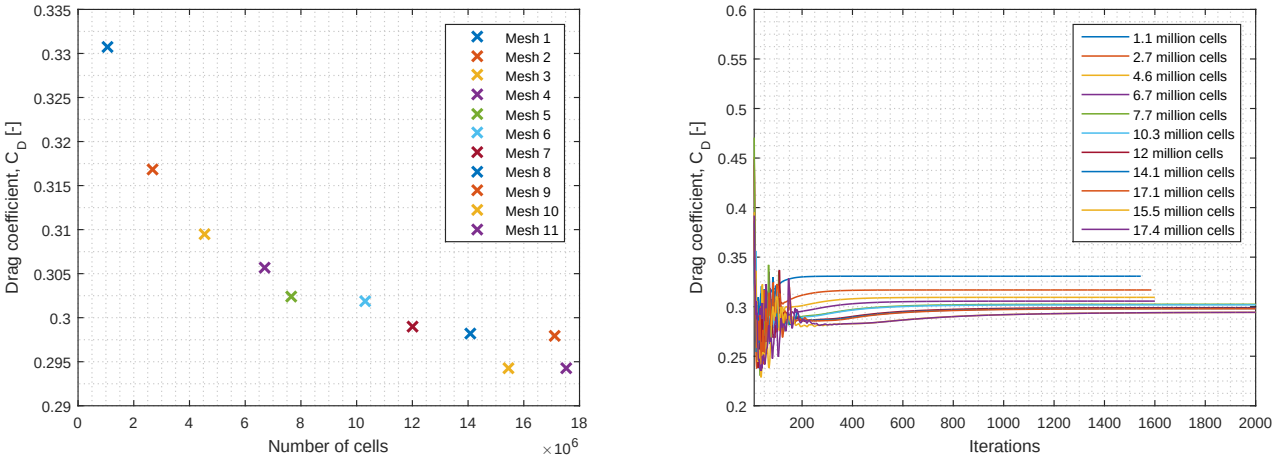

(a) Drag coefficient

(b) Convergence residuals

Figure 2.8: Mesh sensitivity results.

In Figure 2.8(a), the asymptotic behaviour of the drag coefficient as a function of the mesh size can be clearly seen. If one looks at the difference between the cases where only the surrounding density box is refined, it can be seen that the effect of increasing the number of cells in the surrounding density box has no effect any more on the accuracy of the results. This is seen from case five to six, case seven to eight and nine and from case ten to eleven. However, if only the wake density box is refined, case seven to ten or case eight to eleven, it is clear that the curve is not totally asymptotic yet. However further refining the mesh would lead to excessive computational costs. The final drag coefficient that is computed is 0.2943. Since, several configurations with multiple models will be tested, it is unrealistic to use the configuration where just one GETS model already has ten million cells or more. The mesh configuration that will be used for the full scale simulations is the fourth mesh. The drag coefficient for this configuration is 0.3056, which is a difference of 3.5% or 11.3 drag counts with the drag coefficient of the finest mesh. Since the aim of this research is to discover trends due to platooning, it is not critical to be able to calculate the exact drag force of the GETS model. Furthermore, the GETS model is only a simplified representation of real trucks, the exact drag coefficient of this model does not resemble that of real trucks.

2.5 Tested configurations

The vehicles that are tested are all variations on the basic GETS geometry. The radius of the frontal edges is varied three times. Also three different tails are added to the model. These variations are tested for two yaw angles. The different variations are listed below

Front curve radius
- $R = 0.135$ m
- $R = 0.27$ m
- $R = 0.54$ m

Tail configurations
- no tail
- tail of 0°
- tail of 0°
- tail of 6°

Yaw angle
- $Y = 0°$
- $Y = 3°$

Beside the vehicles in isolation, five platoon configurations are tested. First a platoon configuration is tested without any tailed vehicles. The second platoon configuration shows the effect of equipping the trailing vehicle with a tail of 12°. For the remaining platoon configurations, the tail of the trailing vehicle remains unaltered while the tail configuration of the first two vehicles is changed. In the platoon, the vehicles are referred to as the lead vehicle (LV), middle vehicle (MV) and trailing vehicle (TV). The different configurations are summed up in Table 2.5. These platoon configurations are tested for the different yaw angles and frontal edge radii and for three inter-vehicle distances. These distances are often expressed as time intervals when the speed of the vehicles is known. For a driving velocity of 25 m/s, the time intervals between the vehicles are set to 0.3 s, 0.6 s and 0.9 s. The largest time interval is the smallest one at which it is currently legal to drive on the highway in Germany [39]. The shortest time interval is chosen based upon a TNO publication where the string stability of platoons with automatic cruise control was simulated. An interval of 0.3 s still proved to be feasible using cooperative adaptive cruise control [40]. Converting these time intervals to distances gives the distances 7.5 m, 15 m and 22.5 m. If these distances, D, are normalised using the vehicle length, 16.5 m, they become 0.45, 0.91 and 1.36. For the first platoon configuration, an even shorter distance is used in order to reproduce a trend that was observed in literature, namely 3.75 m or 0.23. A distance as close as this lies beyond the scope of this research, therefore only one simulation is performed for this distance.

Table 2.5: The five tested platoon configurations.

Platoon configuration	**Tail configuration**		
	LV	MV	TV
'nnn'	n/a	n/a	n/a
'nnt12'	n/a	n/a	12°
't0t0t12'	0°	0°	12°
't6t6t12'	6°	6°	12°
't12t12t12'	12°	12°	12°

2.6 Limitations

Like every study, the chosen method implies that several limitations are going to be present. These limitations will limit the accuracy and application of the results.

The first limitation is the use of the steady RANS equations combined with a closure model for the effects of turbulence. While results from this system can give good agreement in steady flow, the flow is highly unsteady in real life, especially in the wake of the vehicles. Studying a single vehicle, this would result in an error in the drag force and a difference in flow structures in the wake. This study however, focuses on the interaction of this wake with a drafting vehicle. This will surely induce additional inaccuracies in the results. In order to estimate the magnitude of these errors, extensive validation tests would need to be done on a platoon of vehicles.

The model that is used to study the effects of platooning is the GETS model. This is a highly simplified truck model. It is stripped from all geometrical details like the gap, wheels, mirrors, undercarriage, mud flaps etc. This simplified model has a drastically reduced drag coefficient. The effects that will be seen with these models are thus the primary effects that occur when considering real heavy-duty vehicle geometries.

Another limitation is the steadiness of the chosen platoon configurations. The inter-vehicle distance is exactly the same between the lead and middle vehicle and between the trailing vehicle. The vehicles are also perfectly aligned. In real situations, lateral and longitudinal misalignments might take place. Besides these steady misalignments, the vehicles could also be moving in lateral or longitudinal direction with respect to each other position. This could reduce the beneficial effects of platooning and could lead to increased side forces or yawing moments that influence the driving stability of the vehicles. The considered incoming flow is also a steady uniform flow. In reality, this incoming flow will be influenced by other traffic and surroundings, like bridges, trees etc. This increases the turbulent intensity of the incoming flow instantaneously.

The last limitation has to do with the fact that, during the time period of the master's thesis, only a limited amount of configurations can be tested. Only five platoon configurations are tested with four tail configurations, three frontal edge radii and two yaw angles. All the platoons also consist of vehicles with the same frontal edge radius. In real situations, the frontal shape of the different vehicles can also be slightly different and different effects might occur if one of the parameters is varied more.

Chapter 3

Analysis and Validation of the GETS model

This chapter shows the results of the performed simulations on a single GETS model as well as some discussions on these results. These results will serve as a baseline for the results of the platoon configurations. Therefore, every variation of the basic vehicle that is used in a platoon configuration needs to be simulated first in isolation. First, the results of the basic GETS model are shown, after which the effects of the frontal edge radius, tails and yaw angle will be shown and discussed. Next, the used methodology is validated using data from wind tunnel experiments and a summary is given on the behaviour of isolated vehicles. Finally, a summary of the aerodynamic characteristics of the isolated GETS model is given. All force coefficients in this report are normalised using the freestream velocity, density and the frontal area of the model.

3.1 Basic configuration

The basic configuration of the GETS model is the first model that is simulated. This model has a frontal edge radius of $R = 0.54$ m. The model had a drag coefficient of 0.2881. Since wall functions are used to model the flow near the walls, the y^+ values on the model are first checked. This can be seen in Figure 3.1. It is seen that the values of y^+ are within the desired range in order to validate the use of wall functions. The use of the wall functions is only invalid in the stagnation region and in the vicinity of the wake. In these regions, Fluent® does not use the wall functions since the enhanced wall treatment is used.

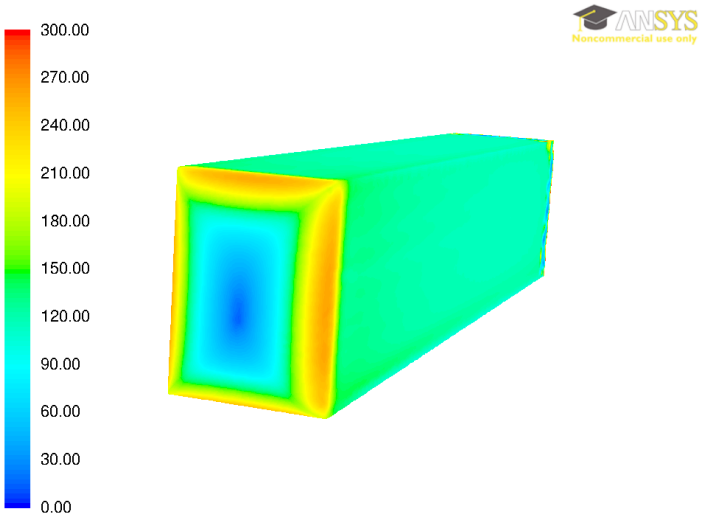

Figure 3.1: Y^+ values on the basic GETS model.

The different contributions to the drag can be seen in Figure 3.2. The model is split up in three different parts: front, side and rear. It is noted that the front surfaces of the model only have a small contribution to the total drag of the model. This is caused by the acceleration of the flow around the frontal edges. This acceleration produces a low pressure region and thus a forward acting suction force at these surfaces. The drag contribution of the front part can be split up further in the four edges and one frontal stagnation surface. These contributions can be seen in Table 3.1 in section 3.2. The low pressure coefficient over the frontal edges is visualised in Figure 3.3.

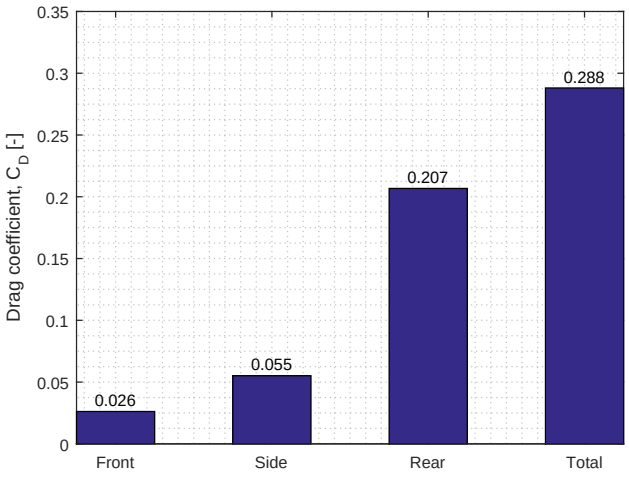

Figure 3.2: Drag contributions of the basic GETS model with $R = 0.54$ m and $Y = 0°$.

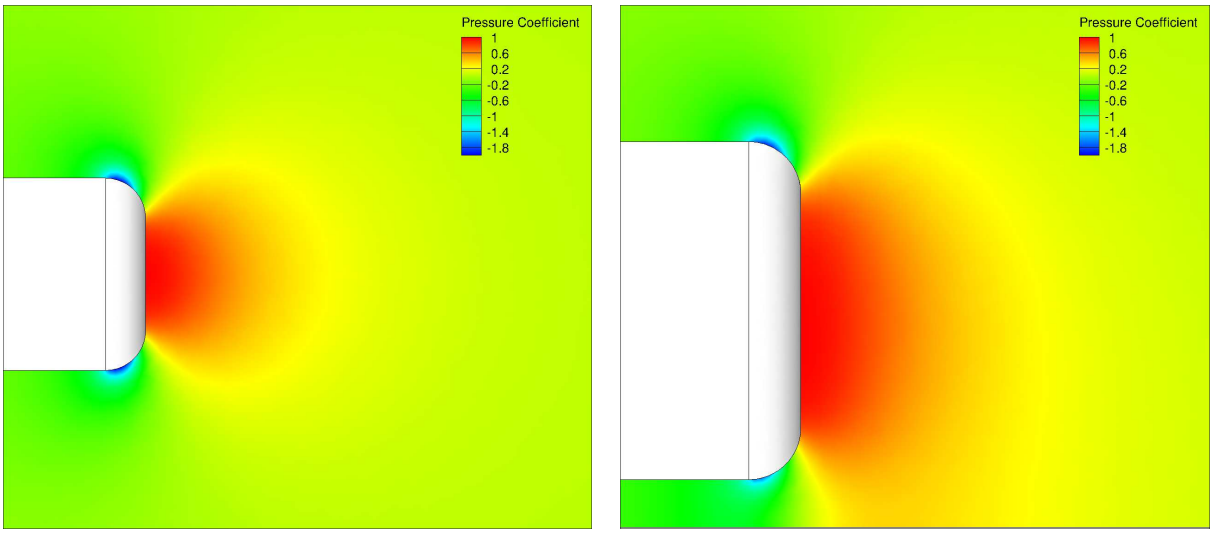

(a) Top view at $z = 2.3175$*

(b) Side view at the $y = 0$ plane

Figure 3.3: Contour of the pressure coefficient around the front part of the model with a radius of 0.54 m.
*the z=2.3175 plane, is the plane halfway the vehicle height.

The simulation of the wake is of great importance for the results since a large contribution of the drag originates from this wake. The visualisation of the wake can be seen in Figure 3.4. The wake is clearly visible within the iso-surface of zero total pressure. Looking at the streamlines shows that there is a toroidal vortex present in the wake. This is confirmed when the vortex cores in the wake are calculated by Tecplot® and shown in Figure 3.4(b). This vortex ring was also observed by Ortega et al [14].

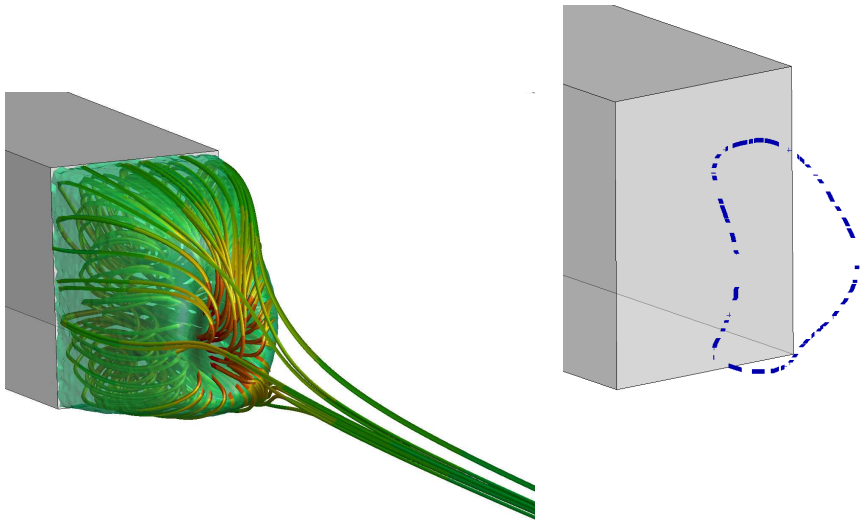

(a) Iso-surface of $p_{total} = 0$ with stream rods

(b) Vortex cores

Figure 3.4: Visualisation of the flow structures in the wake of the model.

3.2 Effect of frontal edge radius

Because of the strong frontal edge suction on the model, the drag contributions of the different vehicle parts did not resemble those found in literature for detailed truck vehicles. Wood stated that the front and rear part of the vehicle produce an equal contribution to the drag [13]. Therefore, the effect of smaller frontal edge radii is investigated. The radius of the GETS model is halved twice, i.e. to a radius of 0.27 m and of 0.135 m. Lowering the radius would lead to an increased suction on the frontal edges. However, these edges then would represent a smaller part of the entire frontal area while the stagnation surface is increased. The contributions to the drag can be compared for the different radii in Figure 3.5.

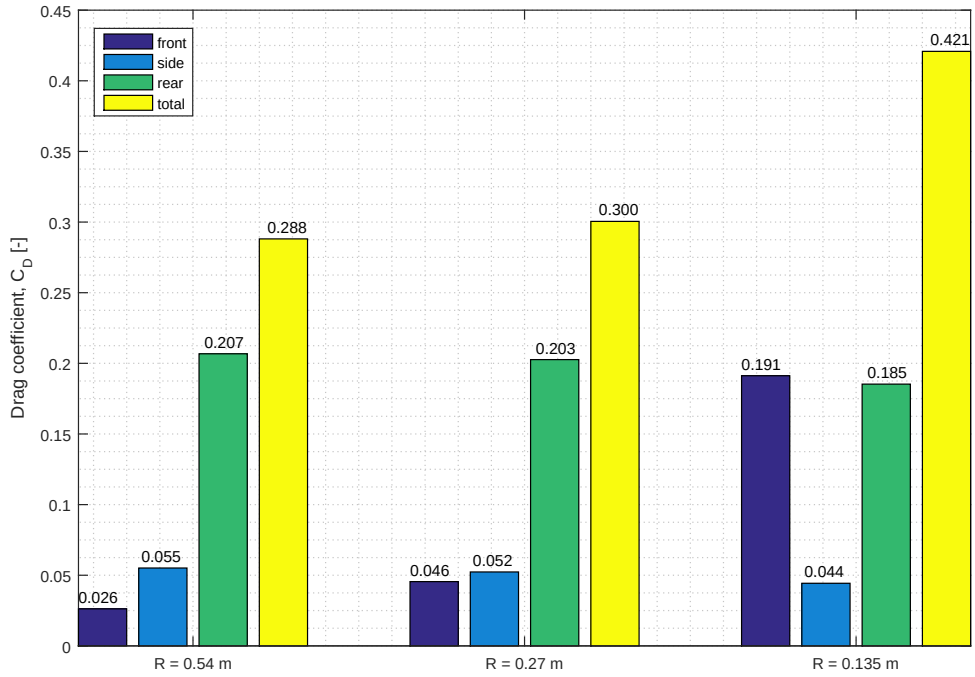

Figure 3.5: Drag contributions of the basic GETS model with $R = 0.54$ m, $R = 0.27$ m and $R = 0.135$ m and $Y = 0°$.

While the drag of the front part increases for decreasing radius, it can also be seen that the drag at the rear of the model decreases slightly. This can be explained by the fact that due to the lower radius of the front curves, the boundary layer thickness over the side surfaces increases. It was already shown in wind tunnel experiments that a thicker boundary layer leads to a decreased back pressure behind the model and thus also to a smaller contribution of the pressure drag at the rear to the total drag [30]. While the drag contributions do not change tremendously when halving the radius from $R = 0.54$ m to $R = 0.27$ m, halving the radius a second time increases the front drag significantly. This is due to flow separation at the frontal edges and the increase of the stagnation surface are due to the smaller edges. The separation at the front part of the vehicle is visualised in Figure 3.6. Reversed flow is clearly seen in Figure 3.6(a). Two areas of high vorticity, representing the free shear layer, are seen on either sides of the vehicle. For the smallest frontal edge radius, the drag contribution resembles that of other studies (when neglecting the gap and undercarriage) [13]. This case thus resembles the drag contribution of currently operating heavy-duty vehicles the best. The cases with a large frontal edge radius represent what happens when more attention is paid to the aerodynamic shaping of the front part of the vehicle.

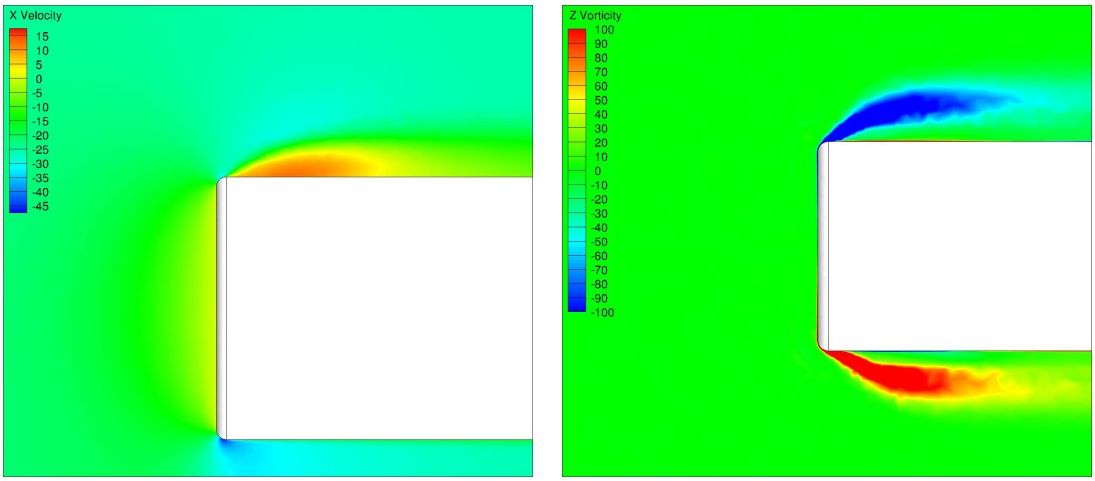

(a) Velocity in x-direction in the vertical plane, $y = 0$

(b) Vorticity in z-direction at the plane, $z = 2.3175$

Figure 3.6: Visualisation of the flow field around the vehicle with a radius of 0.135 m.

The relative drag contribution of the different parts to the total drag can be seen in the pie charts in Figure 3.7. Figure 3.8 shows the contribution of the pressure drag and the viscous drag. As can be expected, reducing the frontal edge radius, and thus making the vehicle less streamlined, increases the contribution of the pressure drag.

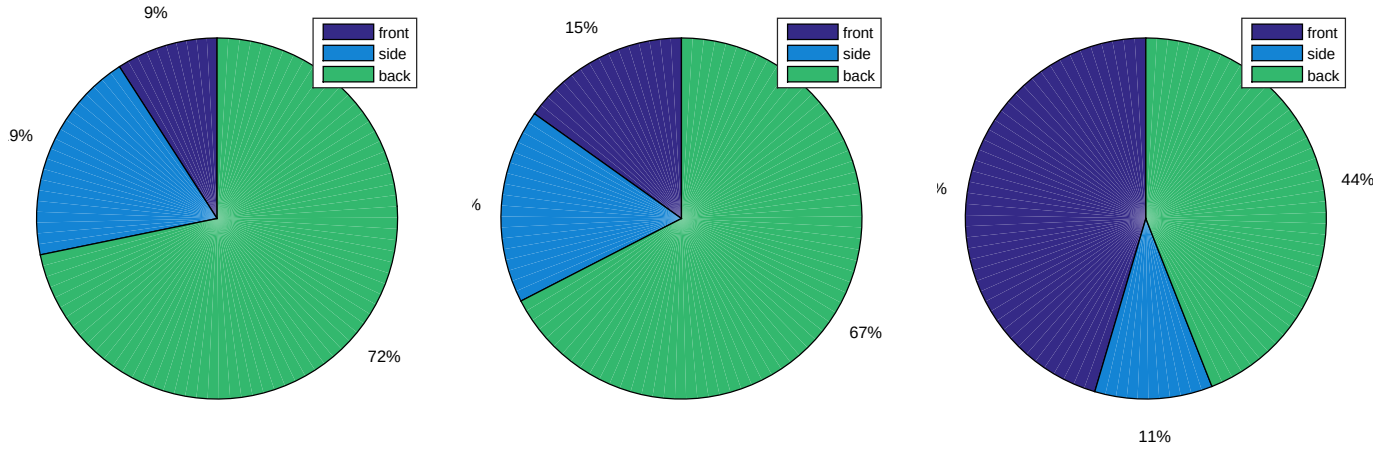

(a) $R = 0.54$ m

(b) $R = 0.27$ m

(c) $R = 0.135$ m

Figure 3.7: Drag contributions of the GETS model with varying frontal edge radius.

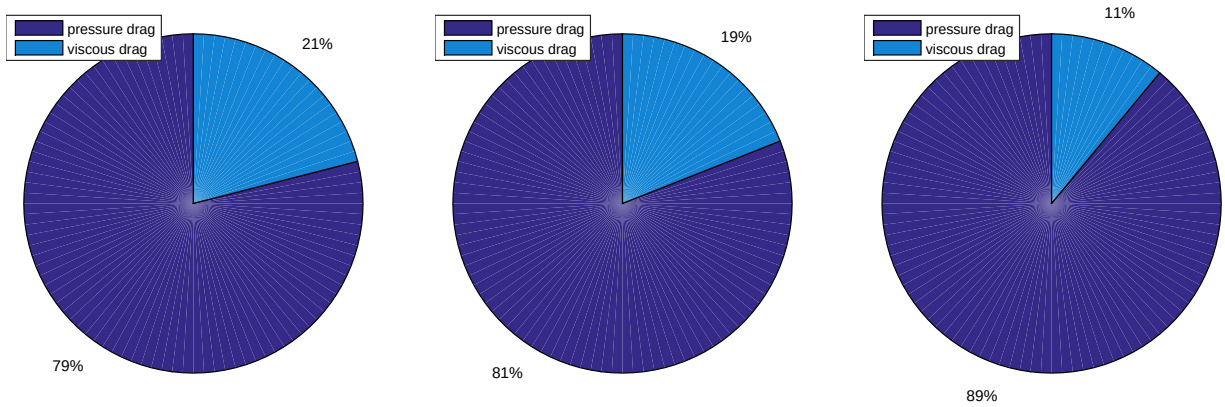

(a) $R = 0.54$ m (b) $R = 0.27$ m (c) $R = 0.135$ m

Figure 3.8: Drag contributions of the GETS model with varying frontal edge radius.

The contributions of the different front surfaces change due to the decreased radii. The drag contributions of the different frontal surfaces can be seen in Table 3.1. While going from $R = 0.54$ m to $R = 0.27$ m increases the suction force, decreasing the radius to $R = 0.135$ m decreases the thrust force due to occurring flow separation. The bottom curve is the only surface where the pressure coefficient keeps decreasing with decreasing radius. This is due to the fact that the presence of the moving floor prevents the flow from separating. It can be noticed that for the vehicle with the smallest frontal edge radius, the difference between the left and right edge is much larger than for the other cases. It is expected that these two contributions are identical in symmetric flow cases. However, due to the sharper corner and the lack of refinement during the meshing, the asymmetry in the mesh leads to difference in separation locations between the left and right edge. This causes a larger difference between the edges than is to be expected. This is a limitation caused by the limiting computation power available to generate the grids.

Table 3.1: Frontal surface drag contributions.

Surface part	**Drag coefficient** [-]		
	$R = 0.54$ m	$R = 0.27$ m	$R = 0.135$ m
frontal surface	0.3529	0.5123	0.5702
top edge	-0.0764	-0.1028	-0.0732
bottom edge	-0.0273	-0.0604	-0.0741
left edge	-0.1115	-0.1518	-0.115
right edge	-0.1115	-0.1518	-0.1167
total front part	0.0262	0.0455	0.1912

The distribution of the pressure coefficient around the front part and the top of the model are shown in Figure 3.9. The pressure peak is clearly higher, but also smaller for the lower radii, this leads to the increase in drag for the front part of the model. For the lowest radius, the adverse pressure gradient is too high and the flow separates from the surface, leading to a small rise after the first pressure drop.

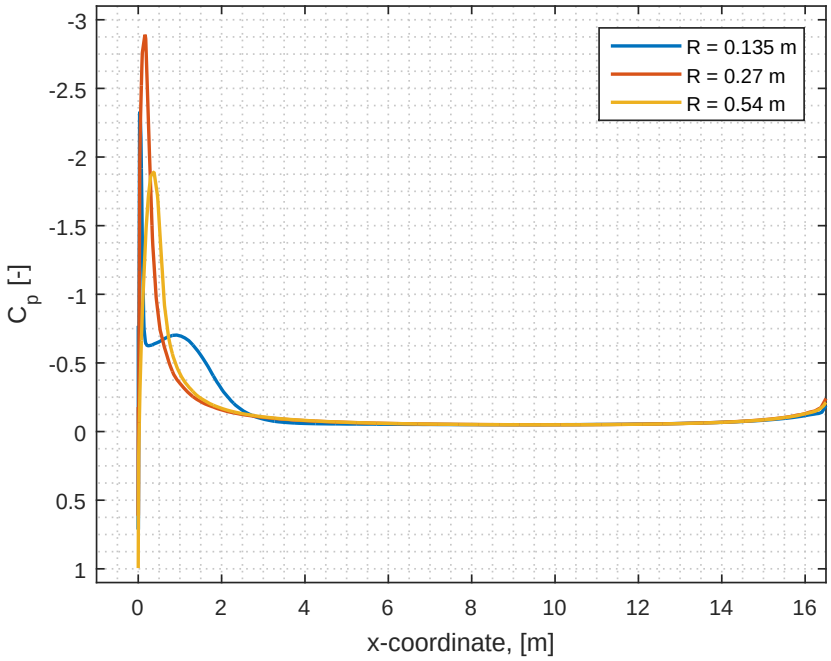

Figure 3.9: Comparison of the pressure coefficient along the front and top of the models with different front radii.

3.3 Effect of tails

The next variable that will be considered is the addition of a tail. The GETS model was equipped with three different tails. All the tails were such that the horizontal length of the model (in x-direction) was increased by 1.5 m, since regulations will limit the horizontal length of the tail instead of the true length. Three different tail angles were used: 0°, 6° and 12°. The effect of the added tails is similar for all frontal edge radii. The drag contributions are shown in Figure 3.10. The tail reduces the pressure drag at the rear of the model significantly, a small part of this drag reduction is again added to the model since the drag of the tail surfaces increases with the tail angle. For some cases, the drag contribution of the rear surface even becomes slightly negative.

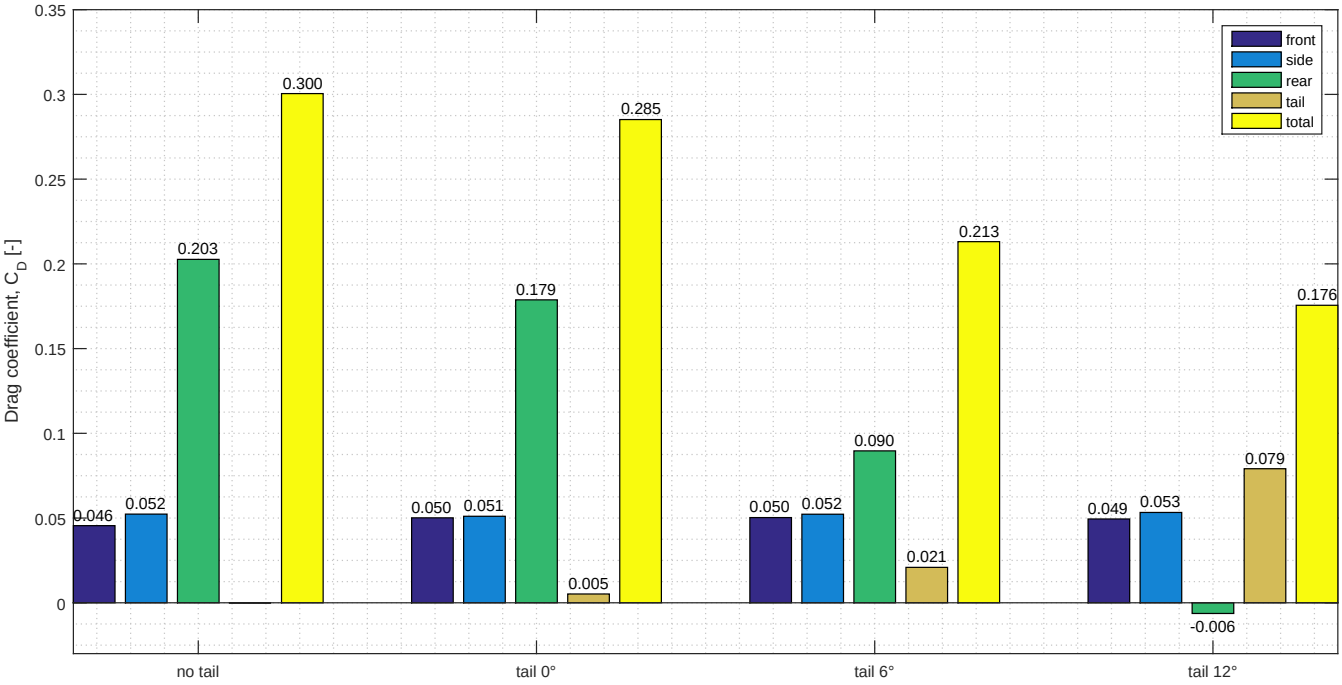

Figure 3.10: Drag contributions of the GETS model for varying tail configuration and a frontal edge radius of 0.27 m. The yaw angle is $0°$.

The pressure coefficient on the back of the vehicles with a frontal edge radius of 0.27 m is plotted in Figure 3.11. A tail without a tail angle shields the base surface from the freestream flow. This reduces the peaks of the pressure variation along the rear surface, i.e. the pressure distribution becomes more constant. Increasing this angle causes the base pressure to rise, leading to a decrease in pressure drag at the rear of the vehicle. For the largest tail angle, the base pressure becomes positive, which results in a slightly negative drag force contribution on the rear surface. This positive pressure coefficient was also measured in wind tunnel experiments [15].

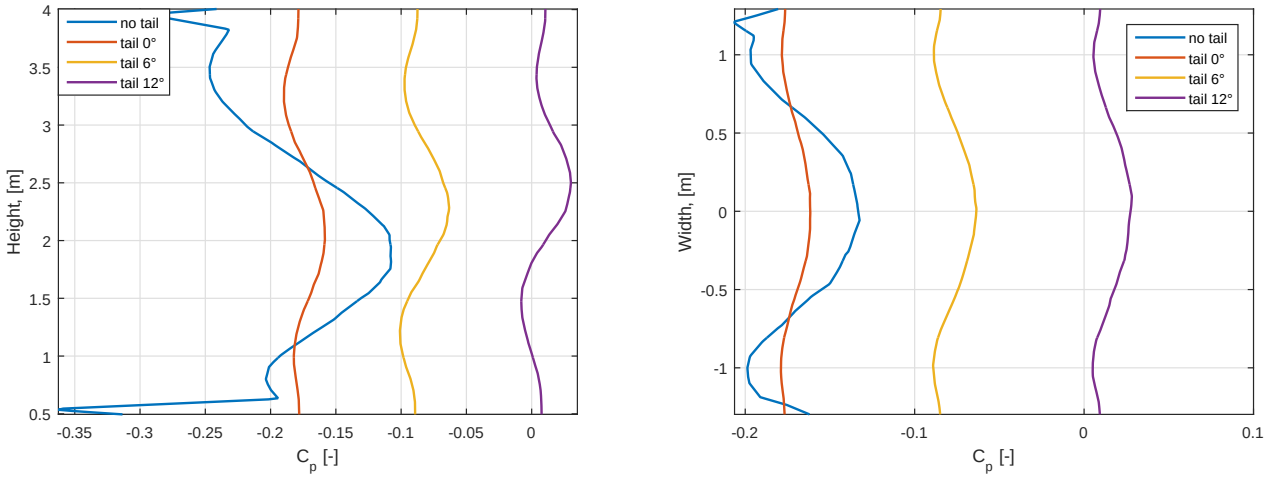

(a) Vertical centreline

(b) Horizontal centreline

Figure 3.11: Effect of tails on the base pressure coefficient along the centrelines.

The tail surfaces also influence the relative drag contributions. When increasing the tail angle, the contribution of the rear surface decreases while that of the tail surfaces increase. Due to the decrease in drag at the rear, the contributions of the front and sides become more important. For the configuration with the largest tail angle, the contribution of the rear surface is entirely removed. It actually gives some net force forward (about 3% of the total drag coefficient).

The effect of the tails on the wake structure is visualised in Figure 3.12. Due to the tail, the streamlines are deflected more inwards and the wake becomes smaller. It is also seen that due to the ground effect, the wake is deflected upward for the configurations with a tail angle of 6° and 12°.

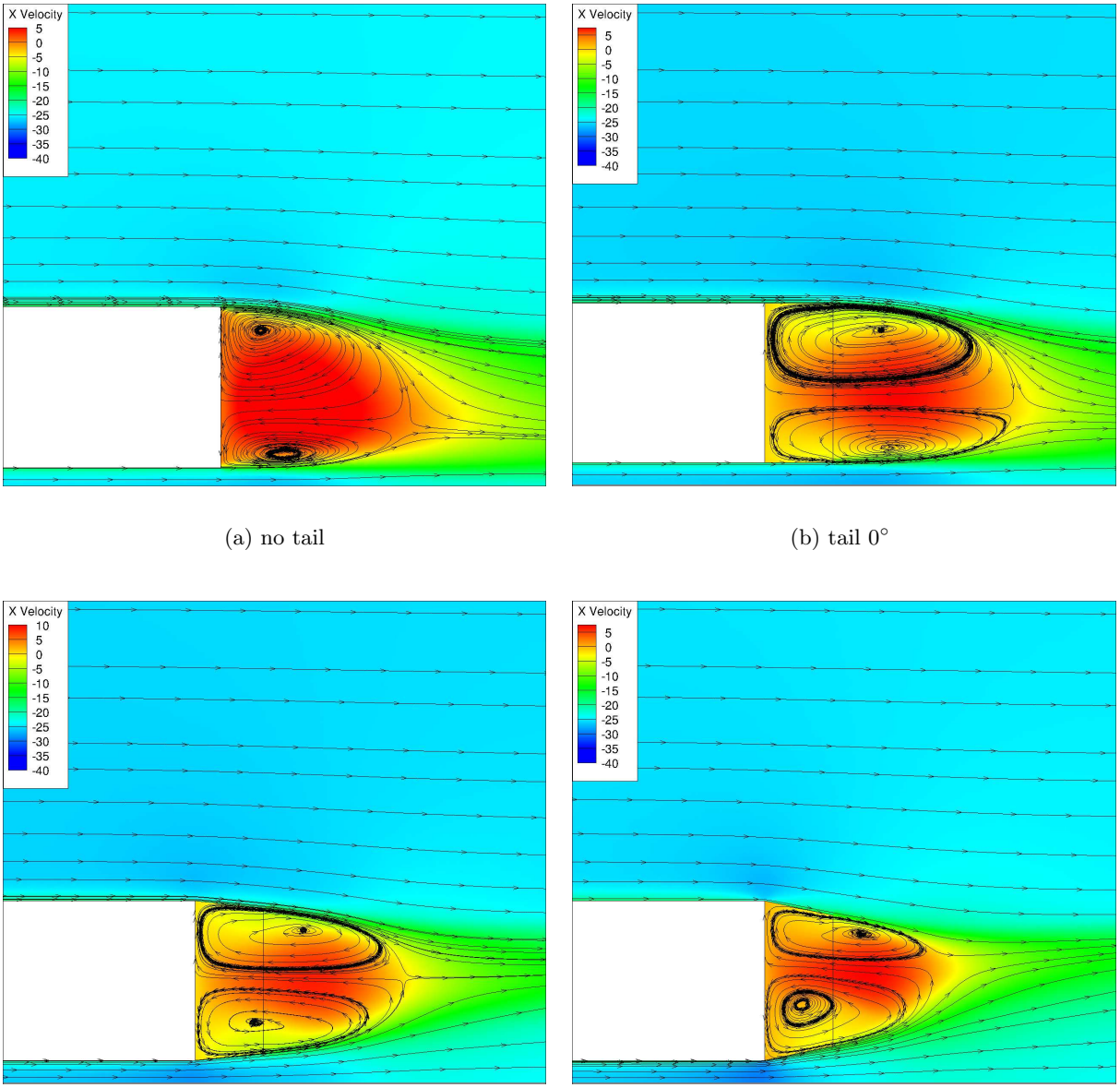

(a) no tail

(b) tail 0°

(c) tail 6°

(d) tail 12°

Figure 3.12: Side contour at the $y = 0$ plane, of the velocity in x-direction and streamlines around the rear part of the model with a radius of 0.27 m.

3.4 Effect of yaw angle

After all geometrical variations of the basic GETS model were studied, a last variable was added. The models were simulated at a yaw angle of 3°. It was expected that the drag coefficient would increase [16, 17, 41]. The change in drag contributions due to the yaw angle can be seen in Figure 3.13 for the vehicles with varying frontal edge radius. The change in drag coefficient is defined as in Equation 3.1.

$$\Delta C_D = C_{D_{Y=3^\circ}} - C_{D_{Y=0^\circ}} \tag{3.1}$$

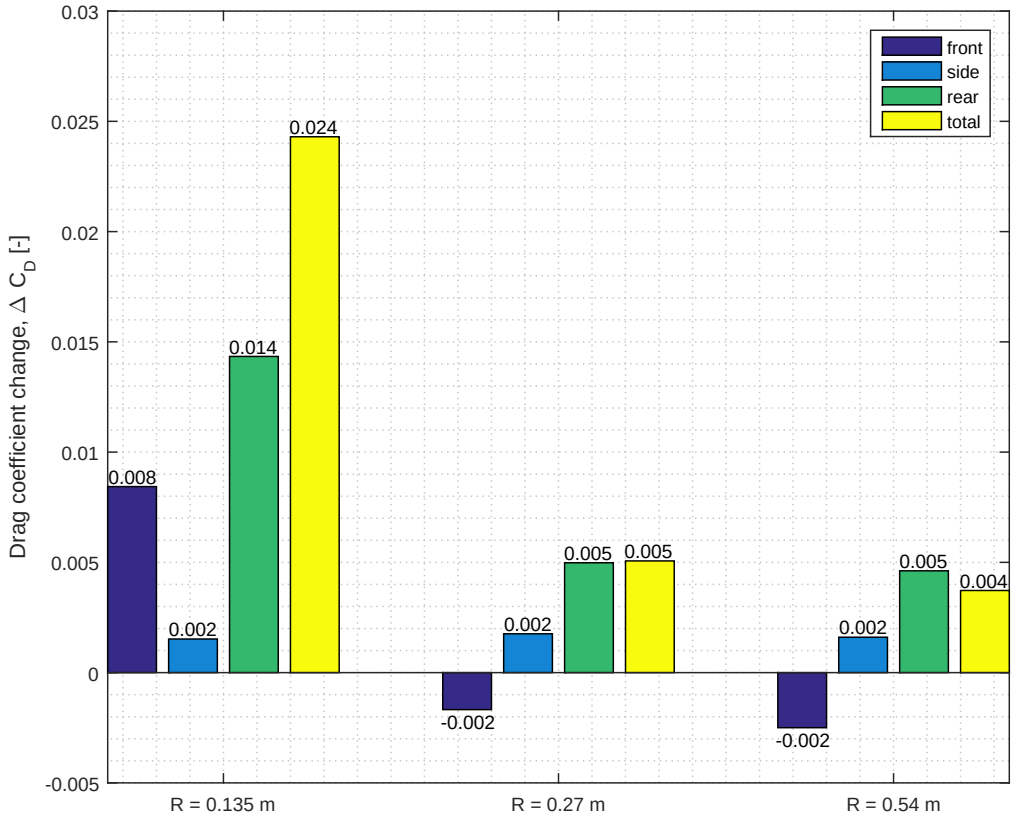

Figure 3.13: Difference in drag coefficient contributions of vehicle due to a yaw angle for different front curve radii. The reference drag coefficient is the one from the same geometry in still wind conditions.

The drag contribution of the front part of the vehicle decreases for the two large radii. The large difference in the effect on the front part of the vehicle is mainly due to the fact that when the flow does not separate at the frontal edges, the drag coefficient of the left (leeward) frontal edge decreases with the same amount as the increase in drag coefficient of the right (windward) frontal edge. The flow accelerates more over the leeward side of the front part and therefore the suction force increases. On the windward side of the front part, the opposite

effect occurs. However, when the radius is small enough to cause separation, both sides of the front part experience a slightly higher drag force. These changes in the front drag contributions can be seen in Figure 3.14.

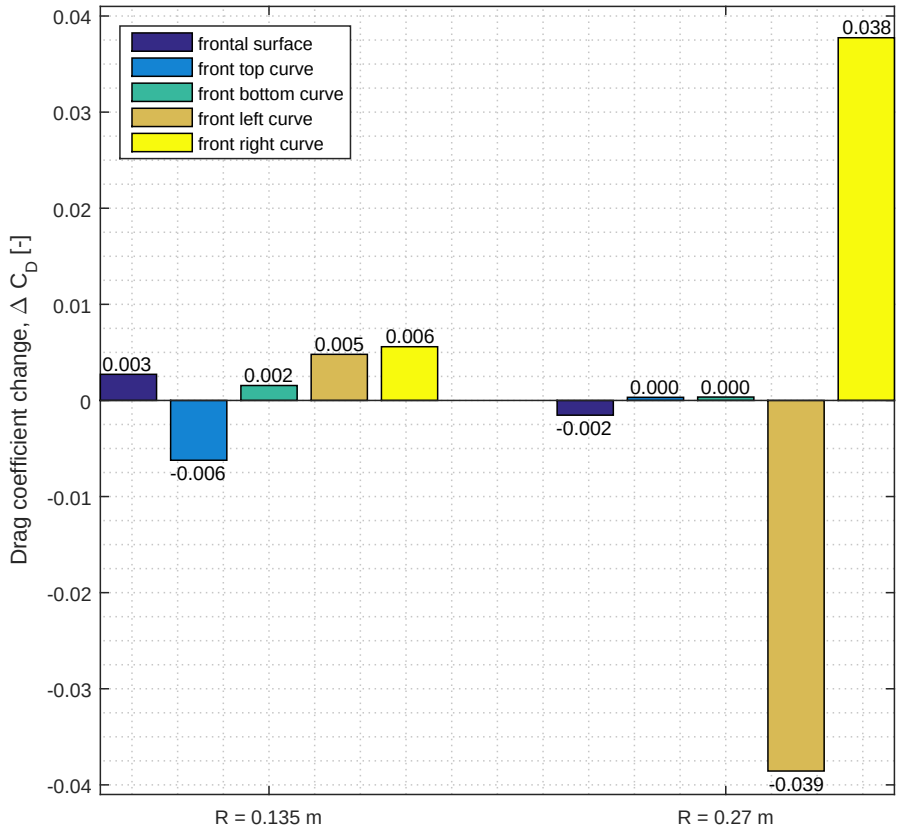

Figure 3.14: Difference in drag coefficient contributions of the front part of the vehicle due to a yaw angle for different frontal edge radii. For each geometry, the reference drag coefficient is the one from the same geometry in still wind conditions.

Besides the radius of the frontal edges, the addition of a tail also influences the sensitivity of the drag coefficient to a yaw angle. The difference in drag coefficient change due to cross wind can be seen for different tails configurations in Figure 3.15. It is seen that for increasing tail angle, the drag increase due to cross wind becomes less pronounced. It can be stated that the more streamlined the vehicle is, the less sensitive its drag force is to yaw angles.

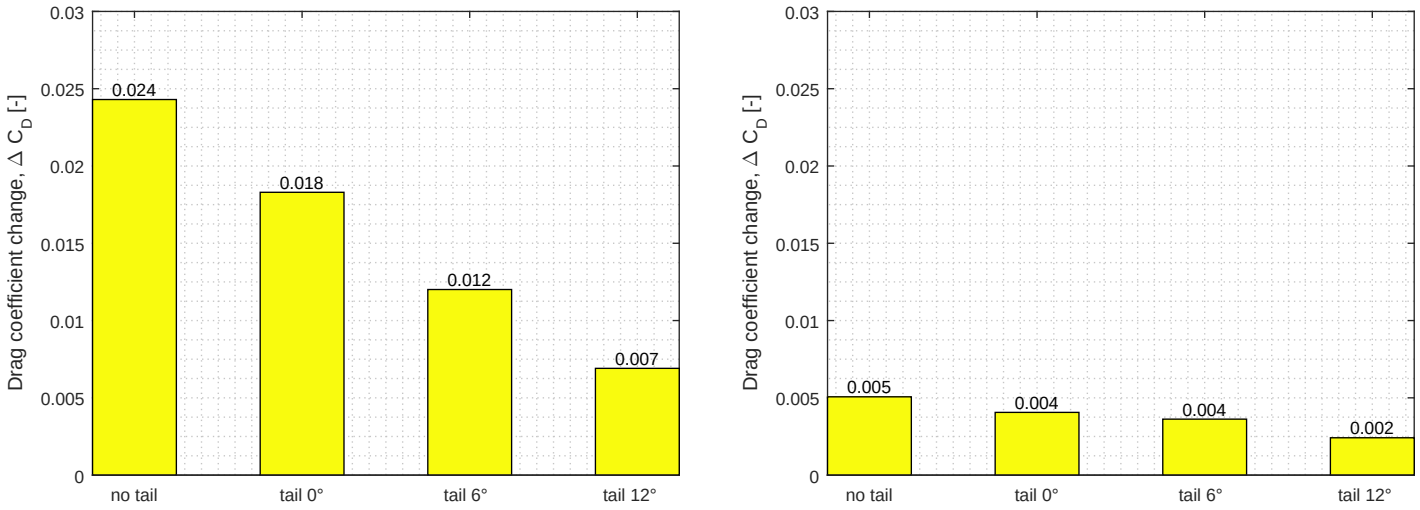

(a) $R = 0.135$ m

(b) $R = 0.27$ m

Figure 3.15: Drag coefficient change due to cross wind conditions for vehicles with different frontal edge radii and tail configurations. The reference drag coefficient is the one from the same geometry in still wind conditions.

Simulating asymmetrical cases also results in side forces. The side force coefficient and its contributions can be seen for different frontal edge radii in Figure 3.16. The side surfaces represent the most important contributions to the side force. The importance of the front part reduces when the frontal edge radius is decreased.

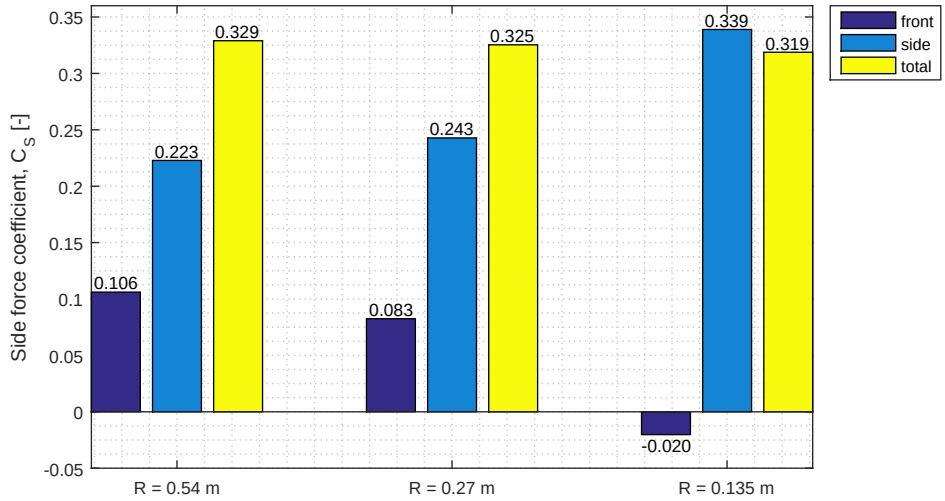

Figure 3.16: Side force contributions of the basic GETS model with $R = 0.54$ m and $R = 0.27$ m.

The side force coefficient of all configurations can be seen in Figure 3.17. It is clear that, while adding a tail reduces the drag, it also significantly reduces the side force experienced by the model. While increasing the frontal edge radius decreased the sensitivity of the drag due to cross wind, it increases the side forces experienced in cross wind conditions. The small increase in side force when adding a tail of 0° is due to the fact that the total vehicle length is increased, while the reference length remained unaltered.

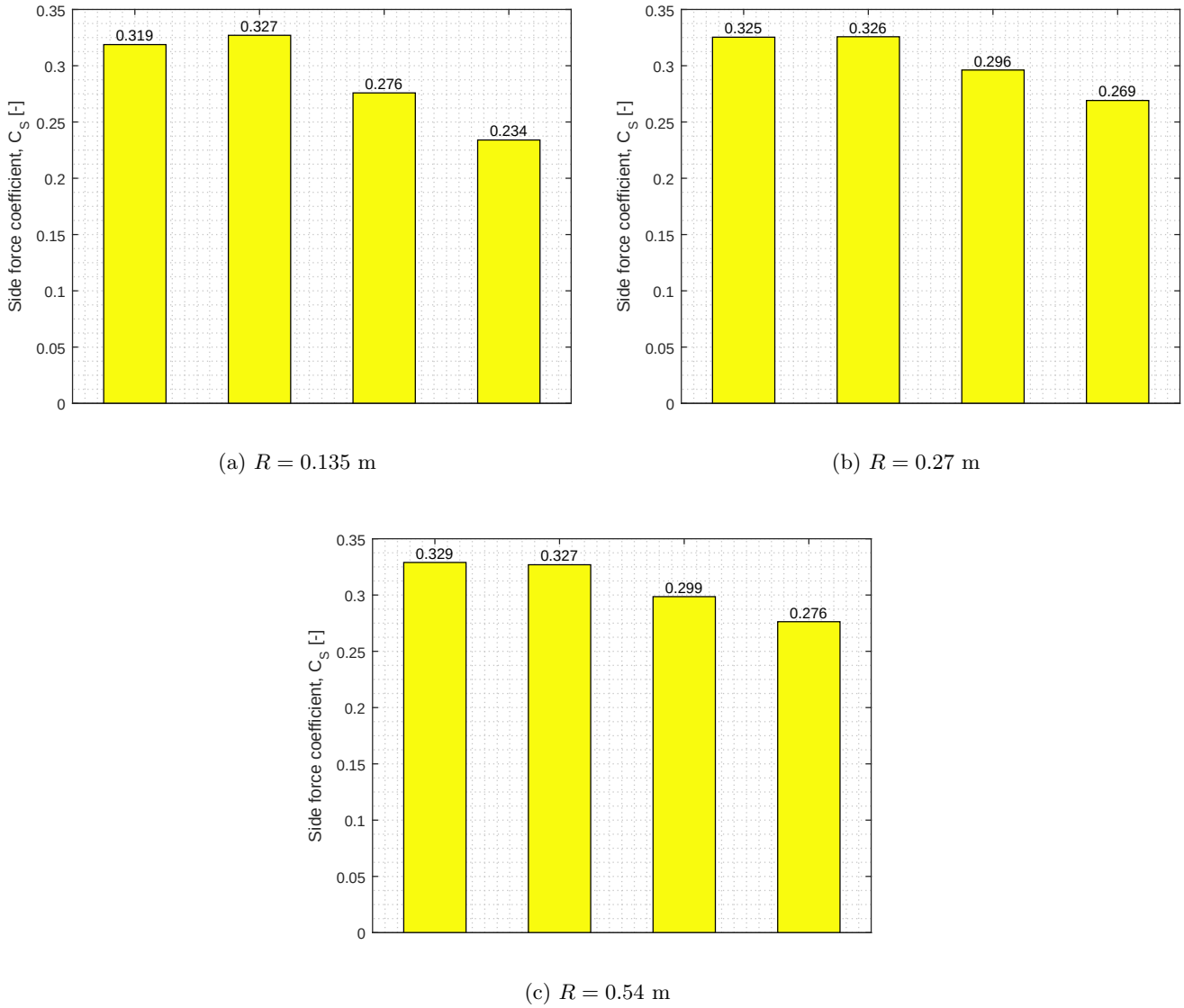

(a) $R = 0.135$ m

(b) $R = 0.27$ m

(c) $R = 0.54$ m

Figure 3.17: Side force coefficients of all the configurations

This reduction of the side force is mainly due to the side force contribution of the side and tail surfaces as can be seen in Figure 3.18.

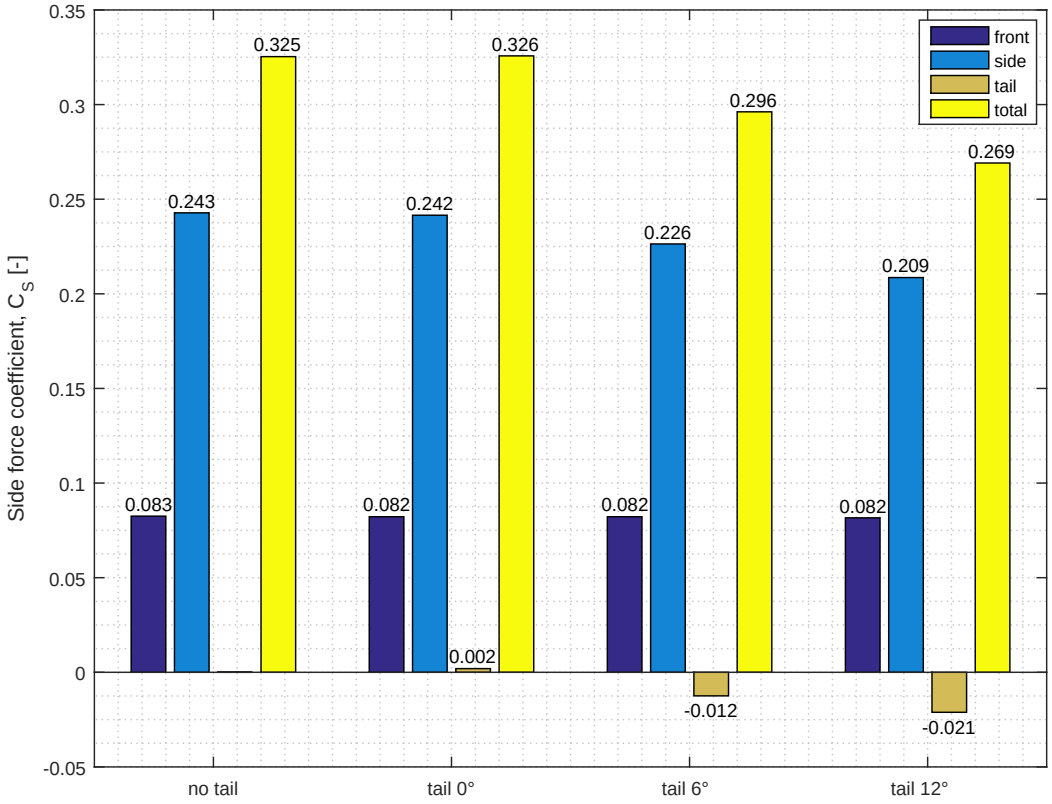

Figure 3.18: Side force contributions of the GETS model with $R = 0.27$ m, with and without a tail.

The side force is the result of an asymmetrical pressure distribution over the model. The pressure distribution over the frontal edges and the sides is shown in Figure 3.19 for two models with a radius of 0.27 m with different tail configurations. It can be seen that the negative pressure drop is smaller on the leeward side than on the windward side. On the side surfaces however, the pressure coefficient is generally lower on the leeward side, this leads to the side force that is experienced by the vehicle. For the configuration with the tail at an angle, there is a second negative pressure peak at the position where the tail starts. Although the difference between the windward and leeward side of the vehicle is more pronounced at the second pressure peak than in the case of a straight tail (0°), the overall difference between the pressure on the leeward and windward side is still larger in the case of a straight tail.

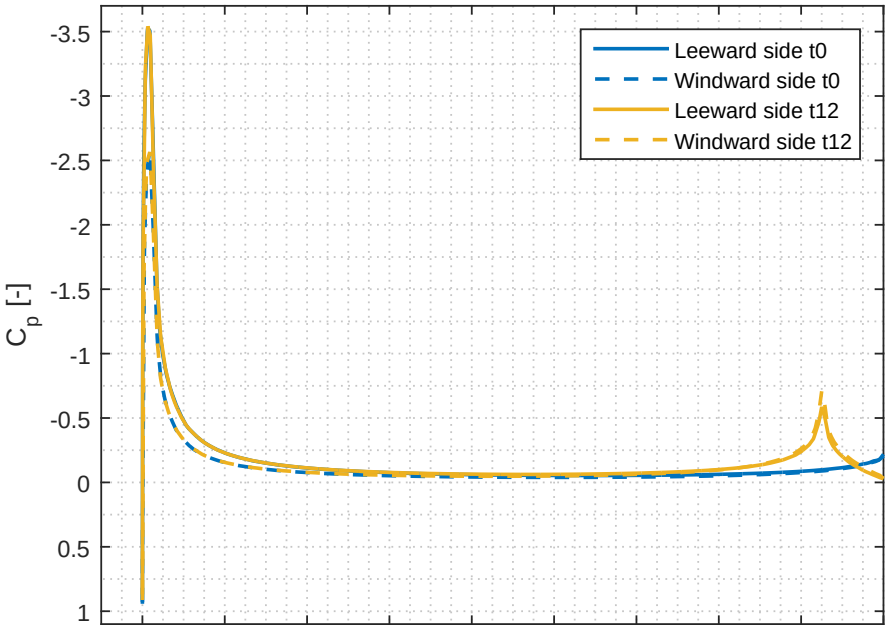

(a) Front, side and tail side surfaces

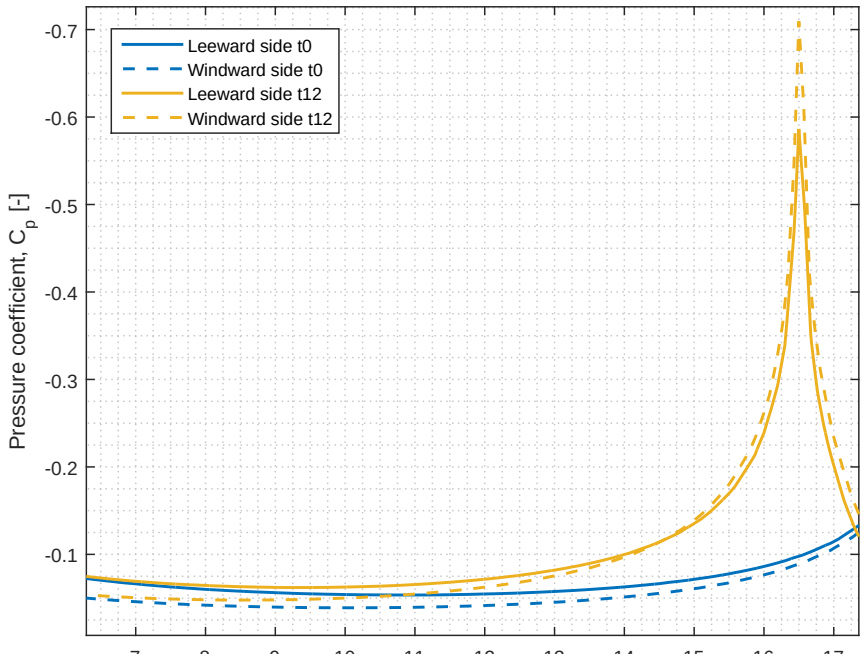

(b) Close-up of the tail region

Figure 3.19: Pressure coefficient distribution over both vertical side surfaces of the vehicle for two different tail configurations.

The non-zero yaw angle also influences the wake of the vehicle. This influence is shown in Figure 3.20. It can be seen that the wake is displaced/deformed in the direction opposite to where the cross wind is coming from. The vehicle bends the air when a yaw angle is applied like an airfoil would do when an angle of attack is applied.

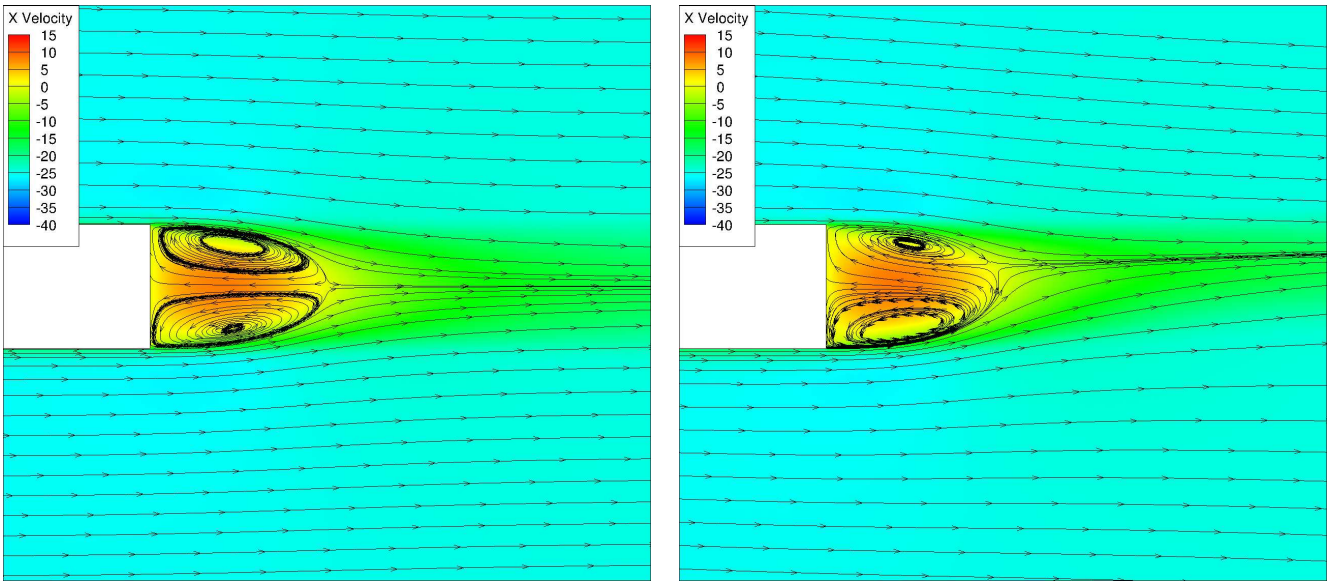

(a) $Y = 0°$ (b) $Y = 3°$

Figure 3.20: Contour of the velocity in x-direction with streamlines around the vehicle for different yaw angles. The contour is plotted at the half of the vehicle height.

3.5 Validation of computational results

Extensive wind tunnel tests were performed on the GETS model by Van Raemdonck [15]. These results are used to validate the numerical simulations in this thesis. The drag forces of both simulations and wind tunnel experiments are compared in Table 3.2. In general, the values are well predicted by the CFD simulations, especially within the scope of this project, where it is more important to observe trends than to accurately predict the exact drag of a GETS model.

Table 3.2: Comparison of the force coefficients from the simulation with data from wind tunnel tests [15].

	$\mathbf{Y = 0°}$		$\mathbf{Y = 3°}$	
	C_D	C_L	C_D	C_S
CFD simulations	0.2881	-0.0332	0.2918	0.3290
Wind tunnel data	0.284	-0.0363	0.300*	0.305*

*these values are the average of the values for two and four degrees.

Besides the force coefficients of the model, the pressure distribution over the surfaces of the model can also be compared to data from wind tunnel experiments. Figure 3.21 shows the pressure distribution on the top surfaces of the model both for CFD simulations and wind tunnel experiments. The pressure peak on the frontal edges is well captured by the RANS simulations. The pressure recovery in the simulations shows a slight offset in pressure coefficient with the experiments. In Figure 3.22 it is seen that the trend of the simulated pressure coefficient on the rear surface of the model and the measured values are not very similar, the order of magnitude however, is similar. The differences between the simulated wake and the measure wake are also seen in Figure 3.23.

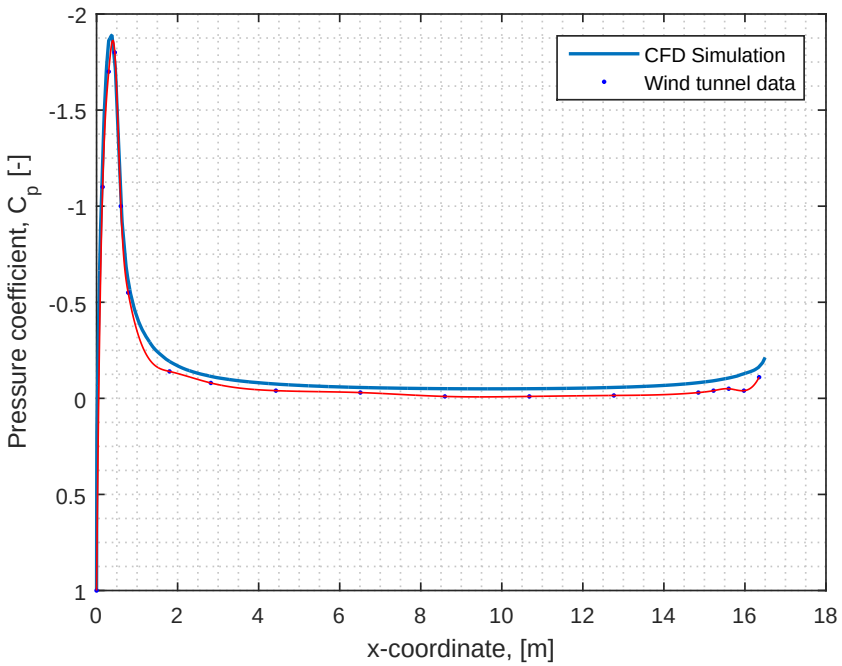

Figure 3.21: Pressure coefficient distribution over the top surfaces of the model for CFD simulations and experiments [15].

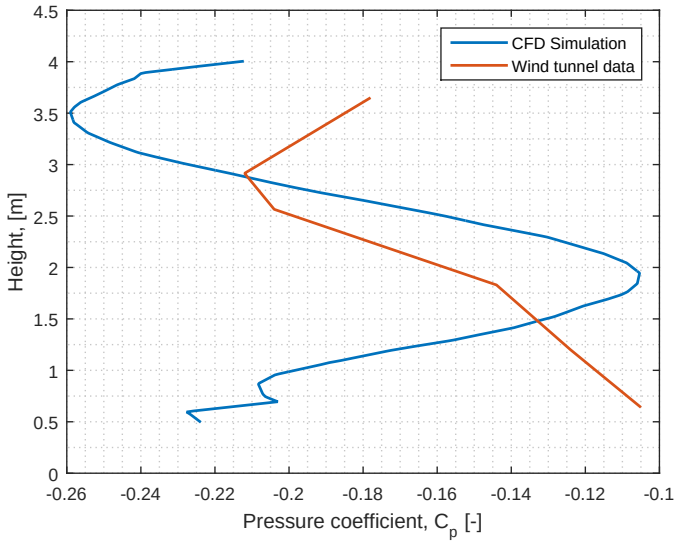

Figure 3.22: Pressure coefficient distribution over the rear surface of the model for CFD simulations and experiments [15].

Using Particle Image Velocimetry (PIV), visualisations of the flow field were made and characteristics of the wake can be studied. These characteristics can be compared to those computed by the simulations. The comparison is shown in Figure 3.23. There are substantial differences between the simulated wake and the wake from the wind tunnel experiments. The vertical size and location of the lower vortex is highly overestimated by the simulations. The dimensions of both vortices in x-direction are also overestimated by the CFD simulations. In reality, this wake structure is highly unsteady and characterised by a large turbulence intensity. Nonetheless, a steady RANS solver is used to simulate the flow, only modelling the effects of turbulence on the mean flow and not computing the turbulence itself. This causes the differences between the simulated and measured wake structures.

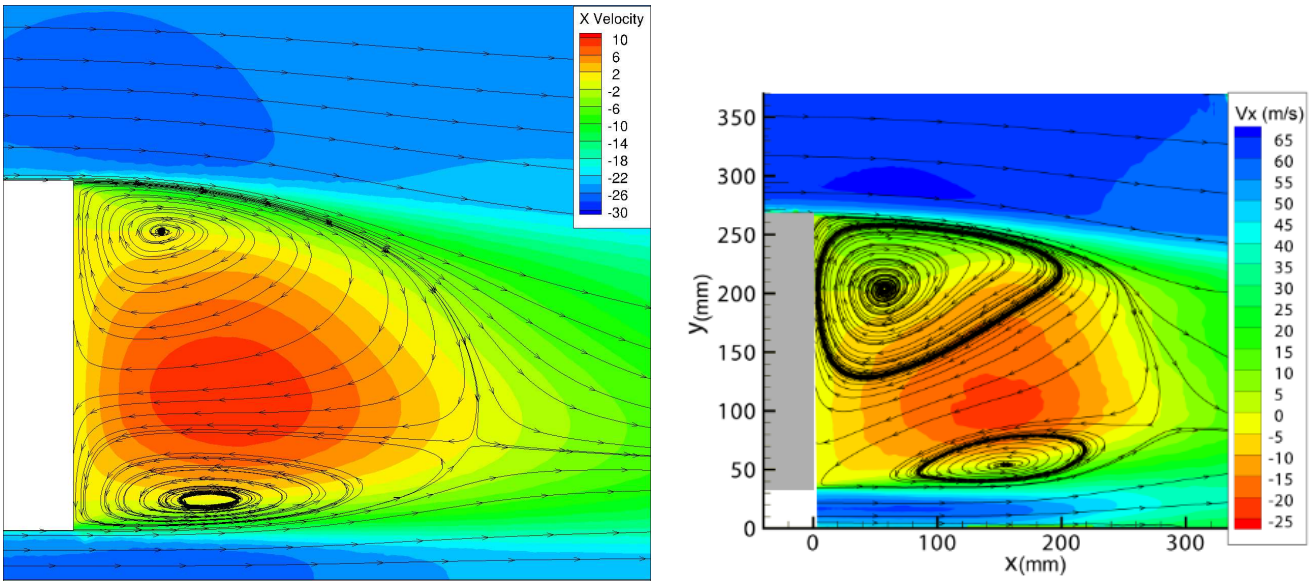

(a) CFD simulations

(b) Wind tunnel experiments

Figure 3.23: Comparison of the wake structures of a model with a frontal edge radius of 0.54 m between the CFD simulations and wind tunnel experiments.

3.6 Summary of the isolated GETS results

The analysis of the GETS model in isolation showed that the frontal edge radius influences the flow behaviour largely. The amount of suction force generated by these edges greatly determines the drag of the vehicle as well as the relative drag contribution of the front part. For the radii of 0.54 m and 0.27 m, the large suction force decreased the drag of the front part of the vehicle significantly such that the drag contribution of the front part was lower than 15% of the total drag while the pressure drag at the rear delivered around 70% of the drag. If the frontal edge radius was halved, the drag contributions of the front and rear part of the vehicle were almost equal, about 45% of the total drag. The total drag also increased largely when the edge radius was lowered. This was mainly due to the fact that the frontal edges were only a small portion of the total frontal surface. With decreasing radii, the stagnation surface became larger. For the smallest edge radius, flow separation occurred. The vehicle with the smallest frontal edge radius also best resembled the drag contributions of a real heavy-duty vehicle.

The addition of tails proved to increase the base pressure of the vehicles significantly. Adding a tail of 0° made the base pressure distribution more constant, increasing the tail angle, increased the base pressure and therefore reduced the drag until the drag contribution of the rear surface was almost zero or even slightly negative for some cases, i.e. a thrust force. Due to the inward deflected tails, the flow in the near-wake was redirected upward and the size of the wake was decreased. Adding a cross wind component to the incoming flow resulted in an increase in drag and a resulting side force. Making the geometries more streamlined by

adding tails or by increasing the frontal edge radius made the drag force less sensitive to yaw angles. The side force on the vehicles was slightly increased by increasing the frontal edge radius, but the addition of tails decreased this side force significantly. The vehicles in cross wind acted like airfoils and redirected the flow in the near wake towards the windward side.

The drag coefficient for all variations of the GETS geometry in cross wind conditions are shown in Figure 3.24. It is seen that increasing the frontal edge radius and adding a tail and increasing its angle decreases the drag coefficient largely. These values will be used to normalise the drag coefficient of the corresponding vehicles in the platoon configurations. The drag coefficients of all the discussed geometry variations can also be found in Table A.1 in Appendix A.

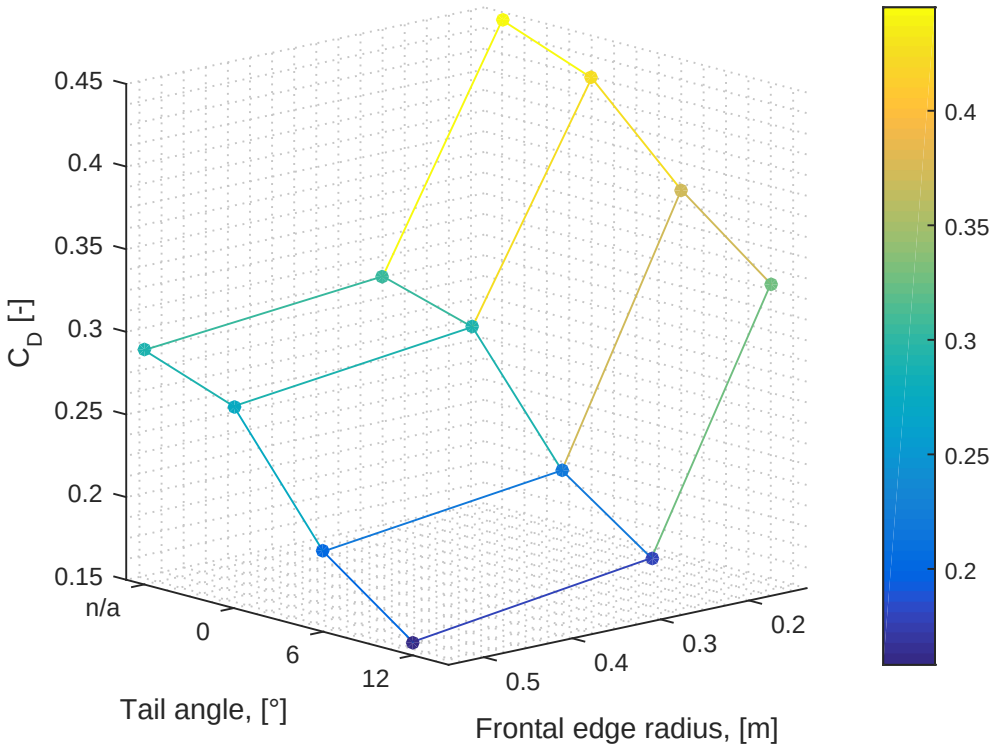

Figure 3.24: Drag coefficients for all variations of the GETS geometry. The yaw angle is 3°.

With the baseline configurations established and validated, platoon configurations are set up and simulated. The results of these simulations can be found in Chapter 4.

Chapter 4

Analysis of the Platoon Configurations

This chapter contains the results of all simulated platoon configurations. All the platoon configurations are divided in three sections. Section 4.1 starts with the most basic platoon, where the vehicles have no tails. Next, a tail is added to the last vehicle of the platoon in section 4.2 and finally all vehicles are equipped with various tails in section 4.3.

In order to avoid excessive nomenclature for platoon configurations, the name of every configuration exists of three letters. An 'n' means that the vehicle has no tail, a 'tX' means that the vehicle has a tail of X degrees. As example: 'nnt12' means that the first two vehicles have not tail, while the last vehicle has a tail of 12°.

4.1 Platoon configuration 'nnn'

The first platoon that is simulated is the most basic one, three vehicles without tails are lined up for three different inter-vehicle distances, two yaw angles and three leading edge radii. This section shows the effects of the different variables, i.e. inter-vehicle distance, frontal edge radius and yaw angle, and explains the differences between the different positions in the platoon formation.

4.1.1 Effect of inter-vehicle distance

The most important variable when studying platoons is the distance between the vehicles. The inter-vehicle distance is defined as the absolute length between the vehicles divided by the vehicle length. The effect of the inter-vehicle distance on both the individual drag coefficients and the average platoon drag coefficient is shown in Figure 4.1. The drag coefficients are scaled using the drag coefficient of a vehicle in isolation, C_{D_p} stands for the drag coefficient

in the platoon while C_{D_i} stands for the drag coefficient in isolation. To be able to compare the results better to results from literature, this configuration was also simulated at an even closer distance as mentioned before. Since the flow field around a model with a frontal edge radius of 0.27 m is similar to that around the model with a radius of 0.54 m, the model with the radius of 0.27 m will be considered as the basic model from now on.

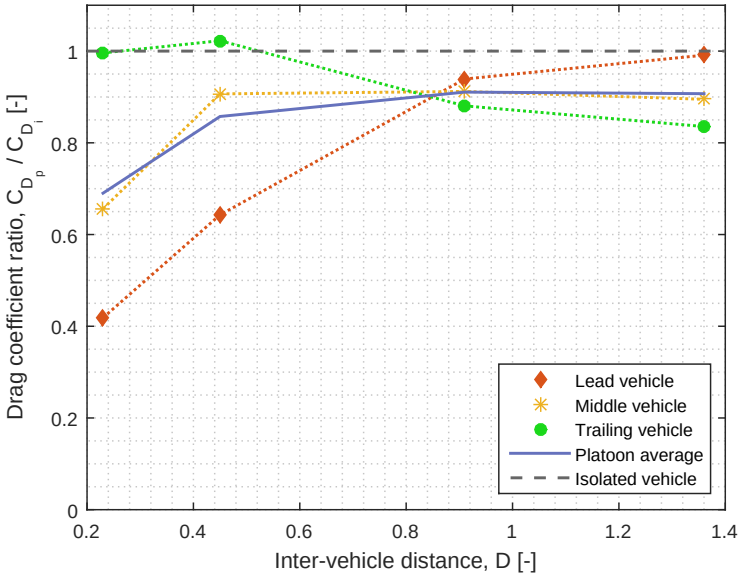

Figure 4.1: Effect of the inter-vehicle distance on the drag coefficient of the models and the entire platoon. The frontal edge radius is 0.27 m.

It is observed that the drag coefficients of the lead and trailing vehicle show opposite behaviour. At very close spacing, the lead vehicle benefits largely from the platoon, the drag coefficient is decreased by almost 60%. This is more than the other vehicles. When the distance is increased, the drag of the lead vehicle increases to the value in isolation in an asymptotic way until it is not influenced anymore by the following vehicles. For the largest distance, the trailing vehicle experiences a drag reduction of almost 20%. When the spacing is getting closer, the drag actually rises up to a value above that in isolation, before it starts to decrease again for the smallest distance. Rajamani [24] also observed, for two Ahmed models, the drag of the trailing vehicle going up when the inter-vehicle distance decreases. After a certain point, the drag started to decrease again for lower distances. Another study showed that the relative drag coefficient of the trailing vehicle can even increase up to 1.4 before decreasing again after passing a critical spacing between 0.3 and 0.4 vehicle length [23]. This study also indicates that this critical inter-vehicle distance lies between 0.23 and 0.45. This critical vehicle length could depend on the size of the wake. For a vehicle length of 0.45, the trailing vehicle is positioned just outside the near wake of the vehicle in front and the drag is still above the value of isolation. When the trailing vehicle is positioned inside the near wake of the vehicle in front, the drag decreases again. This is however not investigated further since more simulations between the distance of 0.23 and 0.45 would be needed in order to map the maximum drag coefficient and relate the corresponding distance to the size of the wake. The effects of both lead and trailing vehicle are combined for the middle vehicle. The drag of the middle vehicle lies very close to the platoon averaged drag. The middle vehicle always

benefits from the platoon formation. For inter-vehicle distances between 0.45 and 1.36, it remains almost constant at about 90%, at the closest spacing, it experiences a steep drop in drag coefficient to about 65% of the value in isolation.

The different drag behaviour of the three vehicles can be explained by looking at the different drag contributions of the three vehicles. In Figure 4.2, the drag coefficient is split up over three different parts of the model: the front, side and rear surface.

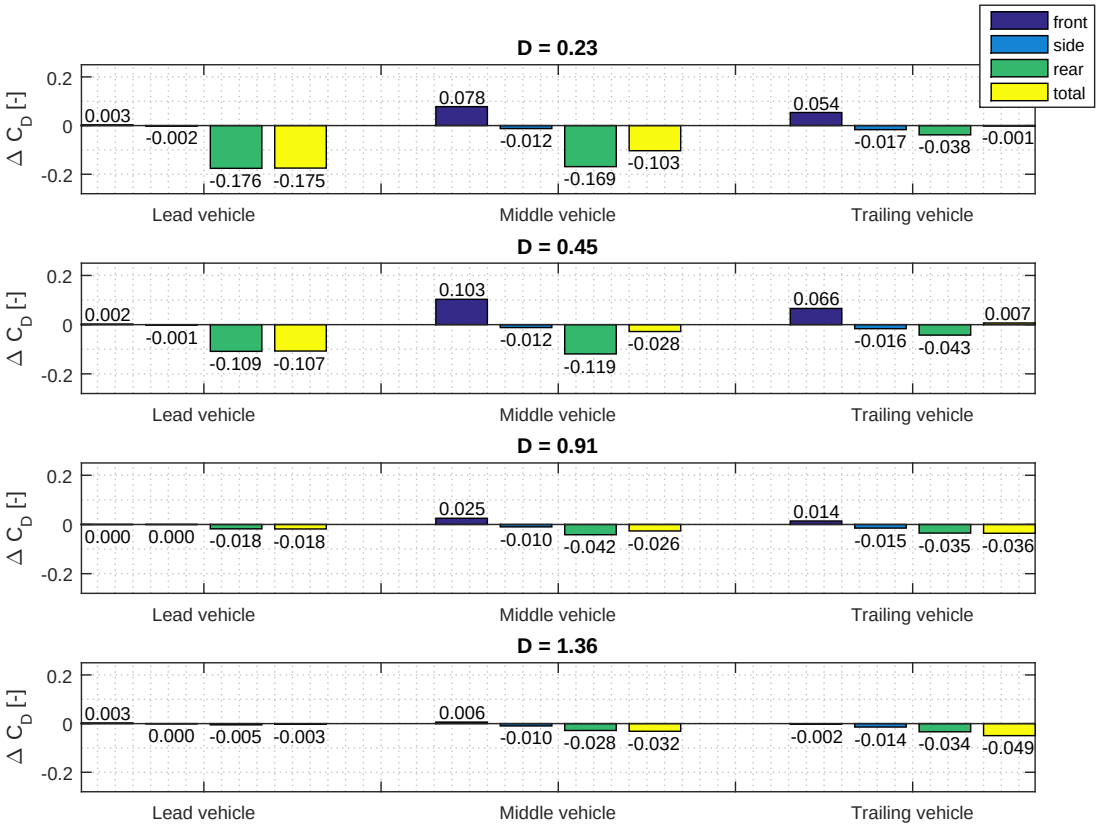

Figure 4.2: Effect of the inter-vehicle distance on the drag contributions experienced by the vehicles with a frontal edge radius of 0.27 m.

The middle and trailing vehicle are influenced by the presence of a vehicle in front. It was seen before in the analysis of vehicles in isolation that the frontal edges produce a suction force that counteracts with the drag of to the stagnation pressure at the frontal surface. The interaction of the front surfaces with a vehicle in front works in two ways. On one hand, the low-pressure wake of the leading vehicle decreases the high stagnation pressure at the front of a following vehicle. On the other hand, the suction force is also decreased significantly. This is due to the decreased flow velocity over the frontal edges and due to the fact that the flow is deflected inwards after the lead vehicle. When the flow then turns to go around the second vehicle, the flow first follows a concave trajectory that increases the pressure on the frontal edges. The latter effect proves to be dominant as the drag of the entire front part increases significantly.

This effect can also be visualised by plotting the pressure coefficient distribution over the top side of the vehicles. Figure 4.3 shows the pressure distribution over the three vehicles in the platoon configuration at the closest inter-vehicle distance. While the pressure peak on the lead vehicle remains unaltered, the middle and trailing vehicle experience a pressure peak that is a lot less negative than in isolation. Figure 4.4 shows the difference between the pressure coefficient on the lead vehicle and on the middle vehicle. This difference is thus defined as follows

$$\Delta C_p = C_{p_{LV}} - C_{p_{MV}} \tag{4.1}$$

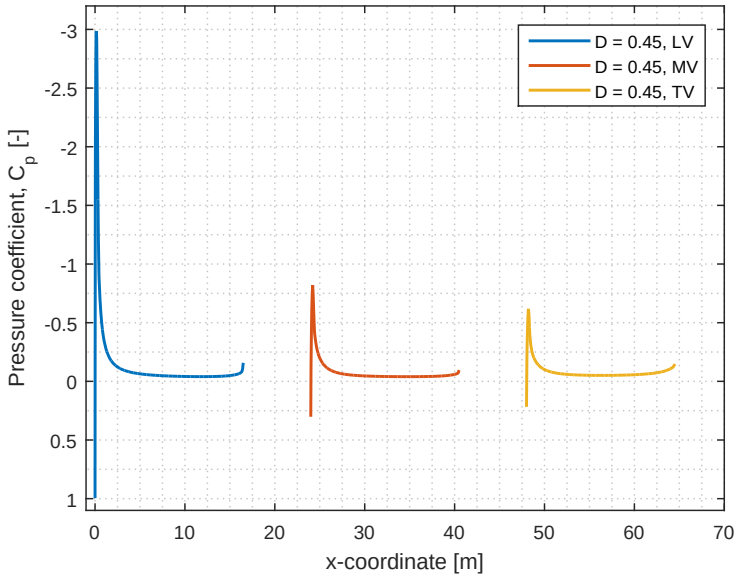

Figure 4.3: Effect of the position in the platoon on the pressure coefficient distribution over the top of the vehicles for an inter-vehicle distance $D = 0.45$ and a frontal edge radius $R = 0.27$ m.

By decreasing the inter-vehicle distance, the stagnation pressure on the frontal surface drops significantly. On the frontal edges, the opposite behaviour is seen: the pressure increases drastically for closer spacings. These two effects thus counteract each other. In Figure 4.2 it is seen that for the distances down to 0.45, the lowering of the negative pressure peaks on the frontal edges is the more dominant effect, leading to a increase in drag on the front part of the vehicle. For the smallest inter-vehicle distance, the loss in stagnation pressure is dominant, which gives a decrease in front drag.

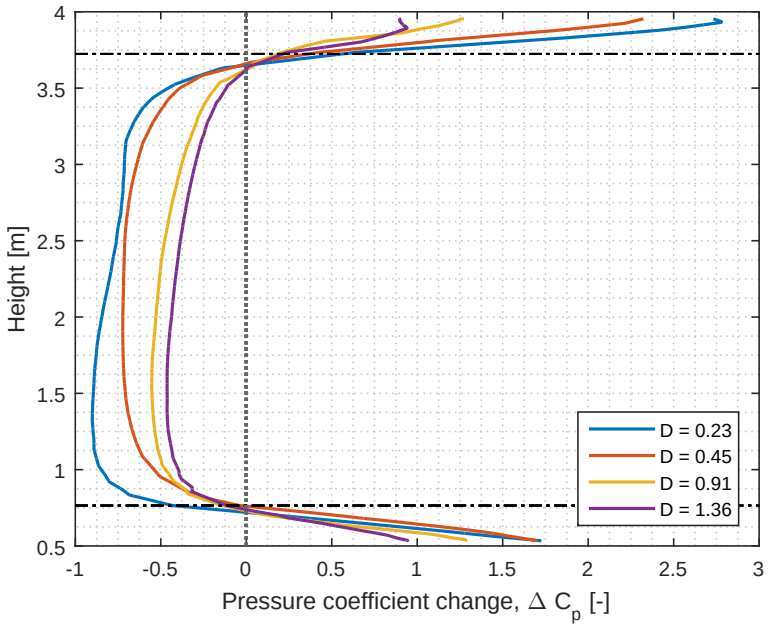

Figure 4.4: Effect of the inter-vehicle distance on the pressure coefficient distribution on the frontal surfaces of the middle vehicle with a frontal edge radius $R = 0.27$ m. The dash dotted lines represent the boundaries between the frontal edges and the frontal stagnation surface.

The drag reductions of the lead vehicle are due to the presence of a following vehicle. The pressure drag at the rear of the lead vehicle is reduced due to the increase in base pressure in the presence of a following vehicle. The effect of a following vehicle on the base pressure is shown by plotting the pressure coefficient distributions. This can be found in Figure 4.5 and Figure 4.6. Figure 4.5 shows the effect of the inter-vehicle distance on the base pressure distribution. The lead and middle vehicle experience a high pressure increase for the smallest distance, for the middle distance the increase in pressure is limited. For the trailing vehicle, nothing much changes besides the shape of the distribution for the closest spacing. Figure 4.6 shows the difference between the tree vehicles in the platoon for different distances. Remarkable is that the trailing vehicle also experience an increase in base pressure. This increase in base pressure is even higher than that on the lead vehicle for the larger inter-vehicle distances as seen in Figure 4.6(b) and Figure 4.6(c).

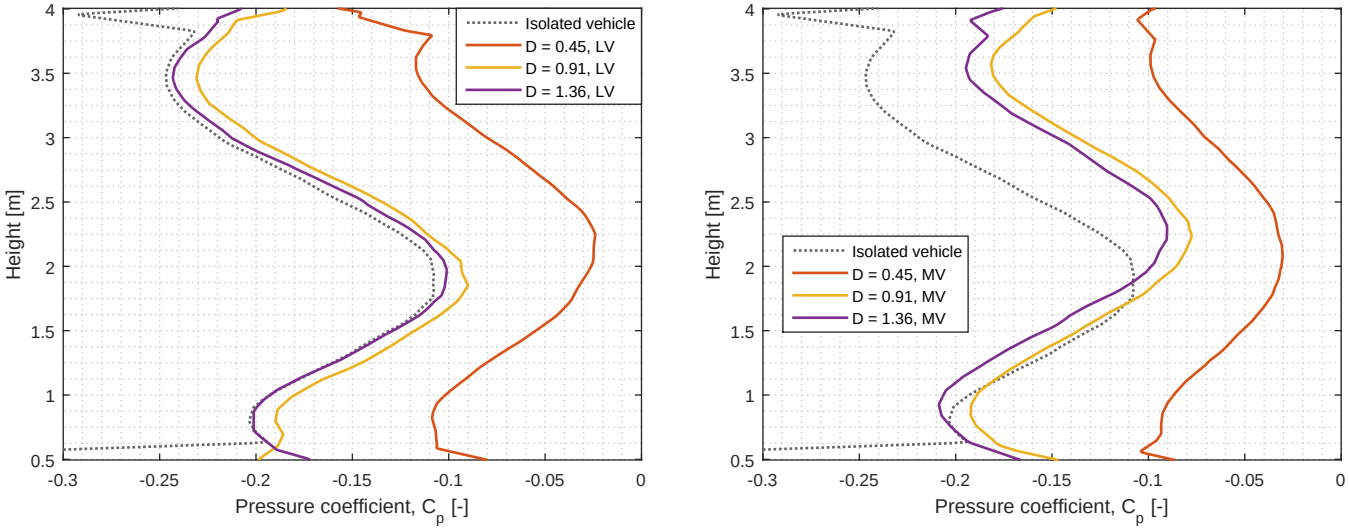

(a) Lead vehicle

(b) Middle vehicle

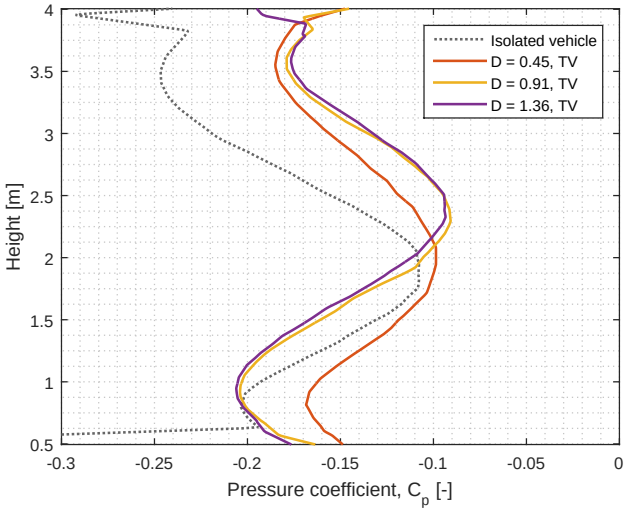

(c) Trailing vehicle

Figure 4.5: Effect of inter-vehicle distance on the pressure coefficient distribution over the top of the vehicles, with a frontal edge radius of 0.27 m.

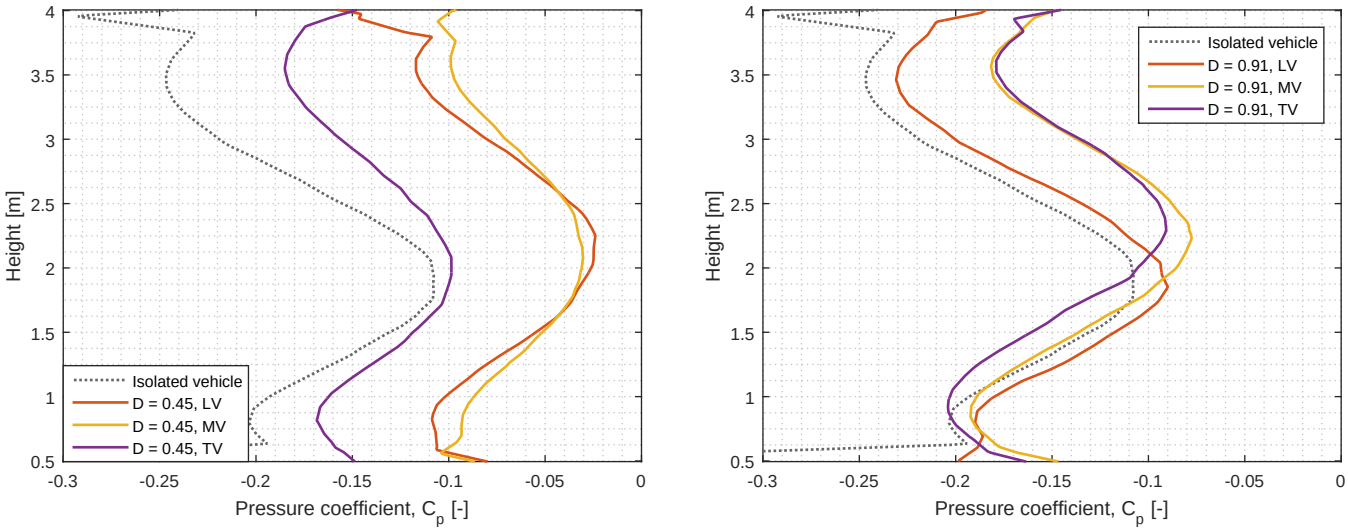

(a) $D = 0.45$

(b) $D = 0.91$

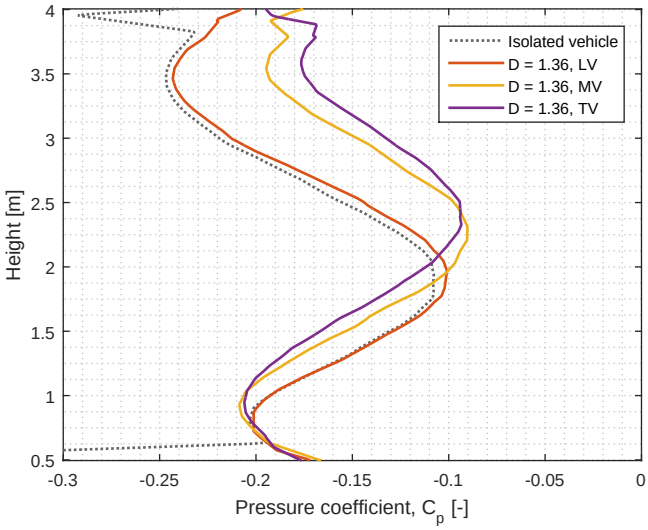

(c) $D = 1.36$

Figure 4.6: Effect of the position in the platoon on the pressure coefficient distribution over the top of vehicles, with a frontal edge radius of 0.27 m, for different inter-vehicle distances.

It was noticed that the trailing vehicle also experiences a decrease in pressure drag at the rear surface, this drag reduction is however less dependent on the inter-vehicle distance than for the other vehicles. For the first two vehicles, this drag reduction at the rear is caused by the presence of a following vehicle in the wake. This is however not the case for the trailing vehicle, another explanation is found for the drag reduction at the rear surface of the trailing vehicle.

In Figure 4.2, it was shown that the decrease in drag becomes less for larger inter-vehicle distances. Besides the drag on the rear surface, the drag of the front and side surfaces of the trailing vehicle is also decreased slightly, compared to the middle vehicle. This could both be due to the fact that the incoming flow field for the following vehicles differs from the flow field that is experienced by the leading vehicle. The effect of the position in the platoon on the incoming flow, experienced by the vehicles, is shown in Figure 4.7, while Figure 4.8 shows the total pressure coefficient at half the vehicle length. This coefficient is obtained by normalising the total pressure with the total pressure in the freestream. These figures explain why even the trailing vehicle experiences a decrease in drag at the rear surface. The following vehicles experience a flow field that has a lower dynamic pressure and a lower total pressure. This causes the drag of the different vehicles parts (except the front) to decrease. The effect is most significant for the trailing vehicle, since this is located in the wake of two vehicles.

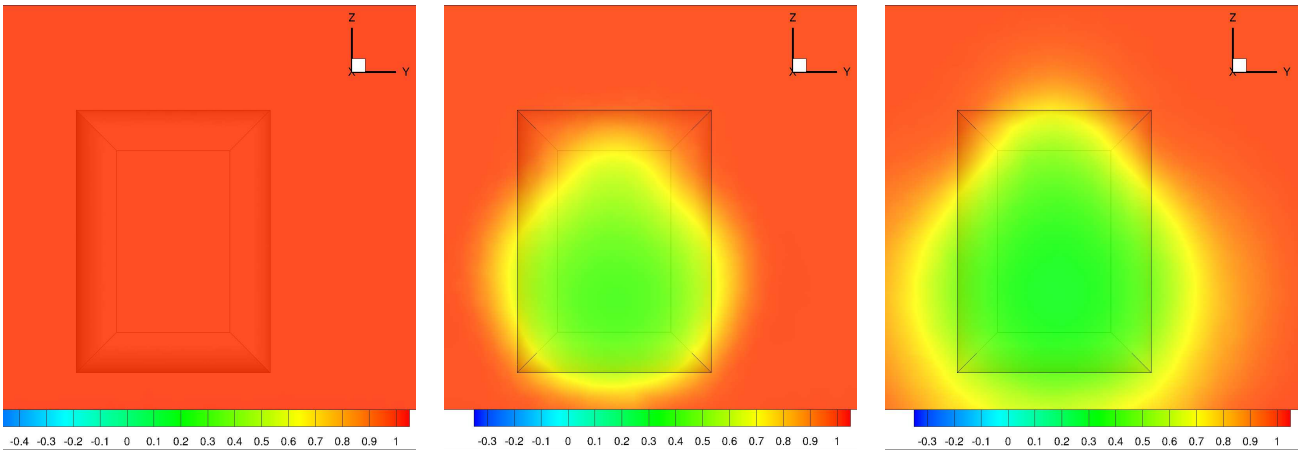

(a) Lead vehicle (b) Middle vehicle (c) Trailing vehicle

Figure 4.7: Contour of the total pressure coefficient at a distance of 2 m in front of the vehicle. The vehicles belong the the platoon formation with an inter-vehicle distance of 0.91 and frontal edge radii of 0.54 m.

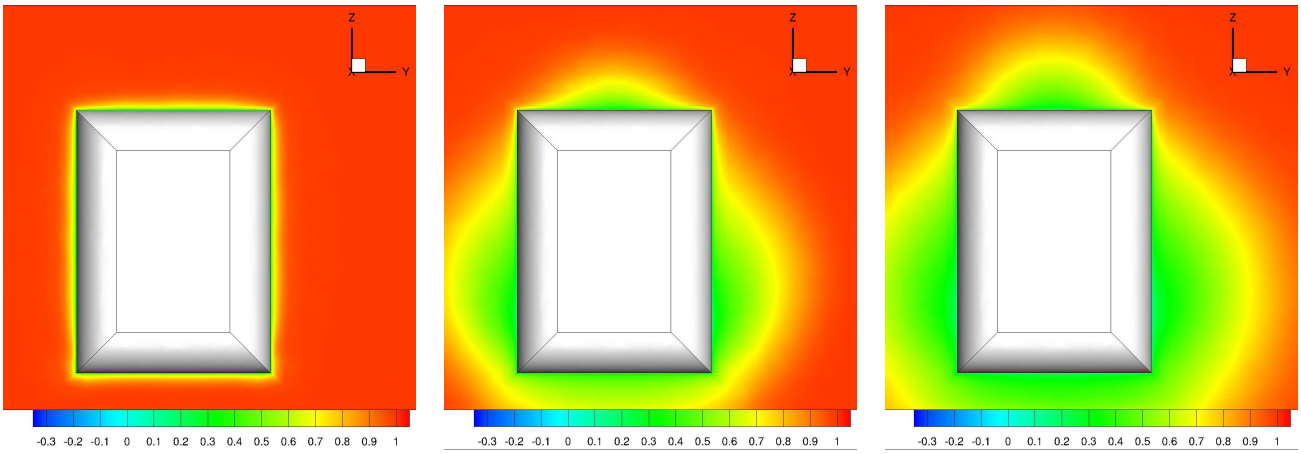

(a) Lead vehicle (b) Middle vehicle (c) Trailing vehicle

Figure 4.8: Contour of the total pressure coefficient halfway of the vehicle. The vehicles belong the the platoon formation with an inter-vehicle distance of 0.91 and frontal edge radii of 0.54 m.

It can be stated that, for a frontal edge radius of 0.27 m, driving in front of a vehicle reduces the pressure drag at the rear surface and driving behind a vehicle increases the drag on the front surfaces. The middle vehicle experiences both the effects of a leading and a trailing vehicle. Despite the increase in drag due to the front surfaces, the total drag of the middle vehicle however is thus still reduced due to the presence of the trailing vehicle in its wake. With increasing distance, both effects diminish.

Considering the flow field around the vehicles, some differences occur between the case for an inter-vehicle distance of 0.45 on one hand and the cases with an inter-vehicle distance of 0.91 and 1.36. This difference can be seen in Figure 4.9. It is seen that for the closest distance, a vortical structure occurs in front of the frontal surface. This recirculation region in front of the following vehicle increases the complexity of the flow around the platoon, while for the larger distances there is no direct interaction between the near-wake of the proceeding vehicle and the stagnation region of the following vehicle.

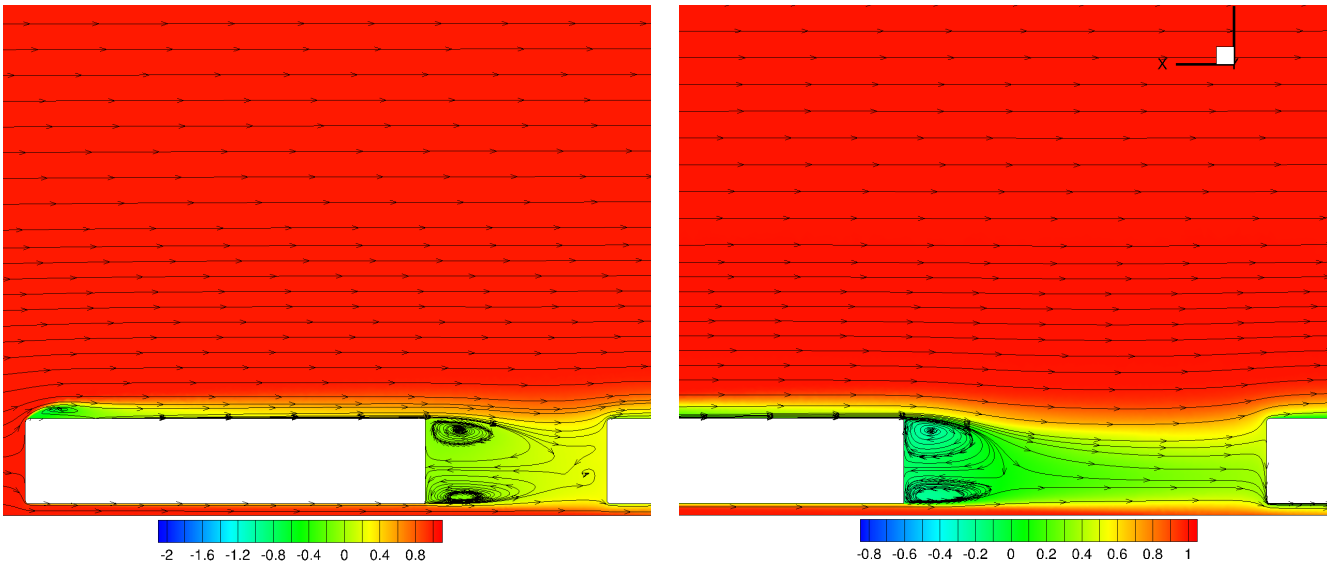

(a) $D = 0.45$ (b) $D = 0.91$

Figure 4.9: Contour of the total pressure coefficient with the streamlines in the $y = 0$ plane. The vehicles belong to the platoon formation with an inter-vehicle distance of 0.45 and frontal edge radii of 0.27 m.

4.1.2 Effect of frontal edge radius

The effect of the frontal edge radius is already discussed in section 3.2. Decreasing the frontal edge radius to 0.135 m increased the front drag of the vehicle significantly and flow separation occurred on the frontal edges. Increasing the radius to 0.54 m did reduce the drag slightly, but no significant changes to the flow field were observed. The analysis, presented above, can be done for a platoon where the models have a frontal edge radius of 0.54 m and 0.135 m. It can be seen that besides the decreased drag coefficient due to the more rounded front surfaces, increasing the radius does not affect the phenomena that occur while driving in a platoon, as can be seen in Figure 4.10(a). Decreasing the radius to 0.135 m however, changes the effectiveness of the platoon significantly. This is seen in Figure 4.10(b).

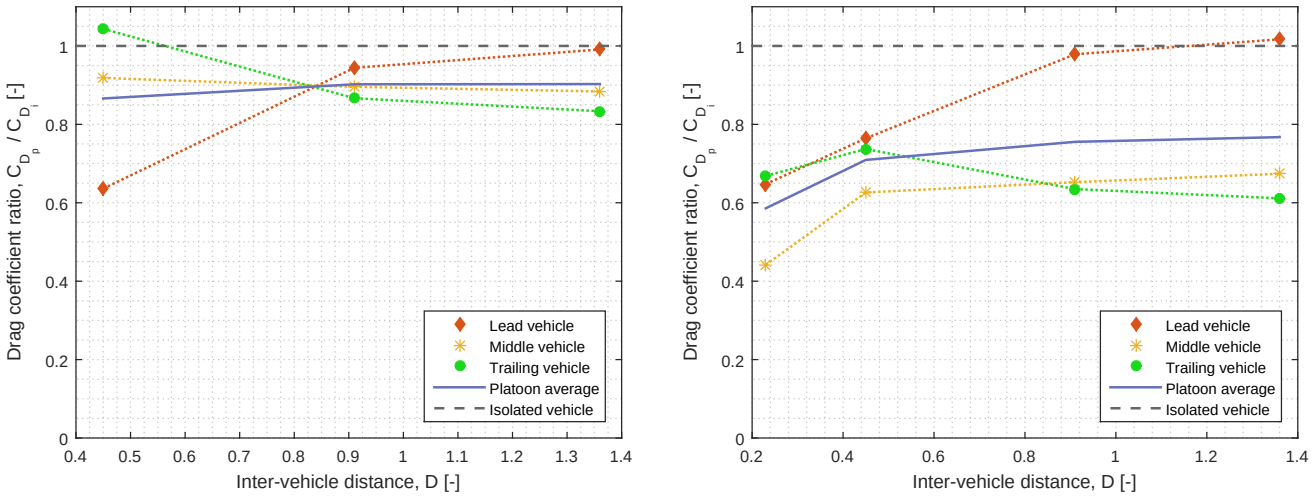

(a) $R = 0.54$ m (b) $R = 0.135$ m

Figure 4.10: Effect of the inter-vehicle distance on the drag coefficient of the models and the entire platoon for two different frontal edge radii.

The trend of the drag of the lead vehicle remained unchanged for the lowest radius, but the relative drag reductions are less than for the larger frontal edge radii. This is due to the fact that if the front of the vehicle is less streamlined, i.e. a lower frontal edge radius, the pressure drag at the rear represents a smaller portion of the total drag. When this pressure drag is then decreased due to the presence of a following vehicle, it has a smaller impact on the total drag decrease. The same is seen for the middle vehicle, the trend did not change but the relative drag reductions become higher for a smaller frontal edge radius. The middle vehicle now becomes the most benefiting vehicle in the platoon, except for a small difference with the trailing vehicle at the largest spacings. The trailing vehicle no longer experiences a relative drag coefficient higher than that in isolation. It is seen that the point at which the drag values of the trailing vehicle and lead vehicle cross each other is shifted towards a larger inter-vehicle distance

The different drag contributions for the configuration with a radius of 0.135 m can be seen in Figure 4.11. Unlike for the configuration with larger radii, the front part of the vehicles now experience a drag reduction due to the platooning effect. This is due to the fact that the front surfaces generating the negative pressure peak are a smaller portion of the total frontal surface and the fact that the flow does not separate on the following vehicles, like on the leading vehicle. Due to the presence of the wake of the lead vehicle and the lower dynamic pressure, the pressure decrease on the frontal edges of the middle vehicle is less pronounced. This leads to a lower adverse pressure gradient and thus no flow separation takes place. This is shown in Figure 4.12 for two different inter-vehicle distances.

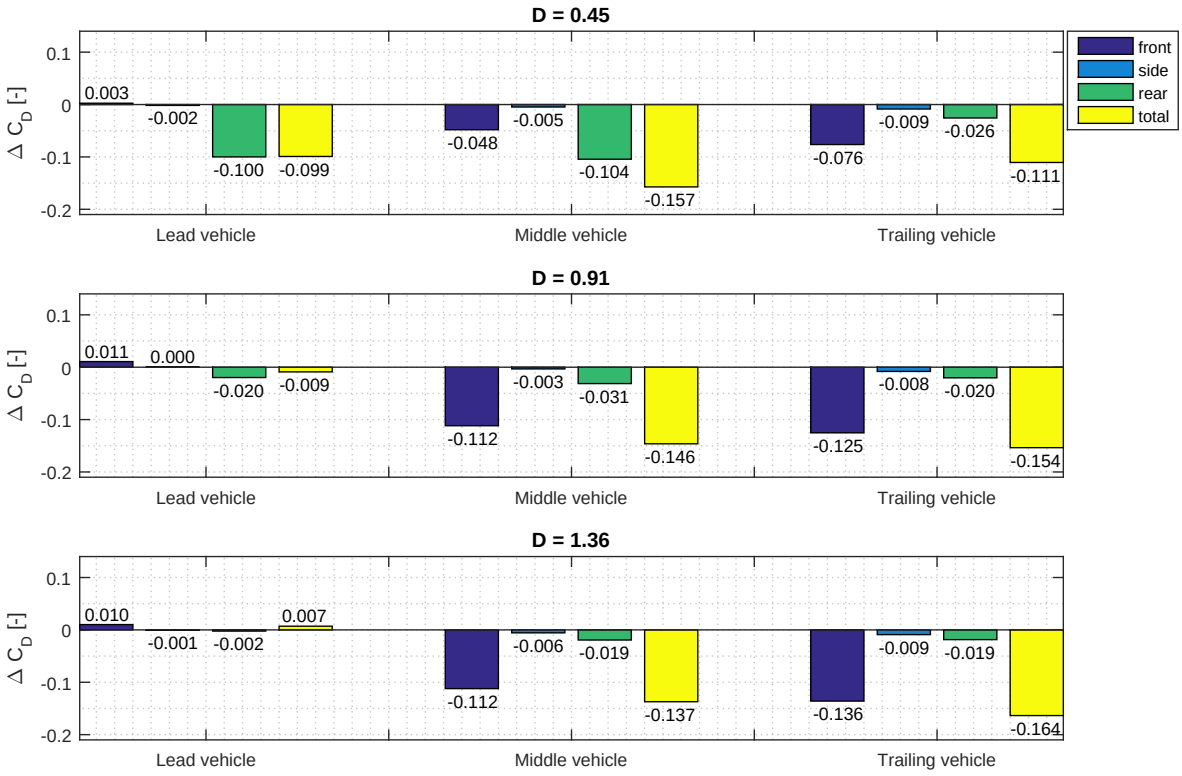

Figure 4.11: Effect of the inter-vehicle distance on the drag contributions experienced by the vehicles with a frontal edge radius of 0.135 m.

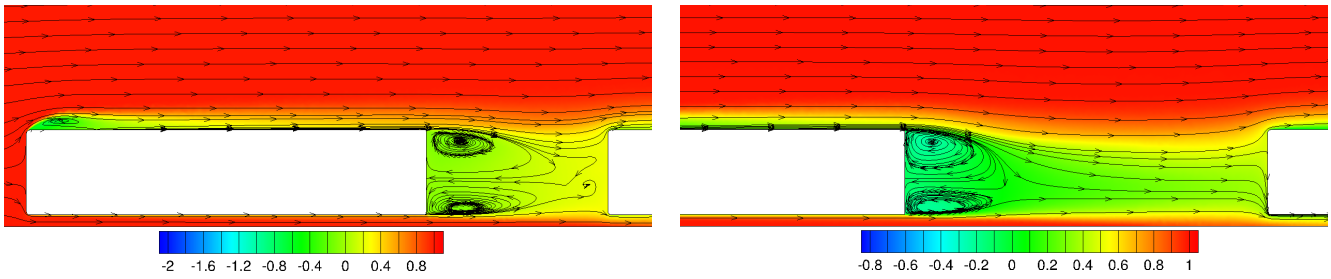

(a) $D = 0.45$ (b) $D = 0.91$

Figure 4.12: Contour of the total pressure coefficient with the streamlines around the lead and middle vehicle in the $y = 0$ plane.

4.1.3 Effect of yaw angle

In this section, the effect of a yaw angle on the platooning vehicles is described as well as what a platoon does with the individual vehicles' response to cross wind. Figure 4.13 shows what happens to the drag reductions from driving in a platoon when a cross wind component is added. The change in drag coefficient, ΔC_D, due to platooning is shown for the two yaw angles. This drag coefficient change is still the drag coefficient of the vehicle in the platoon, subtracted by the value in isolation. The cross wind does not have a drastic effect on the drag reductions in a platoon.

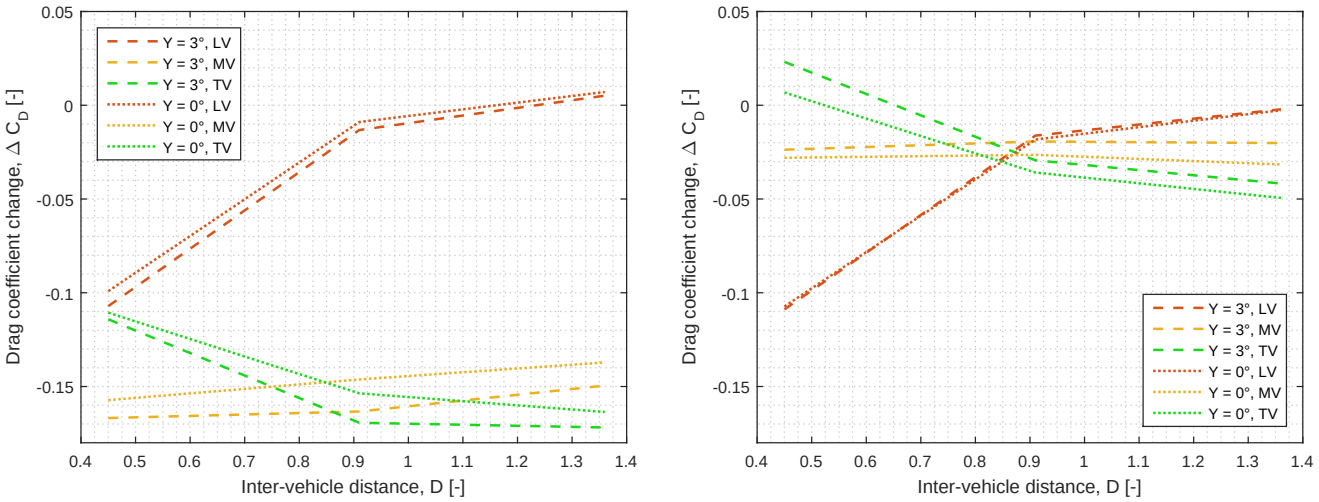

(a) $R = 0.135$ m

(b) $R = 0.27$ m

Figure 4.13: Effect of the yaw angle on the drag reductions of the different vehicles in a platoon. The reference drag coefficient is the drag coefficient of the corresponding vehicle in isolation.

The yaw angle mainly affects the drag reductions of the middle and trailing vehicle. For the largest frontal edge radii, the yaw angle has a negative influence on the drag reductions. The drag reductions decrease for a case with cross wind. If the vehicles have a frontal edge radius of 0.135 m, the drag reductions are increased in a cross wind condition. The drag reduction per vehicle part for the two yaw angles is shown in Figure 4.14. It is seen that the yaw angle has a different effect on the different parts of the vehicles. Due to the yaw angle, the drag reductions at the rear part increase, while those at the front part are reduced. Figure 3.13 in section 3.4 showed that for the vehicle with the lowest radius, the rear part was more affected by the cross wind then for the vehicles with larger frontal edge radii. Therefore, for the vehicles with the lowest frontal edge radius, the increase in drag reductions at the rear part is dominant over the decrease in drag reductions at the front part. For the vehicles with the larger frontal edge radius, this is reversed.

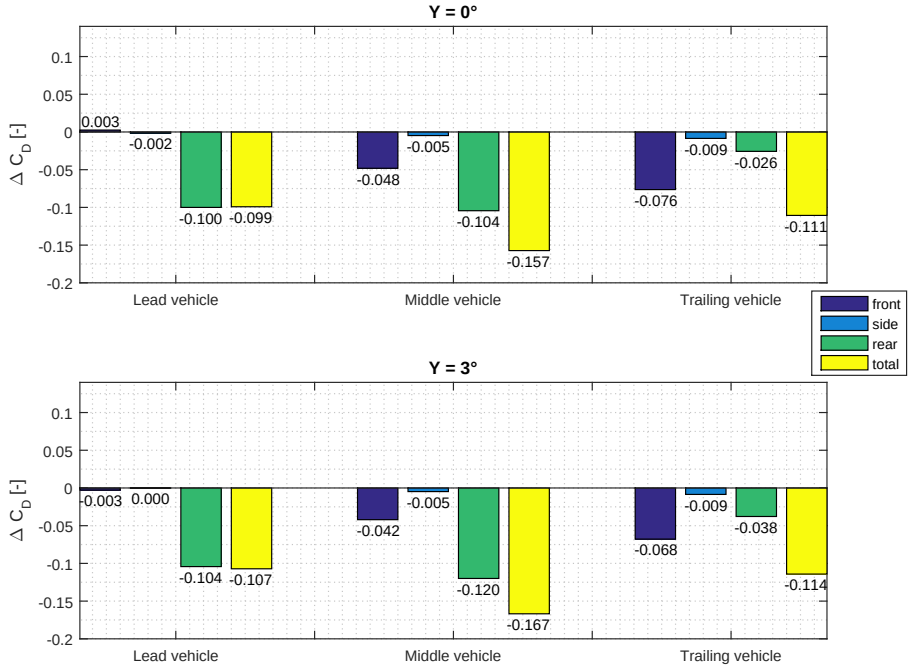

(a) $R = 0.135$ m

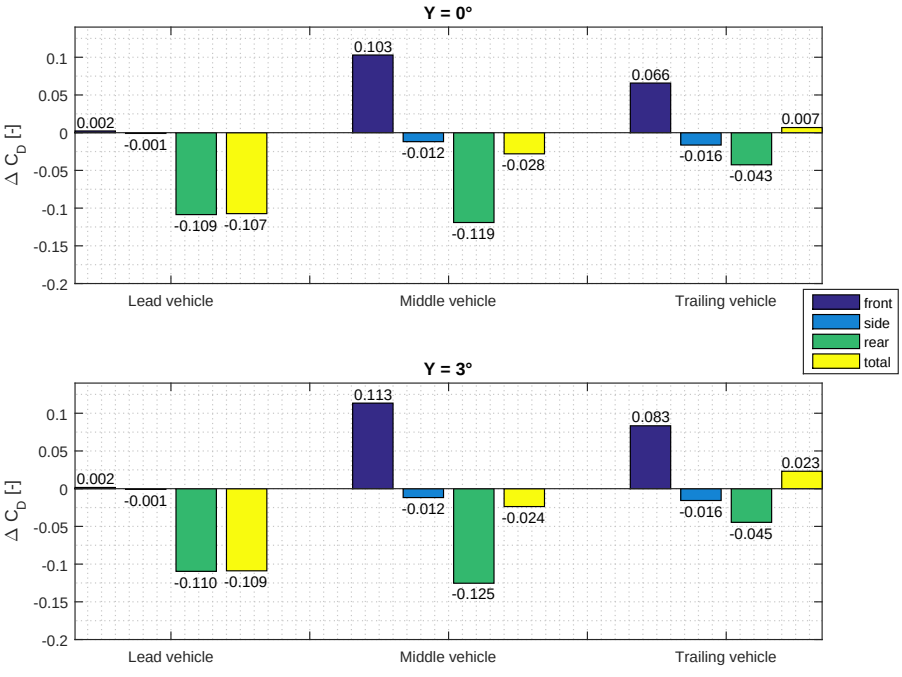

(b) $R = 0.27$ m

Figure 4.14: Effect of the yaw angle on the drag contributions of the different vehicles in a platoon for an inter-vehicle distance of 0.45. The reference drag coefficient is the drag coefficient of the corresponding vehicle in isolation.

Cross wind has been studied in a platoon that was yawed ten degrees with respect to the wind tunnel axis by Marcu and Browand [29]. They found that the drag reductions gained by platooning are still present under side wind conditions. The average platoon drag coefficient was approximately 61% of that of a yawed vehicle in isolation. The platoon drag coefficient for a zero yaw condition was only 58% of the value in isolation (zero yaw). The models used in this study were models of passenger cars. They can thus be seen as more streamlined models than the GETS model with a radius of 0.135 m. In this study, it was also seen that the lead vehicle redirects the incoming flow such that the following vehicles experience less cross wind [29]. This could lead to the statement that the drag reductions in a platoon increase due to a yaw angle, however it is seen that it is the other way around. This is due to the higher drag increase of the front part of the vehicle when cross wind is considered. This will be explained in following paragraphs.

Besides investigating the effect of a yaw angle on the drag reductions in a platoon, one can investigate the effect of driving in a platoon on the drag increase due to a yaw angle. As seen in section 3.4, the addition of a non-zero yaw angle (i.e. adding cross wind) increases the drag. Lining up vehicles in a platoon makes this effect more complicated. The change in drag coefficient due to a yaw angle of $Y = 3°$ can be seen in Figure 4.15 and Figure 4.16. For the larger radii, almost the entire drag increase due to yaw angles comes from the front surfaces for the middle and trailing vehicle. In the configuration of the vehicles with the lowest radius, the drag contribution of the rear part compensates this extra drag increase of the front part.

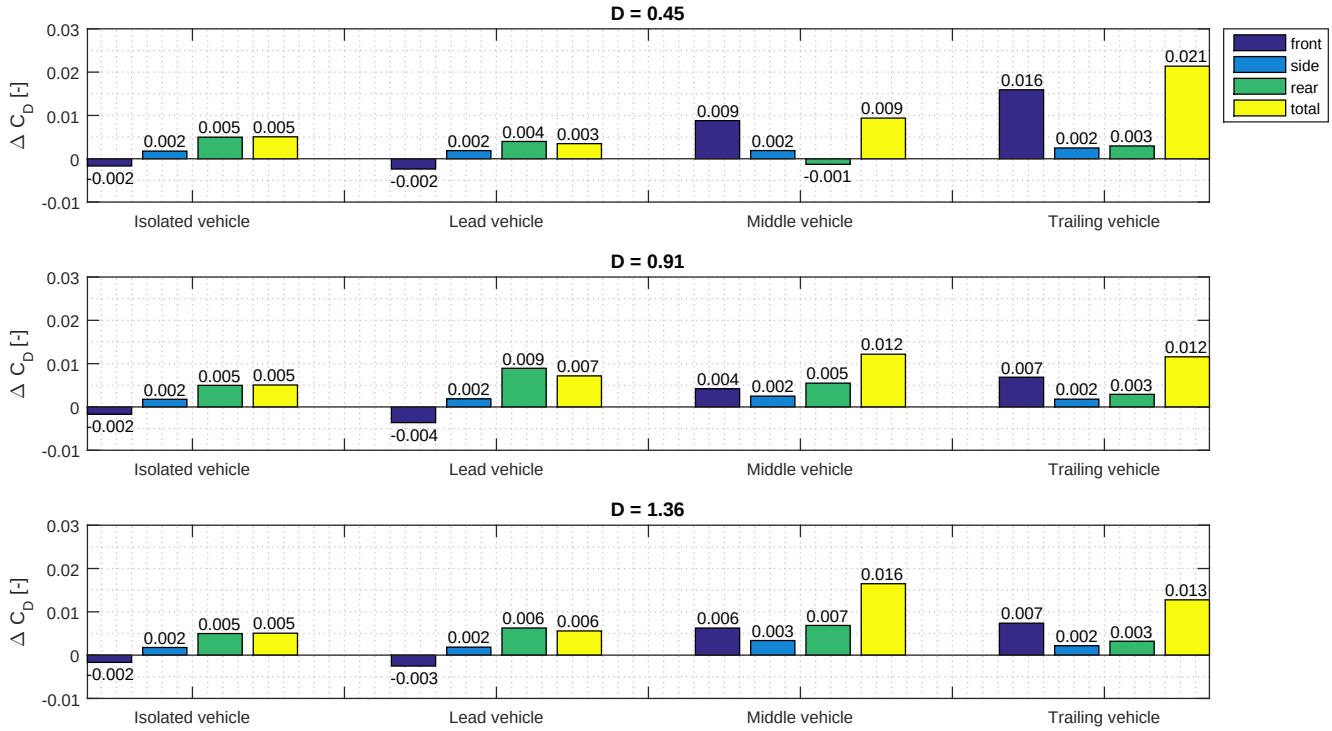

Figure 4.15: Effect of the inter-vehicle distance and the position in the platoon on the drag changes due to a yaw angle of 3°. The reference drag coefficient is the one from the same vehicle in the same platoon without cross wind. The frontal edge radius is 0.27 m.

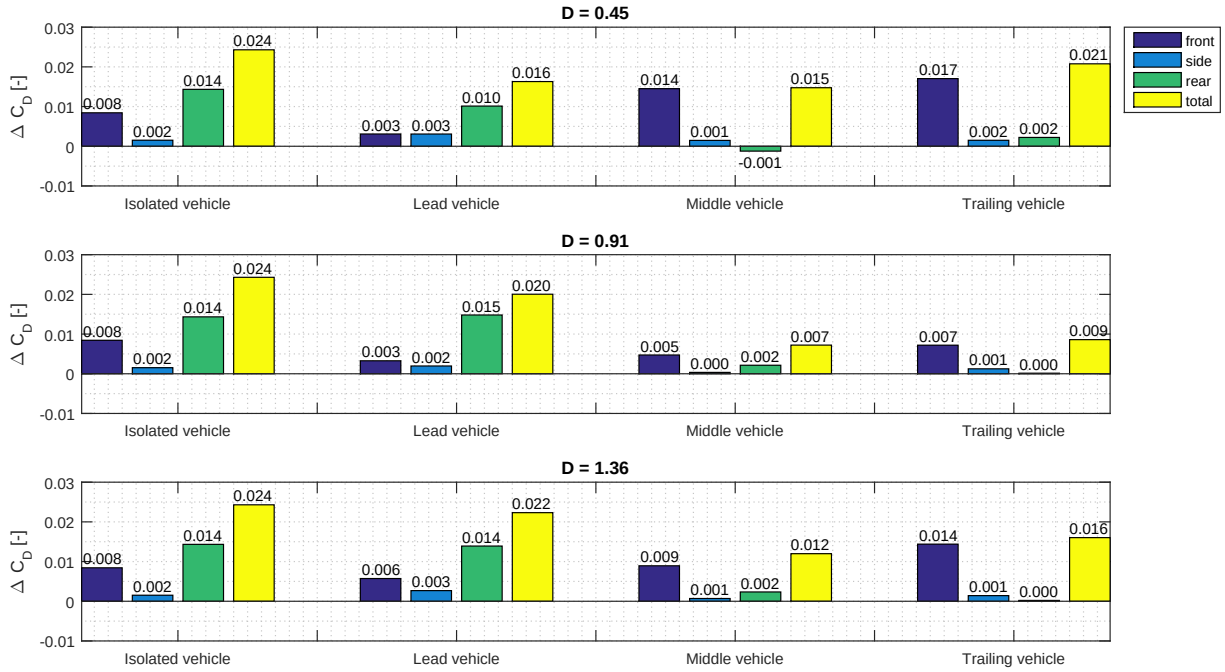

Figure 4.16: Effect of the inter-vehicle distance and the position in the platoon on the drag changes due to a yaw angle of $3°$. The reference drag coefficient is the one from the same vehicle in the same platoon without cross wind. The frontal edge radius is 0.135 m.

The most significant change that is noticed is the fact that the front part becomes more sensitive to changes in yaw angle if the vehicle is following another vehicle. The drag increase due to cross wind is enlarged when following another vehicle. This effect can be explained by the fact that when a non-zero yaw angle is applied, the vehicle acts like an airfoil and bends the air in the opposite direction. The yaw angle is similar to the angle of attack for an airfoil. This leads to streamlines hitting on a different position on the frontal surface, resulting in a different pressure distribution over the front part. The streamlines can be seen in Figure 4.17, while the resulting pressure coefficient on the front surfaces is compared for different platoon positions and yaw angles in Figure 4.18. The pressure coefficient for the $Y = 3°$ case is subtracted by the pressure coefficient for the $Y = 0°$ case. This way, the effect of the position in the platoon on the pressure change due to cross wind can be investigated. It is clear that for the lead vehicle, the main pressure increase due to cross wind occurs on the windward edge, while the leeward edge experiences a pressure decrease. On the middle and trailing vehicle however, there is a region of pressure increase on the leeward edge due to the deflection of the streamlines as seen in Figure 4.17. Thus, instead of shielding the following vehicles from the incoming cross wind, the lead vehicle redirects the flow such that more flow is impinging on the frontal surface of the following vehicles.

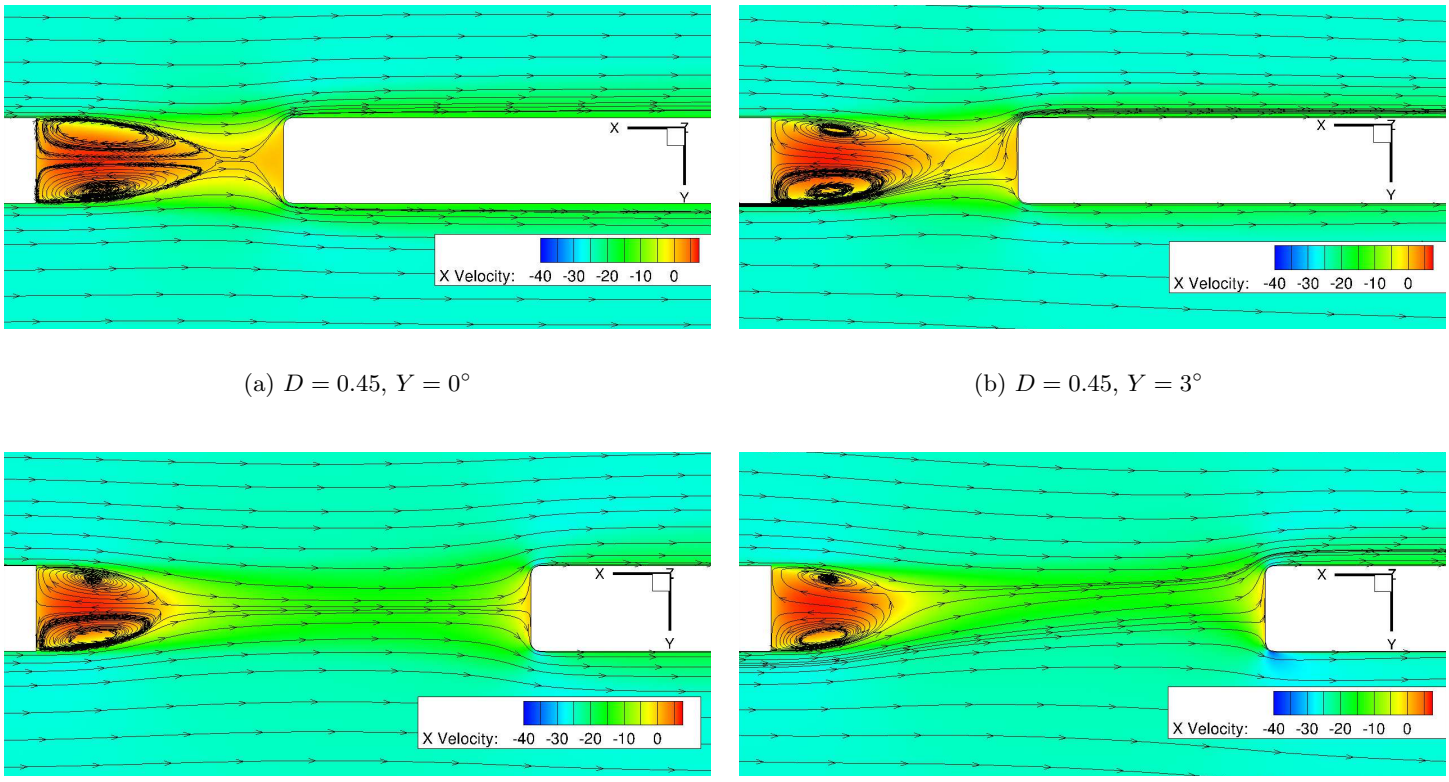

(a) $D = 0.45$, $Y = 0°$

(b) $D = 0.45$, $Y = 3°$

(c) $D = 0.91$, $Y = 0°$

(d) $D = 0.91$, $Y = 3°$

Figure 4.17: Contours of the velocity in x-direction with streamlines in the plane at half the vehicle height for different yaw angles and inter-vehicle distances. The frontal edge radius is 0.27 m.

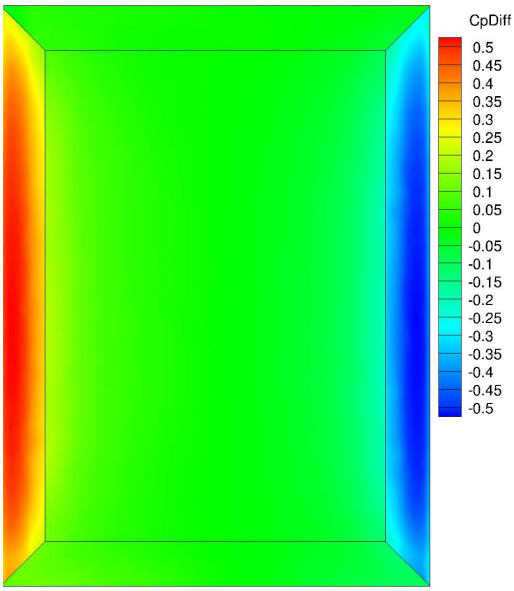

(a) Lead vehicle

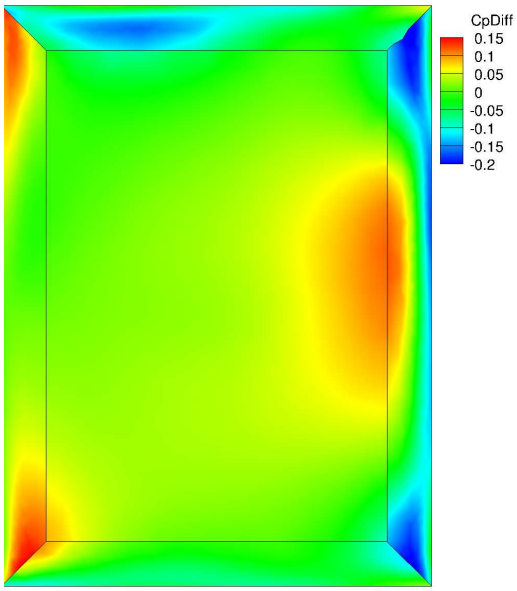

(b) Middle vehicle

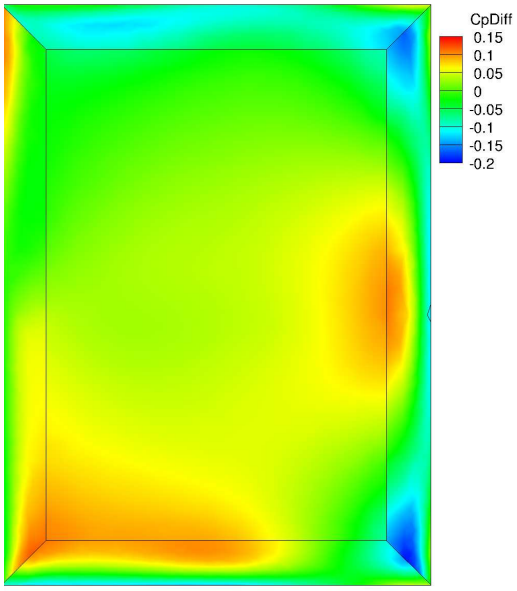

(c) Trailing vehicle

Figure 4.18: Contour of the difference in pressure coefficient between $Y = 3°$ and $Y = 0°$ on the front surfaces of the vehicles. The frontal edge radius is .27 m.

The effect of the yaw angle on the drag coefficient is investigated by showing the difference in drag coefficient between the two yaw angles of 0° and 3°. These differences are in the order of 0.01 drag coefficient. It is debatable whether the accuracy of the RANS simulation is higher than this. Small differences exist in the meshes of different configurations. Also no symmetrical meshes are used, this gives rise to small asymmetric flow features and side forces experienced in the zero cross wind case. While these are usually in the order of one drag count, and thus not significant, for the configurations with the lowest front curvature radius, these are in the order of 10 drag counts. These non-physical asymmetric forces add up to the differences due to the different meshes. Therefore care needs to be taken when drawing conclusions using these results. Not every difference in drag is caused by physical phenomena.

The side force coefficients can also be used to see the effects of cross wind on a vehicle platoon. The total side force coefficient of all the vehicles and the entire platoon can be seen in Figure 4.19. The different contributions that lead to these side force coefficient can be seen in Figure 4.20. This is again illustrated in Figure 4.21 by the distribution of the pressure coefficient.

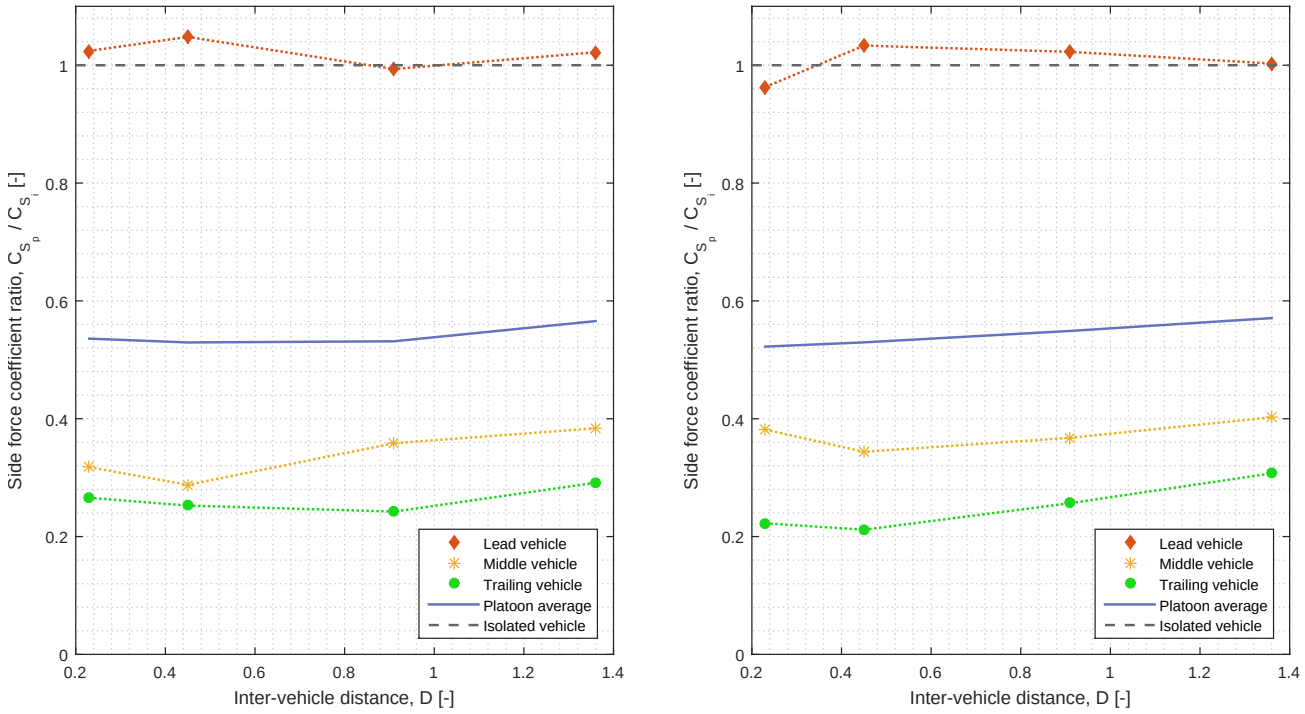

(a) $R = 0.135$ m

(b) $R = 0.27$ m

Figure 4.19: Side force coefficients of the vehicles in the platoon as well as the platoon average as a function of the inter-vehicle distance for two different frontal edge radii and a yaw angle of 3°.

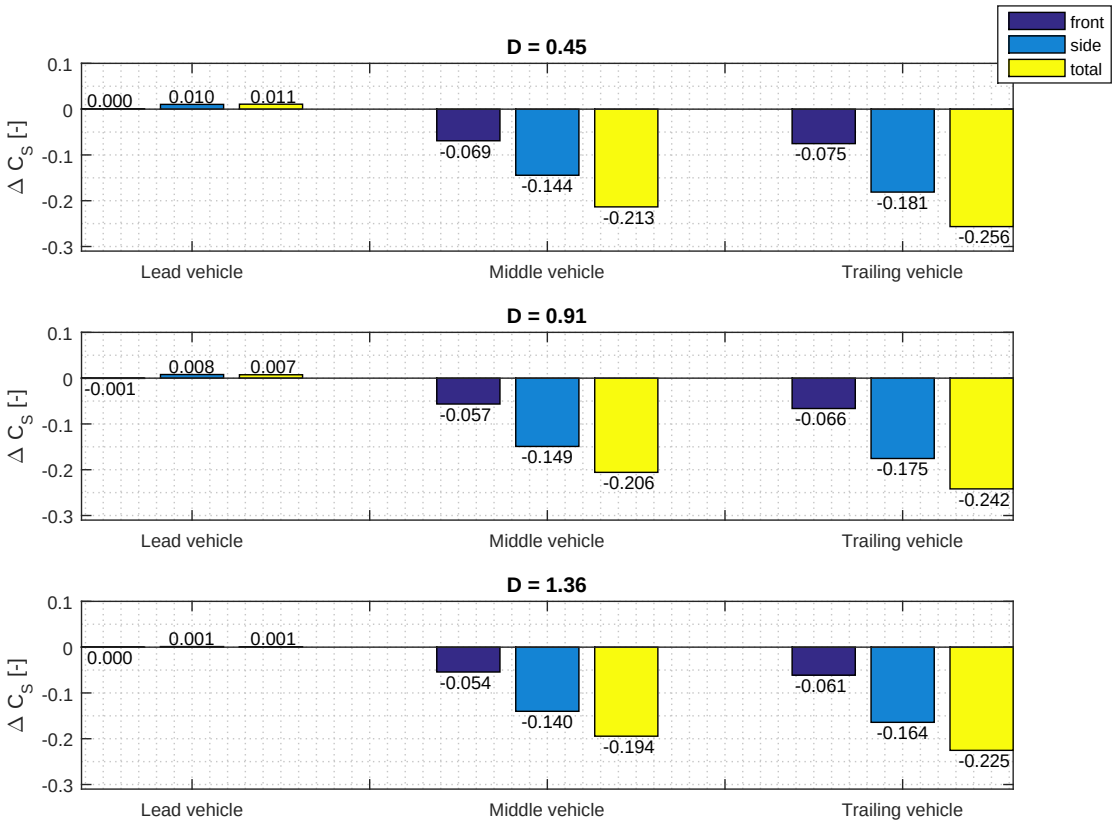

Figure 4.20: Side force coefficients of the vehicles in the platoon as well as the platoon average as a function of the inter-vehicle distance, with $R = 0.27$ m.

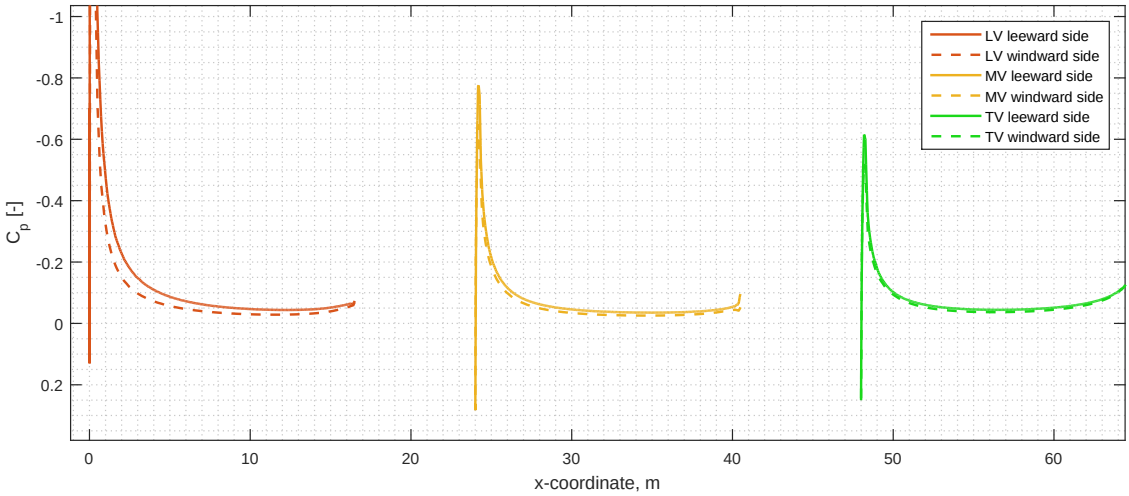

Figure 4.21: Pressure coefficient distribution on the side surfaces of the vehicles in the platoon with $D = 0.45$ and $R = 0.27$ m.

It can be seen that the side forces are decreased for the middle and trailing vehicle. The lead vehicle redirects the flow in such a way that the following vehicles experience less cross wind and hence have a smaller side force than the lead vehicle or the vehicle in isolation. The side force on the lead vehicle itself is practically insensitive to the presence of trailing vehicles. This effect was also seen in wind tunnel experiments by Marcu and Browand [29]. Because of this effect, the hypothesis was stated that driving in a platoon could lead to larger drag reductions for non-zero yaw angles. Since the platoon shields of part of the cross wind, the drag increase due to the yaw angle could become less significant. This however turned out not to be true for every case. While the leading vehicle shields the cross wind such that the side force on the following vehicles decreases, it also turns the streamlines in such a way that they increase the stagnation pressure on the frontal surface of the following vehicle.

4.1.4 Absolute drag values

All the effects of platooning are illustrated by showing the drag and side forces relative to those in isolation. This way, the effect of the different configurations on the effectiveness of a platoon is studied. However, a comparison can still be made with absolute values in order to check whether a less streamlined configuration suddenly outperforms a more streamlined configuration if both are placed in a platoon. $3D$ plots are generated that combine the effect of the inter-vehicle distance and the frontal edge radius on the drag coefficient of the different vehicles and the platoon average. The results are seen in Figure 4.22. The most remarkable result is seen in Figure 4.22(b) and Figure 4.22(c). Decreasing the frontal edge radius almost always increases the drag, however, for the smallest inter-vehicle distance, the drag of the trailing vehicle is decreased when the radius is decreased to its lowest value. For the middle vehicle this occurs at the two smallest distances. Due to the large drag decrease when the middle or trailing vehicle have a large frontal edge radius, it can be beneficial to have a less streamlined front vehicle part, i.e. a smaller radius.

A small remark must be made: the colors on the data points resemble the true values, while the colors on the lines represent the average between the data point. This explains the non-matching of the colors. All the resulting drag coefficients of the vehicles in the 'nnn' configuration can be seen in Table A.2 and Table A.3 in Appendix A.

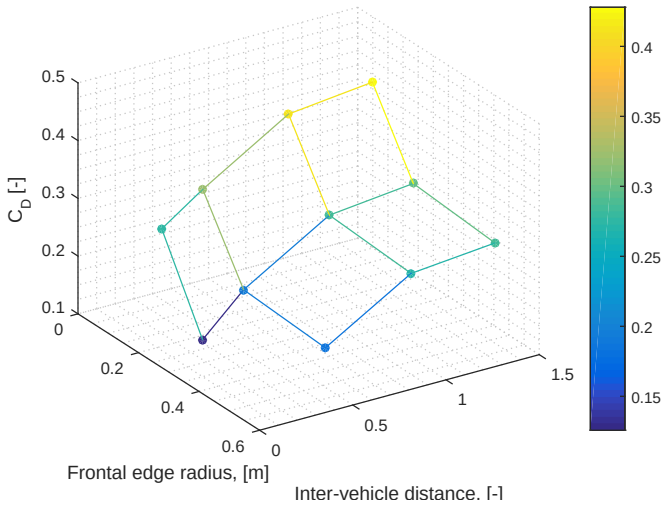

(a) Lead vehicle

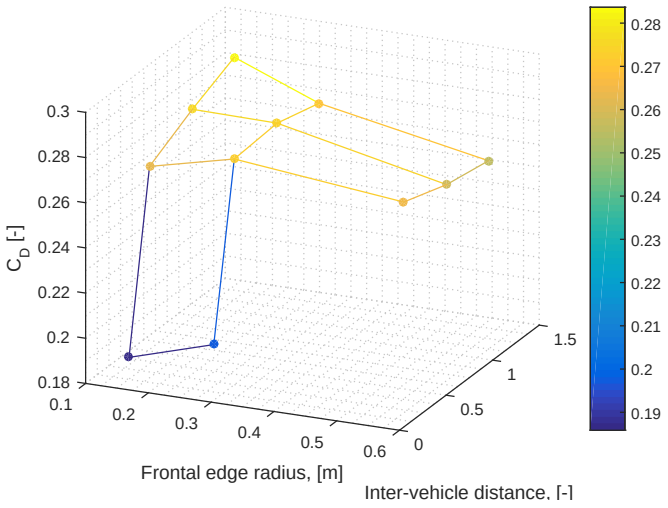

(b) Middle vehicle

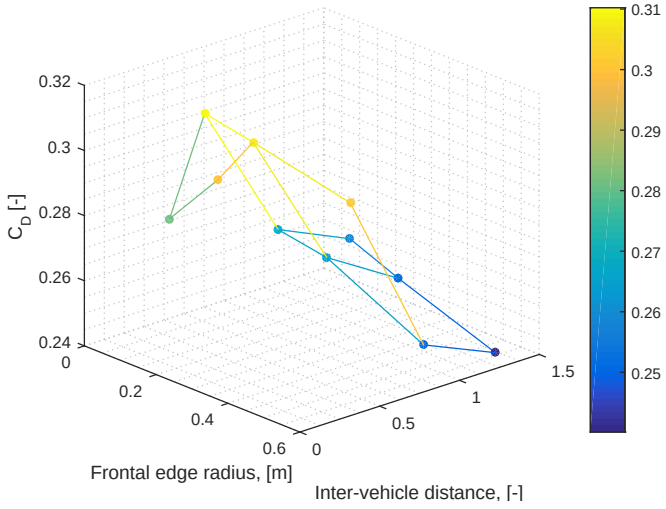

(c) Trailing vehicle

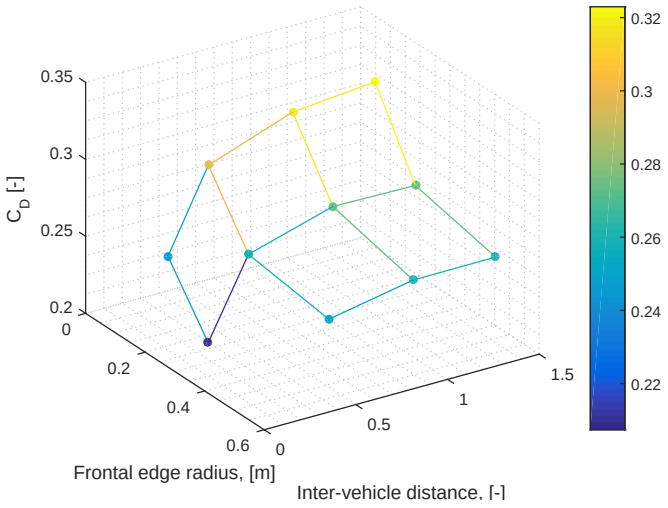

(d) Platoon average

Figure 4.22: Drag coefficients for all vehicles and the platoon average for different inter-vehicle distances and frontal edge radii. The yaw angle is $0°$.

4.1.5 Summary of the 'nnn' configuration

This section showed that for every simulated configuration, the platoon average drag coefficient was decreased with about 10% at least for the larger frontal edge radii and more than 20% for the smallest frontal edge radii. The individual vehicles however, did not always benefit from the platoon formation. The lead vehicle always experienced a drag decrease. Due to the presence of the middle vehicle, the pressure in the wake of the vehicle is increased and the pressure drag is thus decreased. This effect is stronger when the front of the lead vehicle is more streamlined, i.e. with a larger frontal edge radius, and the pressure at the rear surface represents a larger portion of the total drag.

The trailing vehicle showed very different behaviour depending on the frontal edge radius. At a certain small inter-vehicle distance, the drag of the trailing vehicle starts to rise above the drag of the leading vehicle (when gradually decreasing the distance). This inter-vehicle distance depends on the specific geometry of the trailing vehicle. It was shown that increasing the frontal edge radius, shifted the 'switching' point further towards the larger distances. The drag values of the trailing vehicle increased with decreasing distance up to a certain critical point where it started to decrease again. This lied between a distance of 0.23 and 0.45. The increase in drag was a result of the inward deflected streamlines from the middle vehicle's wake that followed a concave trajectory, leading to an increased pressure on the frontal edges. The suction force on those edges decreased drastically, increasing the drag more than the drag decrease due to the lower stagnation pressure on the frontal surface. For the configuration with the larger frontal edge radius, the drag coefficient of the trailing vehicle even increased up to values above the drag in isolation. The reason for this is that the frontal edges of this model are a large part of the total frontal area. Both effects working on the lead and trailing vehicle are combined when considering the middle vehicle. When increasing the inter-vehicle distance, both effects are diminished. Therefore the drag did not change a lot when changing the distance, except for the distance of 0.23 where the drag increase of the front part was drastically decreased. The middle and trailing vehicle also experienced a general decrease in drag for all vehicle parts due to the decreased velocity in the incoming flow field due to the wake of the lead vehicle.

When the cross wind term was added to the incoming flow, the drag reductions due to platooning increased for configurations with a short frontal edge radius. They decreased however for configurations with a larger edge radius. The yaw angle makes the drag reductions at the rear part more effective, while those at the front part become less effective. For the vehicles with the lowest frontal edge radius the increase in drag reductions at the rear part is more pronounced than the decrease in drag reductions at the front part. This is reversed for the larger frontal edge radii. Vehicles in a platoon were found to experience a larger front drag increase than in isolation. This was due to the deflection of the streamlines around a proceeding vehicle. These streamlines impinges on the front of the vehicle and increase the drag of the front part. When driving in a platoon, the lead vehicle redirects the flow towards the platoons axis. This ensures that the middle and trailing vehicle experience almost no side force due to the cross wind. The side force on the lead vehicle is not changed significantly. None of the vehicles in the discussed configurations was equipped with a tail. The addition of a tail on the trailing vehicle will be discussed in section 4.2.

4.2 Platoon configuration 'nnt12'

The next platoon configuration that is tested is the 'nnt12' configuration, where the last vehicle of the platoon is equipped with a tail of 12°. It must be noted that the drag coefficients of the individual vehicles are always scaled using the drag coefficient of the corresponding vehicle in isolation. An example for this platoon is given in following equations.

$$\begin{aligned} \text{ratio}_{\text{LV}} &= \frac{C_{D_{\text{LV}}}}{C_{D_{\text{no tail}}}} \\ \text{ratio}_{\text{MV}} &= \frac{C_{D_{\text{MV}}}}{C_{D_{\text{no tail}}}} \\ \text{ratio}_{\text{TV}} &= \frac{C_{D_{\text{TV}}}}{C_{D_{\text{tail 12°}}}} \end{aligned} \tag{4.2}$$

$$\begin{aligned} \Delta C_{D_{\text{LV}}} &= C_{D_{\text{LV}}} - C_{D_{\text{no tail}}} \\ \Delta C_{D_{\text{MV}}} &= C_{D_{\text{MV}}} - C_{D_{\text{no tail}}} \\ \Delta C_{D_{\text{TV}}} &= C_{D_{\text{TV}}} - C_{D_{\text{tail 12°}}} \end{aligned} \tag{4.3}$$

4.2.1 Effect of inter-vehicle distance

The effect of the inter-vehicle distance on both the individual drag coefficients and the average platoon drag coefficient is shown in Figure 4.23. If this is compared to the results from the 'nnn' platoon in Figure 4.1, it is seen that adding a tail to the trailing vehicle increases the drag coefficient ratio for an inter-vehicle distance of 0.45 largely, from about 1 to a value higher than 1.2. For the other distances no significant changes are observed. As can be expected, the lead and middle vehicle are not affected by the addition of the tail.

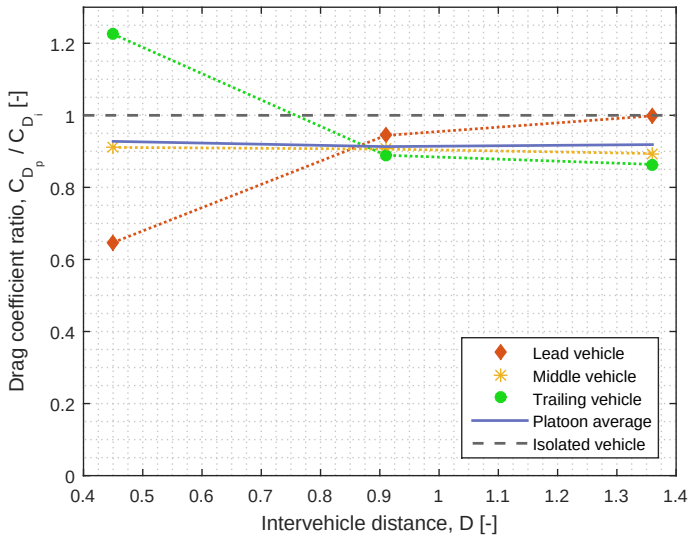

Figure 4.23: Effect of the inter-vehicle distance on the drag coefficients of the models and the entire platoon.

The drag contributions of the vehicles can be seen in Figure 4.24. Comparing these results with the results in Figure 4.2 shows that the relative drag increase, compared to the 'nnn' configuration, for the trailing vehicle is due to the fact that the drag at the rear surface increases instead of decreases due to the platoon formation, unlike the 'nnn' configuration. Driving in a platoon increases the drag of the rear part of the trailing vehicle with 0.16 or 0.18, while in Figure 4.2, the drag of the rear surface was decreased with 0.043. The drag reductions experienced by the tail surfaces do not entirely counteract this difference between drag reduction and drag increase.

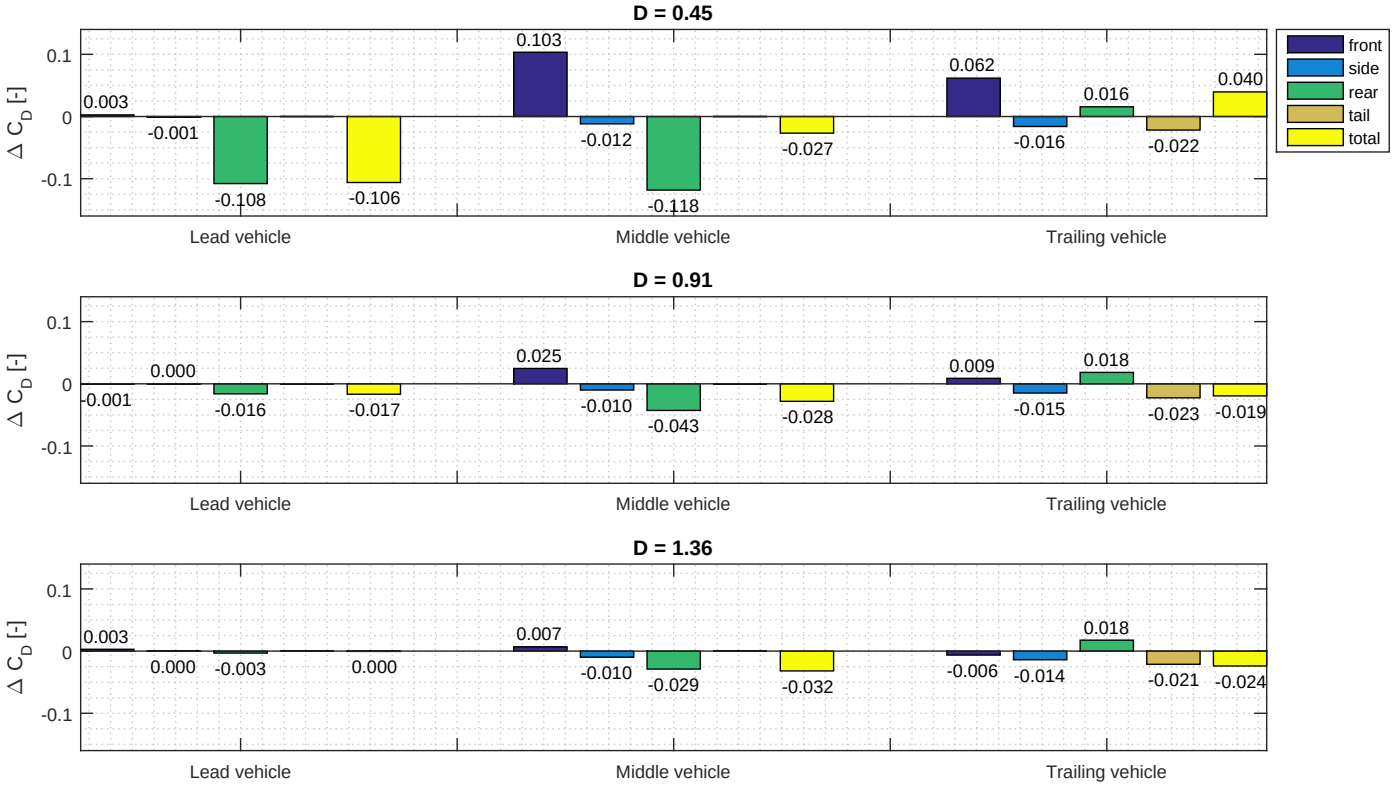

Figure 4.24: Effect of the inter-vehicle distance on the drag contributions experienced by the models with a frontal edge radius of 0.27 m in the 'nnt12' platoon. ΔC_D is defined as the difference between the platoon value and the value in isolation.

The increase in pressure drag at the rear of the surface could be due to the fact that, like illustrated in Figure 4.7, the trailing vehicle experiences a lower incoming velocity field. In Figure 3.12(d), it was already shown that two counter-rotating vortices exist in the wake of the tailed vehicle, these two vortices are larger than the tail cavity. If the velocity of the air, flowing over the tail and separating at the end of the vehicle, decreases, the magnitude of these vortices also decreases, because the trailing vehicle is moving in the middle vehicle's wake. The flow that is rotating and impinging back on the rear surface thus has a lower velocity and thus does not increase the back pressure as they would in perfect freestream conditions,

i.e. like for the leading vehicle. This can be seen in Figure 4.25, where the pressure coefficient on the rear surface is compared between a vehicle in isolation and a trailing vehicle in a platoon, both with a tail of 12°. The pressure coefficient is significantly higher on the rear surface of the vehicle in isolation. The average pressure coefficient of the vehicle in isolation is $C_{p_{avg}} = 0.00369$, while for the vehicle in the platoon $C_{p_{avg}} = -0.01194$. The corresponding velocity in the x-direction can be seen in Figure 4.26. It can be noticed that for the platoon case, the backflow velocity is lower than in the isolated case.

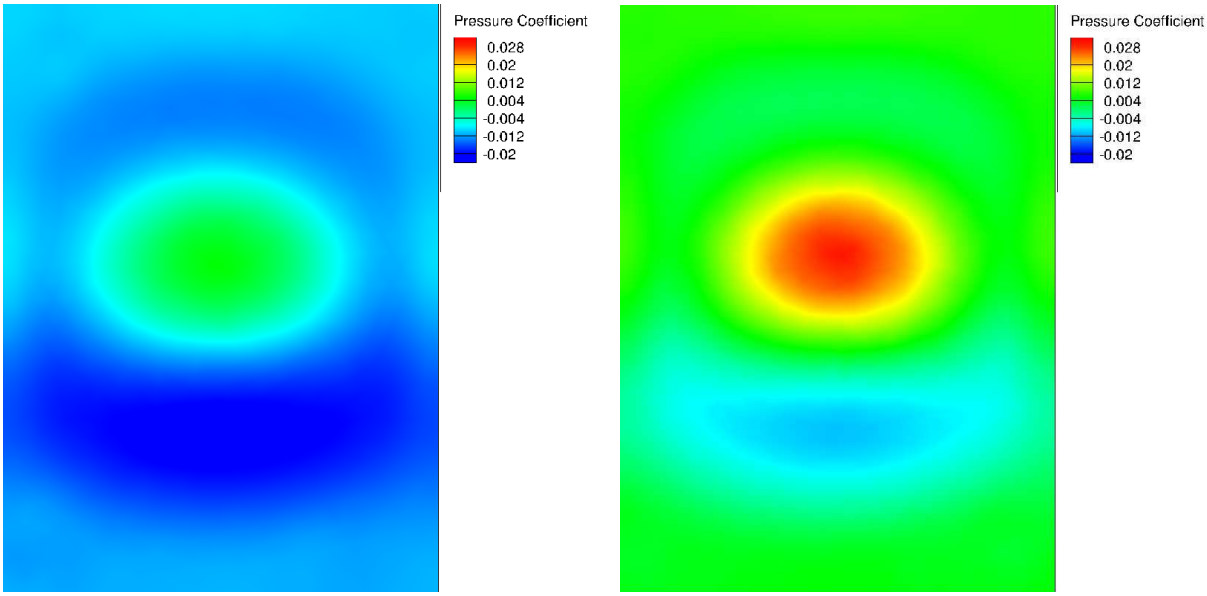

(a) Trailing vehicle, $C_{p_{avg}} = -0.01194$ (b) Vehicle in isolation, $C_{p_{avg}} = 0.00369$

Figure 4.25: Pressure coefficient distribution on the rear surface of a vehicle with a tail of 12°.

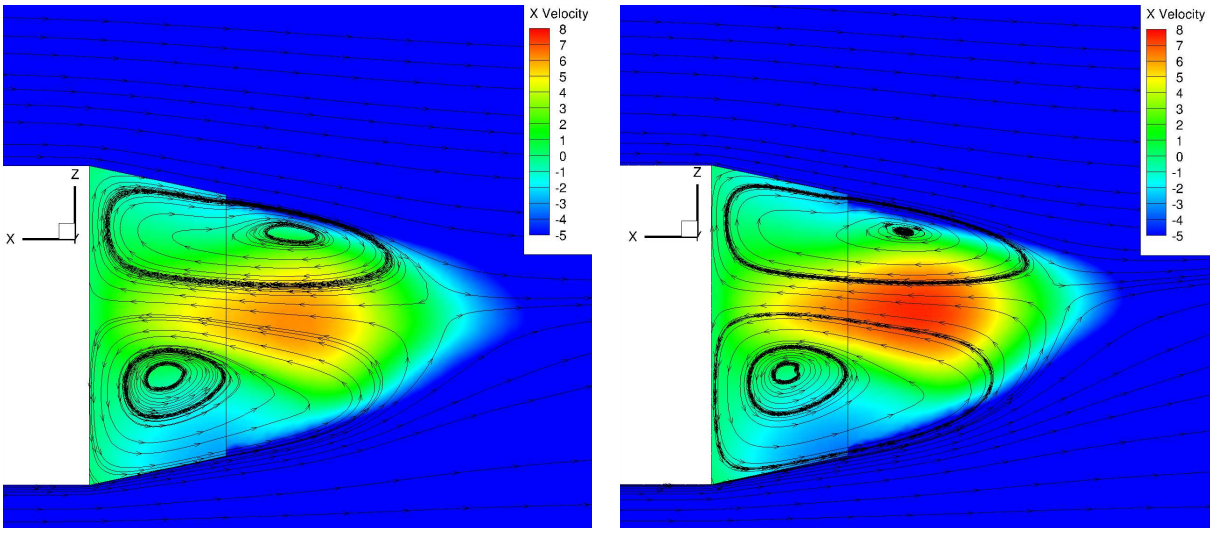

(a) Trailing vehicle

(b) Vehicle in isolation

Figure 4.26: Velocity in x direction in and around the 12° tail of the vehicle.

4.2.2 Effect of frontal edge radius

The same analysis as presented above can be done for a platoon where the models have a frontal edge radius of 0.54 m. This can be seen in Figure 4.27 and Figure 4.28. It was stated before in section 3.2, that the differences between a frontal edge radius of 0.54 m and 0.27 m are very small. The drag of a vehicle only decreases slightly when the frontal edge radius is increased. Also in the case of the 'nnt12' platoon, the behaviour of the vehicles in the platoon remain almost identical when changing the frontal edge radius. The drag contributions also show very similar before to the platoon with a frontal edge radius of 0.27 m. This platoon was not simulated for the shortest radius of 0.135 m.

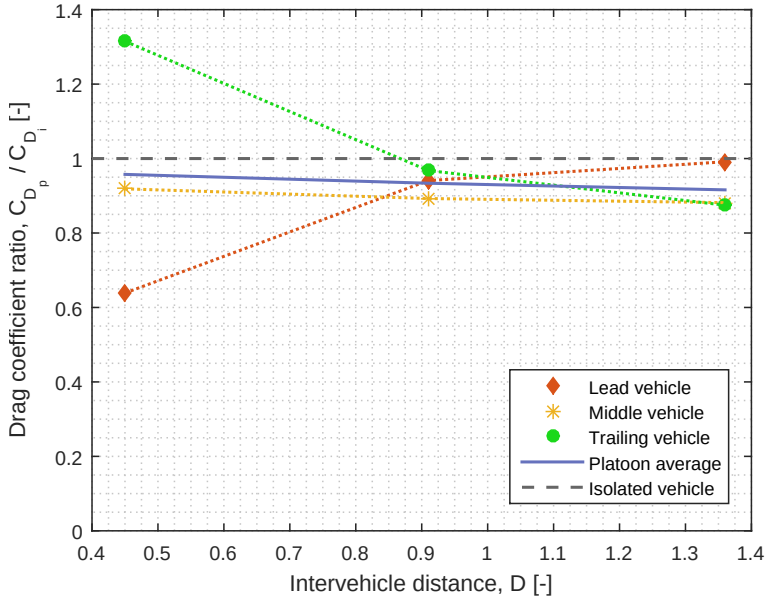

Figure 4.27: Effect of the inter-vehicle distance on the drag coefficient of the models and the entire 'nnt12' platoon. The frontal edge radius is 0.54 m.

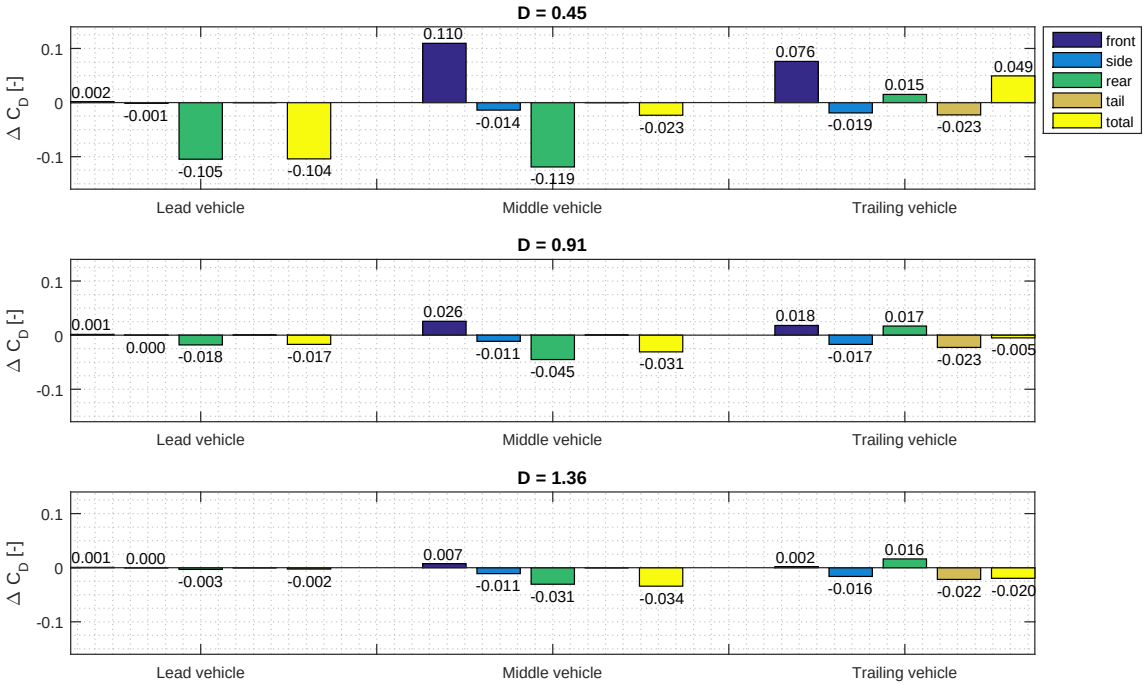

Figure 4.28: Effect of the inter-vehicle distance on the drag contributions experienced by the vehicles in the 'nnt12' platoon with a curvature radius of 0.54 m.

4.2.3 Effect of yaw angle

It was seen that cross wind reduces the drag reductions in a platoon for larger frontal edge radii. The drag reductions due to platooning also slightly decrease in this platoon when a yaw angle is applied. This can be seen in Figure 4.29.

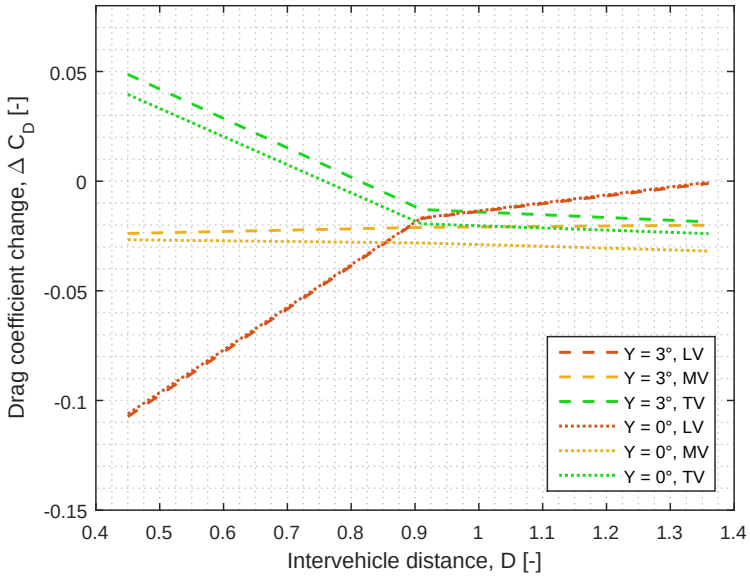

Figure 4.29: Effect of the yaw angle on the drag reductions experienced by the vehicles with a frontal edge radius of 0.27 m.

The side force coefficients can also be used to see the effects of cross winds on a platoon of vehicles. The side force coefficient of all the vehicles and the entire platoon can be seen in Figure 4.2.3. The different contributions that lead to these side force coefficient are very similar to those of the 'nnn' configuration in Figure 4.19(b). Again, the addition of a tail at the end of the platoon formation does not cause large differences in the behaviour of the relative side coefficient.

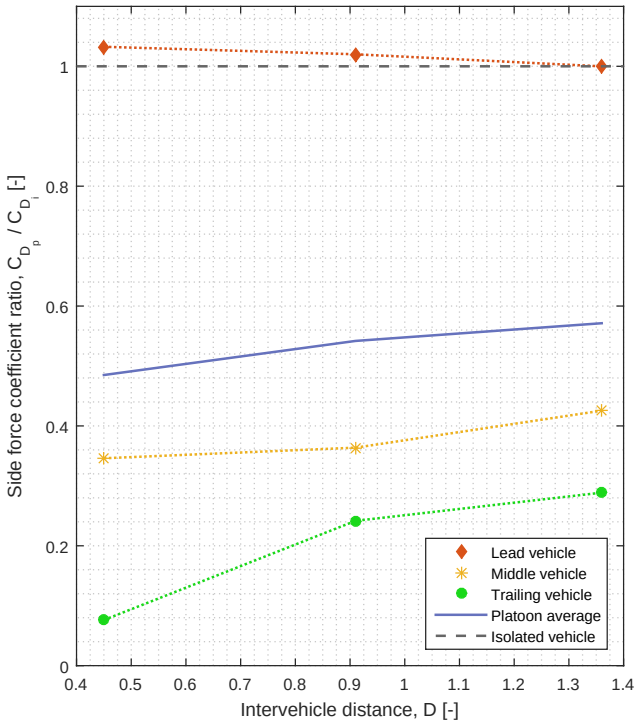

Figure 4.30: Side force coefficients of the vehicles in the 'nnt12' platoon as well as the platoon average as a function of the inter-vehicle distance. The frontal edge radius of the vehicles is 0.27 m.

4.2.4 Absolute drag values

The effects of platooning are illustrated by showing the drag and side forces relative to those in isolation. This way, the effect of the different configurations on the effectiveness of a platoon is studied. However, a comparison is also made with the absolute drag values. $3D$ plots are generated that combine the effect of the inter-vehicle distance and the frontal edge radius on the drag coefficient of the different vehicles and the platoon average. The results are seen in Figure 4.31. The behaviour of the absolute drag values resembles that of the relative drag coefficients.

A small remark must be made: the colors on the data points resemble the true values, while the colors on the lines represent the average between the data point. This explains the non-matching of the colors. Similarly to the previous platoon configurations, all the results for the 'nnt12' configuration can be seen in Table A.4 in Appendix A.

4.2.5 Summary of the 'nnt12' configuration

Adding a tail to the trailing vehicle did not change the trend of the drag coefficiens in the platoon. Besides the drag decrease of the trailing vehicle, another remarkable conclusion can be drawn. Contrary to what happened in the 'nnn' platoon configuration, the presence of the proceeding vehicles increased the base pressure on the rear surface of the trailing vehicle. This could be due to the decreased velocity in the incoming flow field that the trailing vehicle experiences, this then decreases the vorticity in the wake and decreases the backflow velocity. This is a large difference between a tailed and a non-tailed vehicle. For the vehicle without a tail, the base pressure decreased due to the presence of the proceeding vehicles. The effect on the total drag however is not very significant, since the decrease in drag of the tail surfaces itself replaces that of the rear surface in the case of a non-tailed vehicle. Now that the trailing vehicle is equipped with a tail, this will remain unchanged while the other vehicles are equipped with different kind of tails in section 4.3.

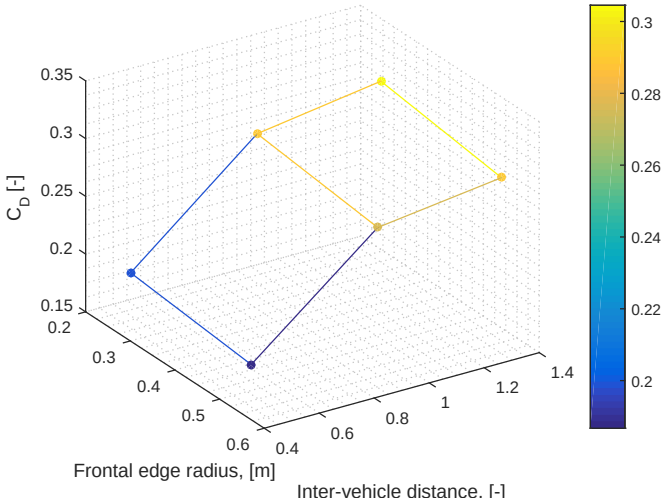

(a) Lead vehicle

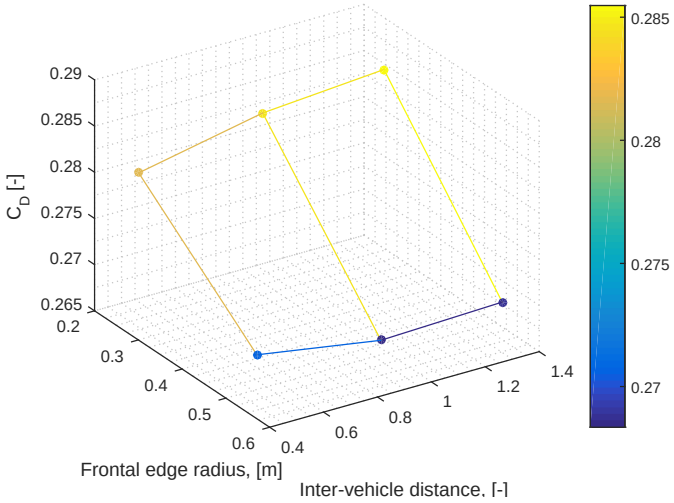

(b) Middle vehicle

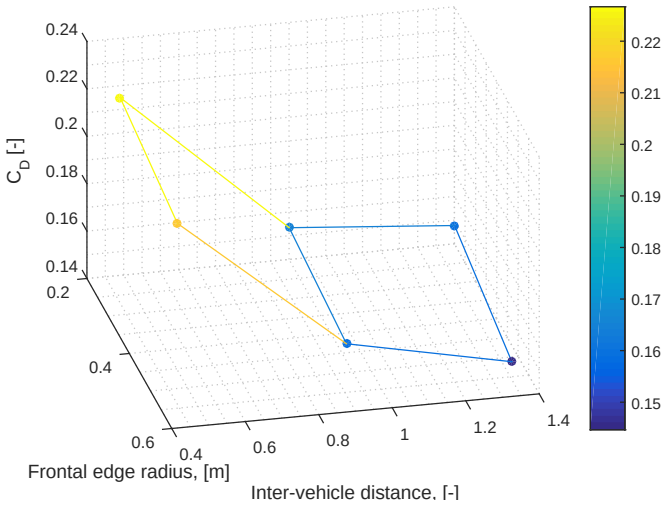

(c) Trailing vehicle

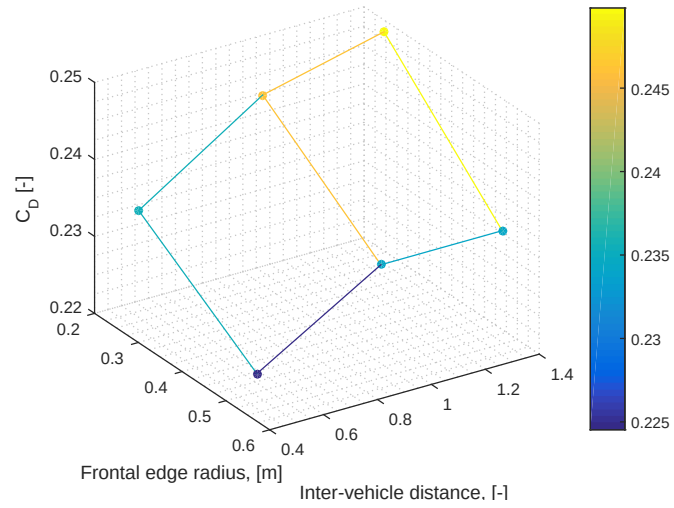

(d) Platoon average

Figure 4.31: Drag coefficients for all vehicles and the platoon average of the 'nnt12' platoon for different inter-vehicle distances and frontal edge radii. The yaw angle is 3°.

4.3 Platoon configurations 'ttt'

This section consists of the results of three different platoon configurations where all the vehicles are equipped with tails. The simulated configurations are: 't0t0t12','t6t6t12' and 't12t12t12'. While previous sections elaborated more on the effect of the platoon formation on the drag of the vehicles, this section focuses on the effect of a changing tail angle on the following vehicle. For the smallest frontal edge radius, only the last two configurations are tested and no simulations are done with the largest radius 0.54 m. This was decided since the differences between this radius and the radius of 0.27 m were small and the phenomena that were occurring were exactly the same, as opposed to the significant differences between $R = 0.135$ m and $R = 0.27$ m.

4.3.1 Effect of inter-vehicle distance

The effect of the inter-vehicle distance on both the individual drag coefficients and the average platoon drag coefficient is shown in Figure 4.32. The effectiveness of the platoon does not vary a lot for the leading vehicle when the tail angle is changed: the drag coefficient ratio remains almost unchanged. However since the drag coefficient of the vehicle in isolation decreases with increasing tail angle, the absolute drag reduction is larger for the vehicles with a smaller tail angle, i.e. the less streamlined vehicles. The same applies for the other vehicles. With the varying tail angles, the same trends are seen as in section 4.1.

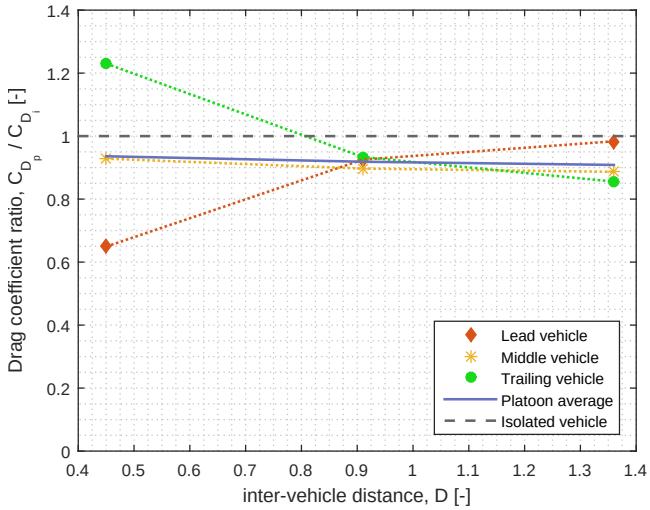

(a) 't0t0t12'

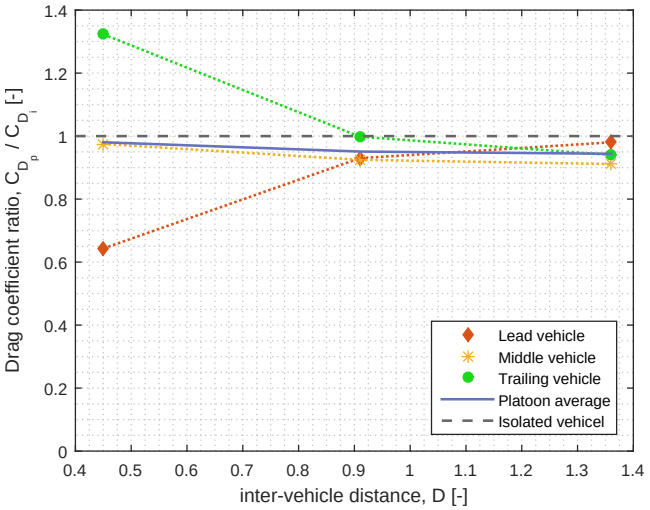

(b) 't6t6t12'

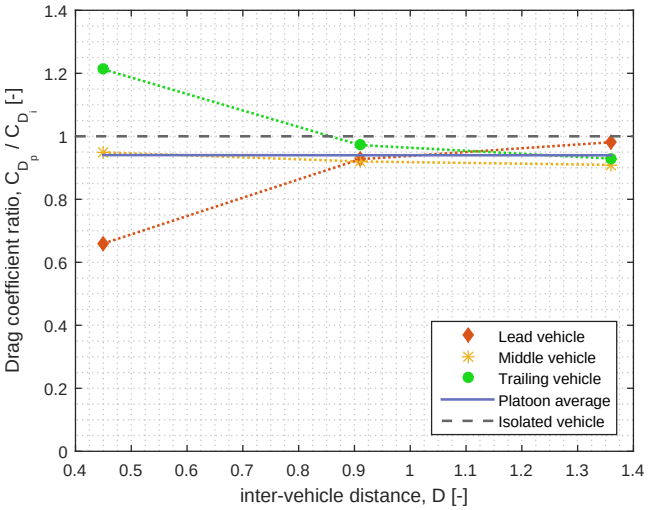

(c) 't12t12t12'

Figure 4.32: Effect of the inter-vehicle distance on the drag coefficient of the vehicles in different platoons. The frontal edge radius is 0.27 m.

As seen in Figure 4.33 and Figure 4.34, the drag of the middle and trailing vehicle is influenced by the varying tail angle. Both the middle and trailing vehicle experience a drag increase at the front part due to the decreased thrust force at the frontal edges. This increase in drag becomes less when the vehicle in front has a tail that is deflected more inwards. The drag contributions of the other parts of the vehicle experience a decrease in drag reductions when the tail is deflected more inward. This is due to the fact that for the middle and trailing vehicle the decrease in dynamic pressure of the incoming flow field is less when the front vehicle's wake is decreased in size by deflecting a tail.

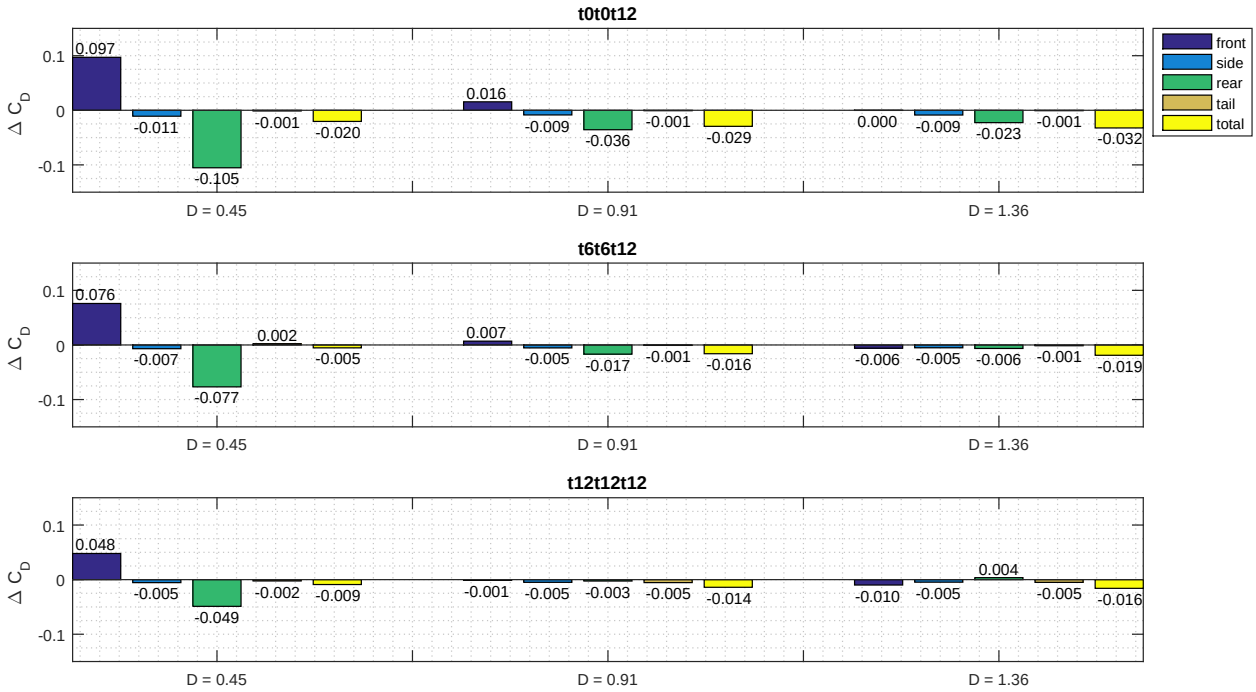

Figure 4.33: Drag contributions of the middle vehicle for the platoon configurations with vehicles with a frontal edge radius of 0.27 m.

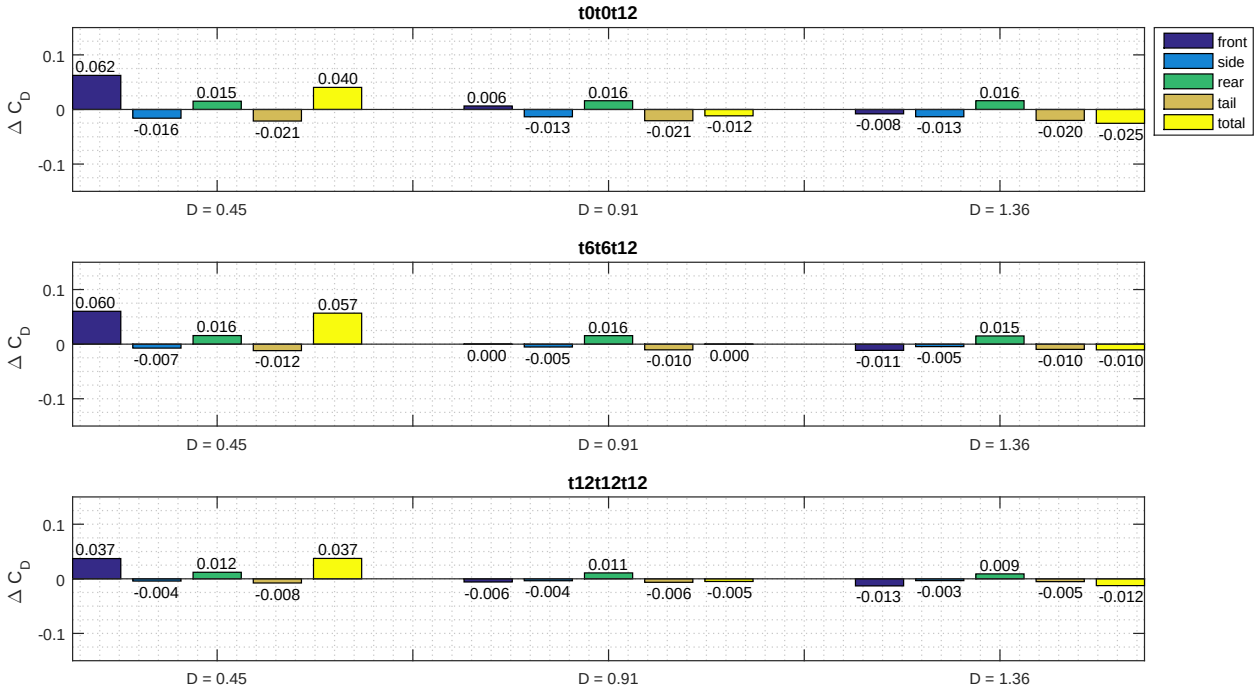

Figure 4.34: Drag contributions of the trailing vehicle for the platoon configurations with vehicles with a frontal edge radius of 0.27 m.

The tail angle of a vehicle largely affects the front part of the following vehicle. To study this effect, the pressure coefficient distribution over the front part of the middle vehicle is plotted in Figure 4.35. The two black horizontal point-dashed lines indicate the borders between the frontal edges and the stagnation surface. Two variations are included in this plot, the inter-vehicle distance and the tail angle. Increasing the inter-vehicle distance increases the pressure on the horizontal surface towards the value of an isolated vehicle. Increasing the tail angle also increases the pressure. On the frontal edges, the situation is reversed. Increasing the inter-vehicle distance and the tail angle lowers the negative pressure on the edges towards the value of a vehicle in isolation. It can thus be stated that the tail angle and the inter-vehicle distance globally have the same effect on the platoon. In Figure 4.36, the change in drag contributions of the frontal stagnation surface and the frontal edges can be seen, it is clear that for this frontal edge radius, the decrease of the pressure on the frontal edges influences the front drag more than the increase of the high stagnation pressure on the frontal surface due to the deflection of the tails. This is the case for both the middle and trailing vehicle.

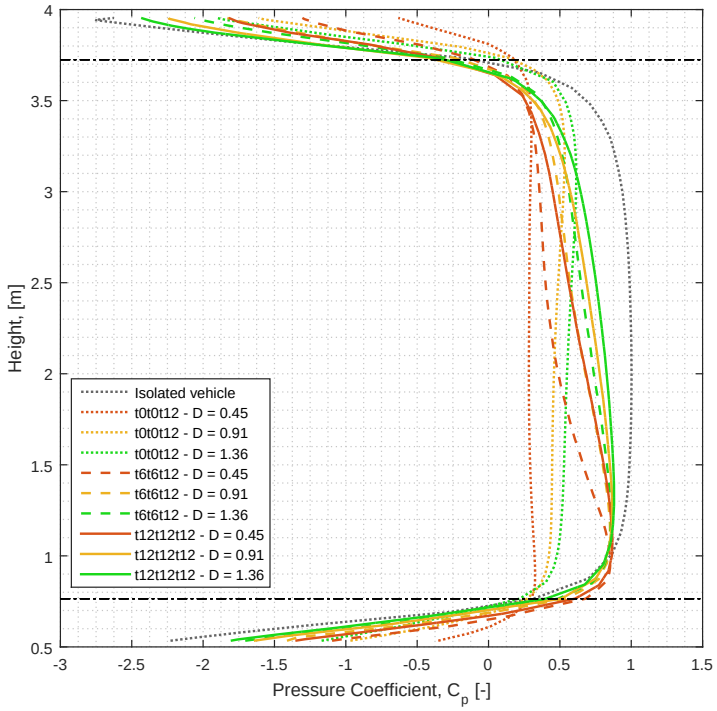

(a) General view

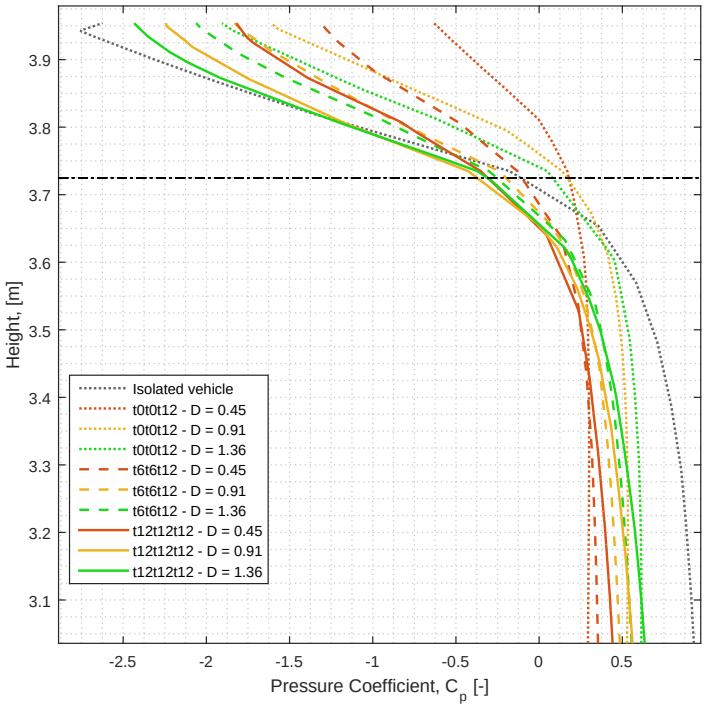

(b) Zoomed in

Figure 4.35: Pressure coefficient over the vertical centreline on the front part of the trailing vehicle in different platoon configurations with a frontal edge radius of 0.27 m.

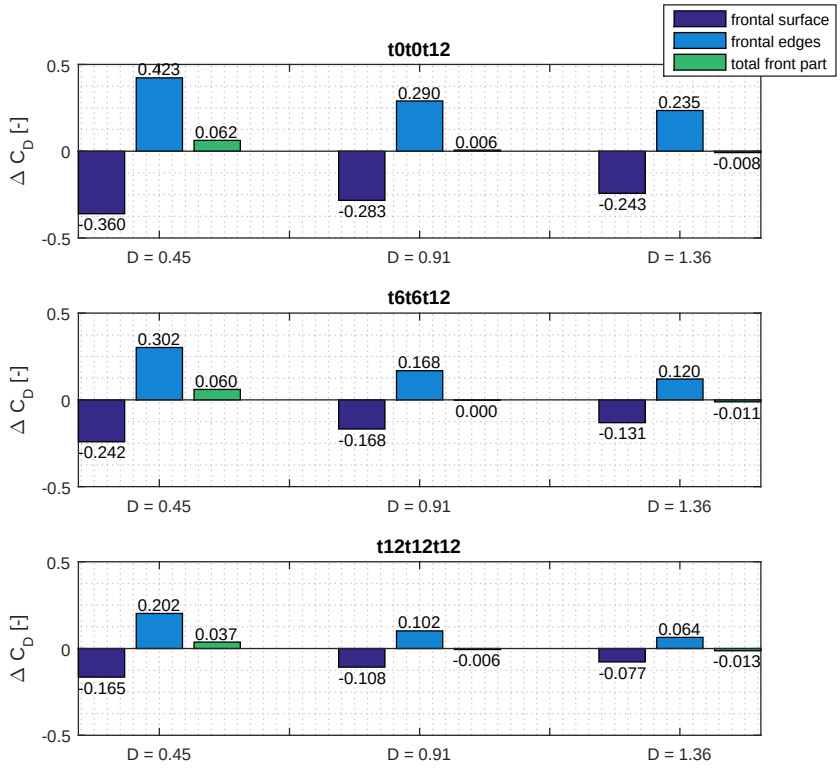

Figure 4.36: Drag contributions of the front of the trailing vehicle for the platoon configurations with vehicles with a frontal edge radius of 0.27 m.

It can be noticed in Figure 4.34 that while the drag of the front part of the trailing vehicle decreases when deflecting the tail inwards, the total drag of the trailing vehicle is first increased when the tail angle is increased from 0° to 6°, but it is decreased when increasing the tail angle from 6° to 12°. Deflecting the tail more inward causes several things. First of all the drag increase of the front part is reduced. Secondly, the small drag reduction of all vehicle parts due to a slower incoming flow field, i.e. lower dynamic pressure, experienced by the trailing vehicle, is also decreased. Changing the tail angle from 0° to 6°, the first effect is less significant and thus the second effect becomes more dominant and increases the total trailing vehicle drag. When changing the tail angle from 6° to 12°, the first effect (on the front drag) becomes more dominant and thus the total trailing vehicle drag decreases again.

The differences between the middle and trailing vehicle are due to the fact that when the tail angle of the lead vehicle is changed, its effect on the flow around middle vehicle is affected by the fact that the simultaneous change of the middle vehicle's tail also affects the flow around the middle vehicle. Another difference is that the effects of the middle vehicle's tail on the trailing vehicle are affected by the fact that the middle vehicle is also positioned in a region with a lower dynamic pressure than in the freestream, unlike the lead vehicle.

It is remarkable in Figure 4.35 that by deflecting the tail inward, the pressure values on the lower part of the frontal surface slightly exceed those of a vehicle in isolation, while on the upper part, there is still a decrease in pressure due to the platoon formation. This is due to

ground effect that increases the flow velocity underneath the tail. When a particle follows a streamline going underneath the vehicle, its velocity at the end of the tail will be higher than in the case where the particle follows a streamline going over the vehicle. This difference in velocity results in the wake being deflect more upward. Figure 4.37 shows the upward deflection of the wake and the interaction with the following vehicle.

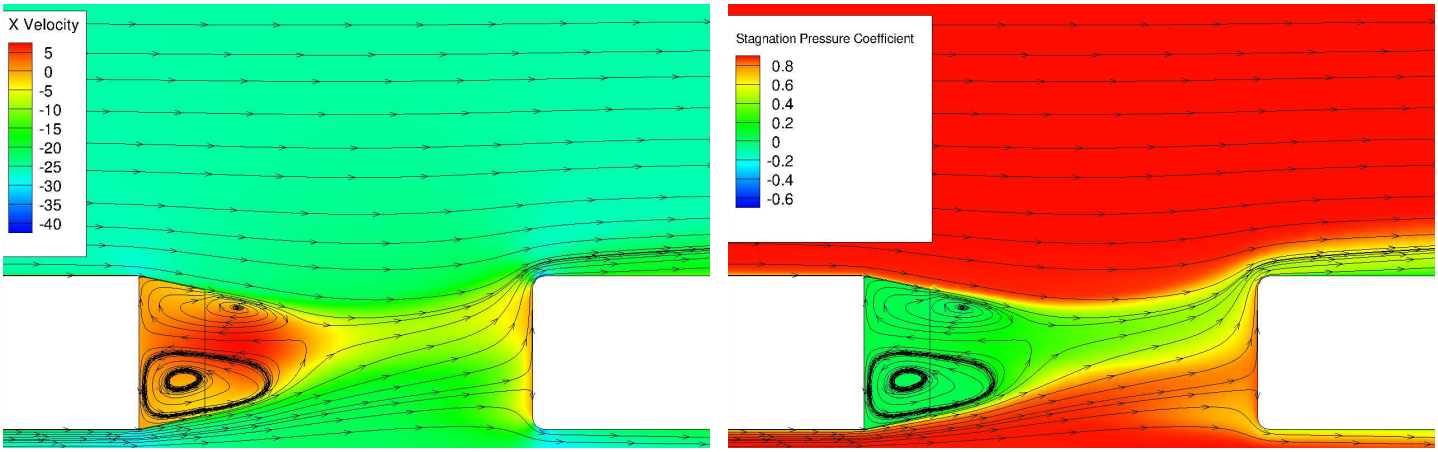

(a) x-velocity (b) Total pressure coefficient

Figure 4.37: Visualisation of the interaction between the wake of the leading vehicle and the front of the middle vehicle.

4.3.2 Effect of frontal edge radius

When the frontal edge radius is decreased to 0.135 m, nothing much changes for the behaviour of the lead vehicle when the tail angle is varied. Changing the tail of the vehicles mainly affects the vehicles driving behind a tailed vehicle. For every inter-vehicle distance, the middle and trailing vehicle benefit a lot more from the platoon when the radius of the frontal edge radius is smaller. The drag of the front part of the middle and trailing vehicles is no longer increased due to the presence of the vehicle in front. This results in the middle and trailing vehicle benefiting more from the platoon than the leading vehicle, which was not the case for larger radii. In Figure 4.38, it is seen that, for both tail configurations, by increasing the inter-vehicle distance, the drag reductions first increase and then decrease again. While for the 'nnn' configuration, the drag reductions increase with increasing inter-vehicle distance, it is expected that the drag value will asymptotically go to the value in isolation if the inter-vehicle is increased further and further. Deflecting a tail on the vehicles in front might have the same effect as it also reduces the influence of the wake on the following vehicle. This explains why the drag of the entire vehicle starts to increase again for the largest inter-vehicle distance, when the vehicles are equipped with deflected tails. The deflection of the tails shows what would happen if the inter-vehicle distance was increased further without tail deflection. This is the main difference between this configuration and the configuration with frontal edge radii of 0.27 m. For a frontal edge radius of 0.27 m, the drag values of the total trailing or middle vehicle are not increasing again when the inter-vehicle distance or the tail angle is increased.

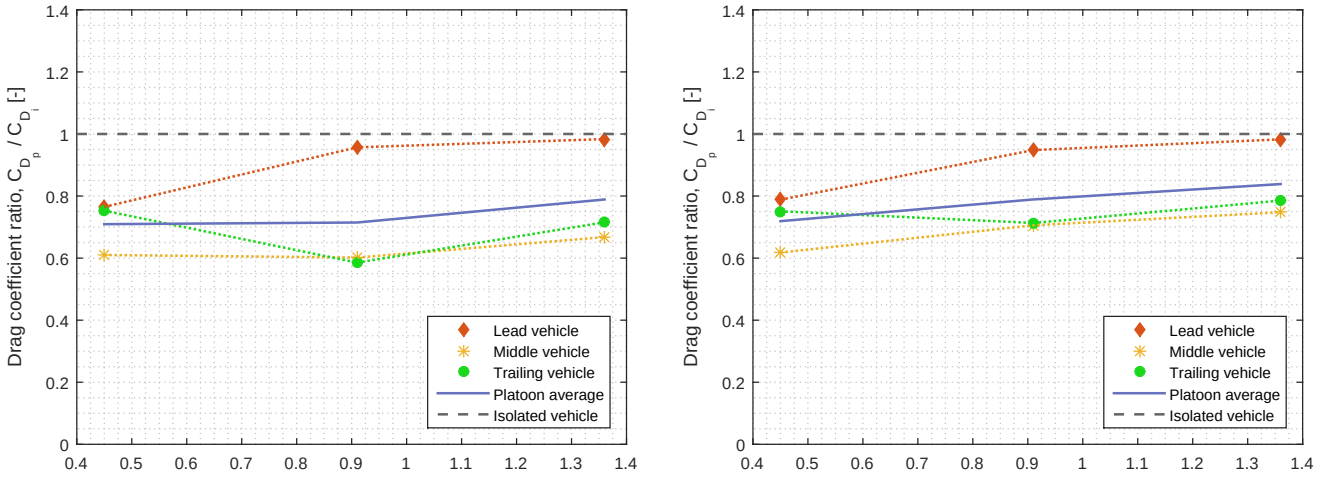

(a) 't6t6t12' (b) 't12t12t12'

Figure 4.38: Drag coefficient reductions for the vehicles in the platoon as a function of the inter-vehicle distance. The frontal edge radius is 0.135 m.

To investigate the effects of the varying tails on the middle and trailing vehicle, all the drag contributions of these vehicles are shown in Figure 4.39 and Figure 4.40 for different platoon configurations. Since no 't0t0t12' configuration is tested for this frontal edge radius, the 'nnn' configuration will serve as the configuration where the tails are not deflected inward. It can be seen that the total drag of the vehicles always increases when the tail angle is increased.

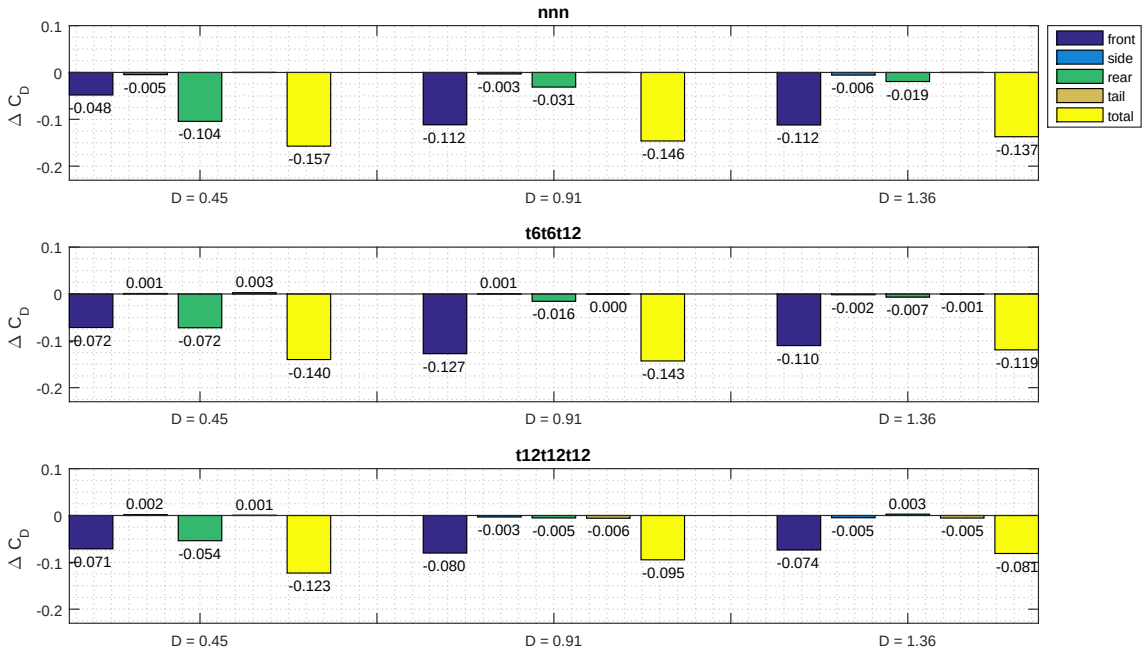

Figure 4.39: Drag contributions of the middle vehicle for the platoon configurations with a frontal edge radius of 0.135 m.

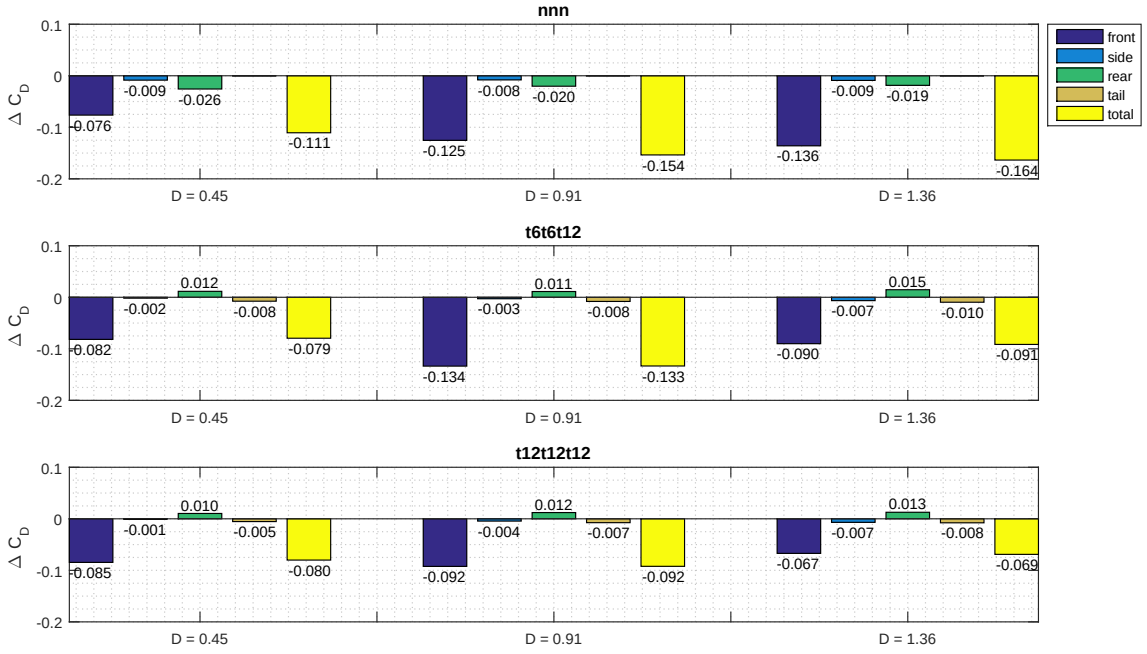

Figure 4.40: Drag contributions of the trailing vehicle for the platoon configurations with a frontal edge radius of 0.135 m.

As opposed to the behaviour of the total drag, the front drag shows a more complicated behaviour when the tail angles are changed. The drag reduction on the front part of the vehicle is split up again in the frontal stagnation surface and the frontal edges in Figure 4.41. The difference between going from 0° to 6° and going from 6° to 12° lies in the fact that, in the first case, the loss in thrust force on the frontal edges is affected more than the drag on the stagnation surface. Going from 6° to 12°, this is reversed. Only when the largest inter-vehicle distance is considered, it can be seen that the drag reductions on the front part are always decreasing with increasing tail angle, i.e. the decrease in stagnation pressure is more significant than the change in thrust force. This shows that the effects of the tail angle and the inter-vehicle distance on vehicles, that follow a tailed vehicle, strongly depend on each other. It can be stated as follows: if the combination of the inter-vehicle distance and the tail angle is low, the front drag reductions are increased by the deflection of the tails. If the combination is high, the front drag reductions decrease when the tails are deflected inwards.

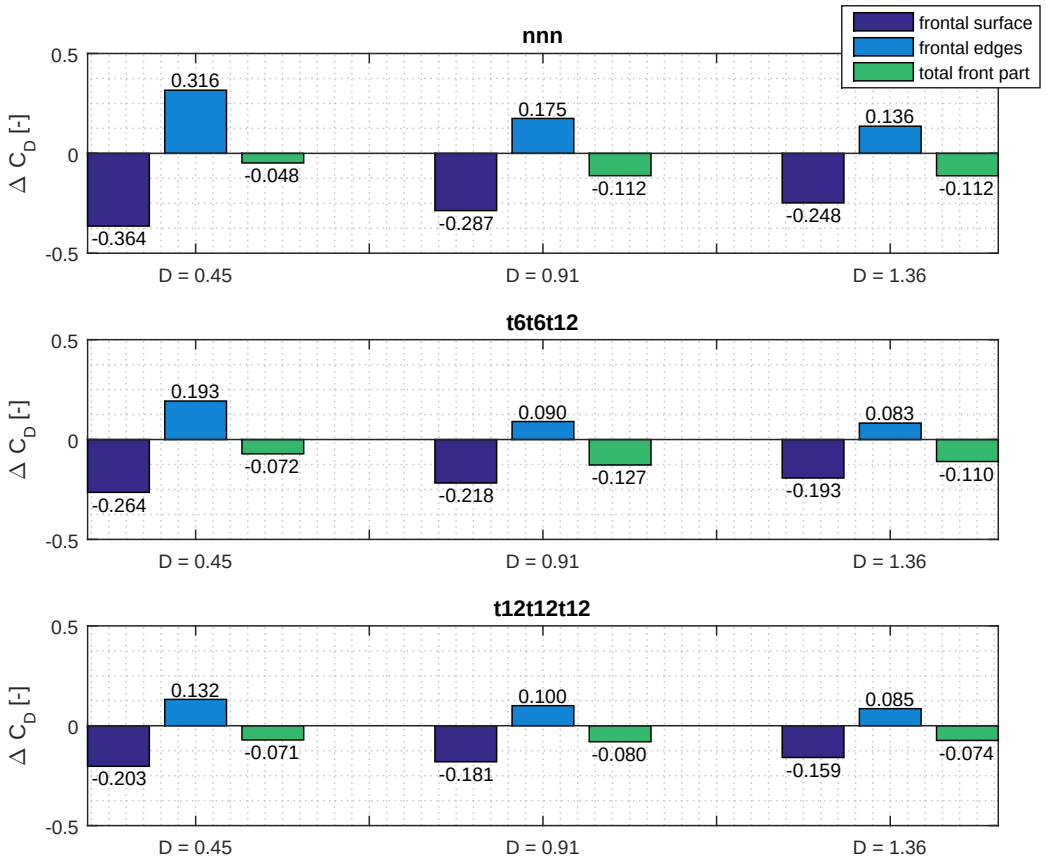

Figure 4.41: Drag contributions of the front of the trailing vehicle for the platoon configurations with vehicles with a frontal edge radius of 0.135 m.

In Figure 4.42, it is seen that by increasing the inter-vehicle distance, the stagnation pressure on the frontal surface of the trailing vehicle increases. If the vehicle in front has a tail angle of 6°, the pressure coefficient on the frontal surface is lower than for the case when the vehicle in front has a tail angle of 6°. This is due to the fact that the tails that are deflected inwards also bend the air flow towards the frontal surface of the trailing vehicle. This effect is most significant at the lowest inter-vehicle distance. At the frontal edges, the opposite trend is observed. The closer a vehicle is to the vehicle in front, the higher the pressure coefficient. This decrease in suction force at the frontal edges is already explained in section 4.1. It seems that the inter-vehicle distance of 0.91 gives the lowest pressure coefficient, i.e. the highest suction force, while its stagnation pressure is still lower than for a distance of 1.36. This results in the largest drag reductions on the front of the vehicle when the inter-vehicle distance is 0.91. Figure 4.43 shows the velocity in the wake of the middle vehicle and over the front part of the trailing vehicle. It can be noticed that the inward deflection of the tails causes a higher acceleration of the flow over the frontal edges of the following vehicle. This leads to the higher negative pressure peak on the edges that was seen in Figure 4.42.

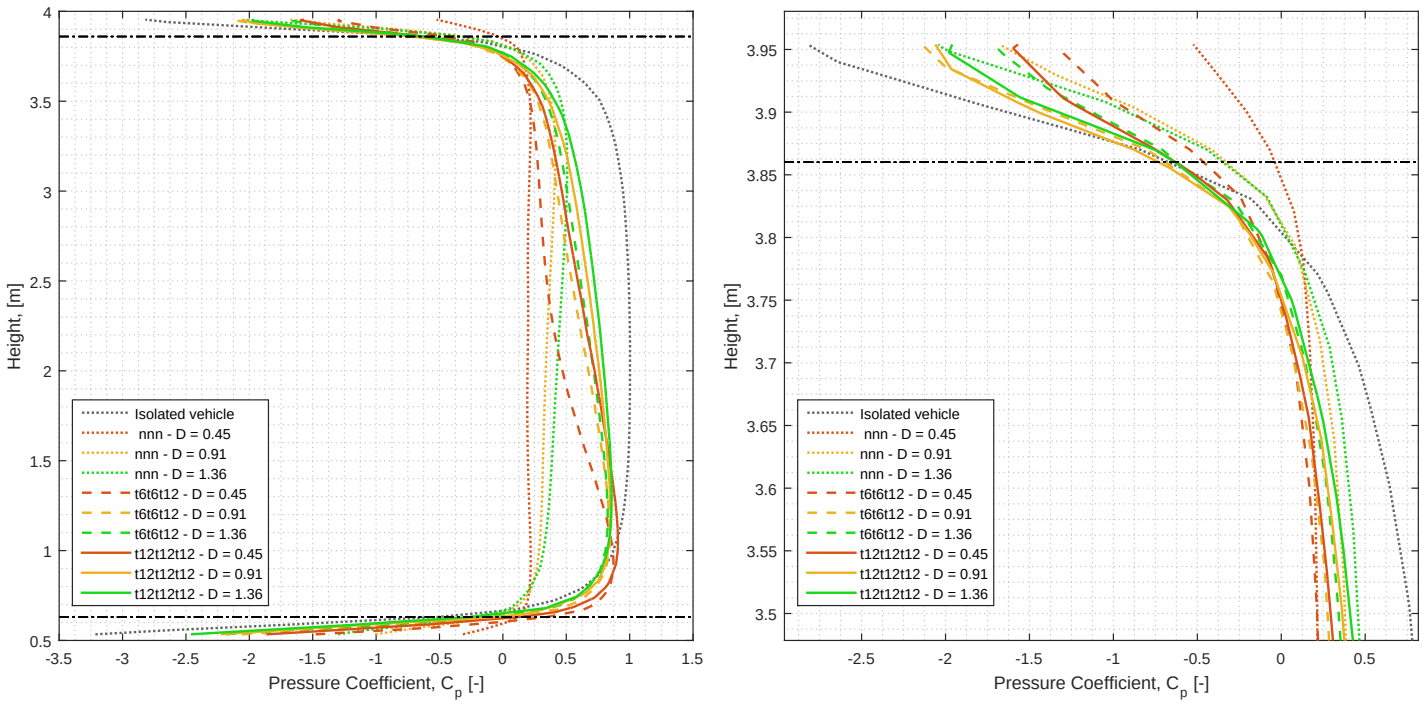

(a) General view

(b) Zoomed in

Figure 4.42: Pressure coefficient over the vertical centreline on the front part of the trailing vehicle in different platoon configurations with a front curvature radius of 0.135 m.

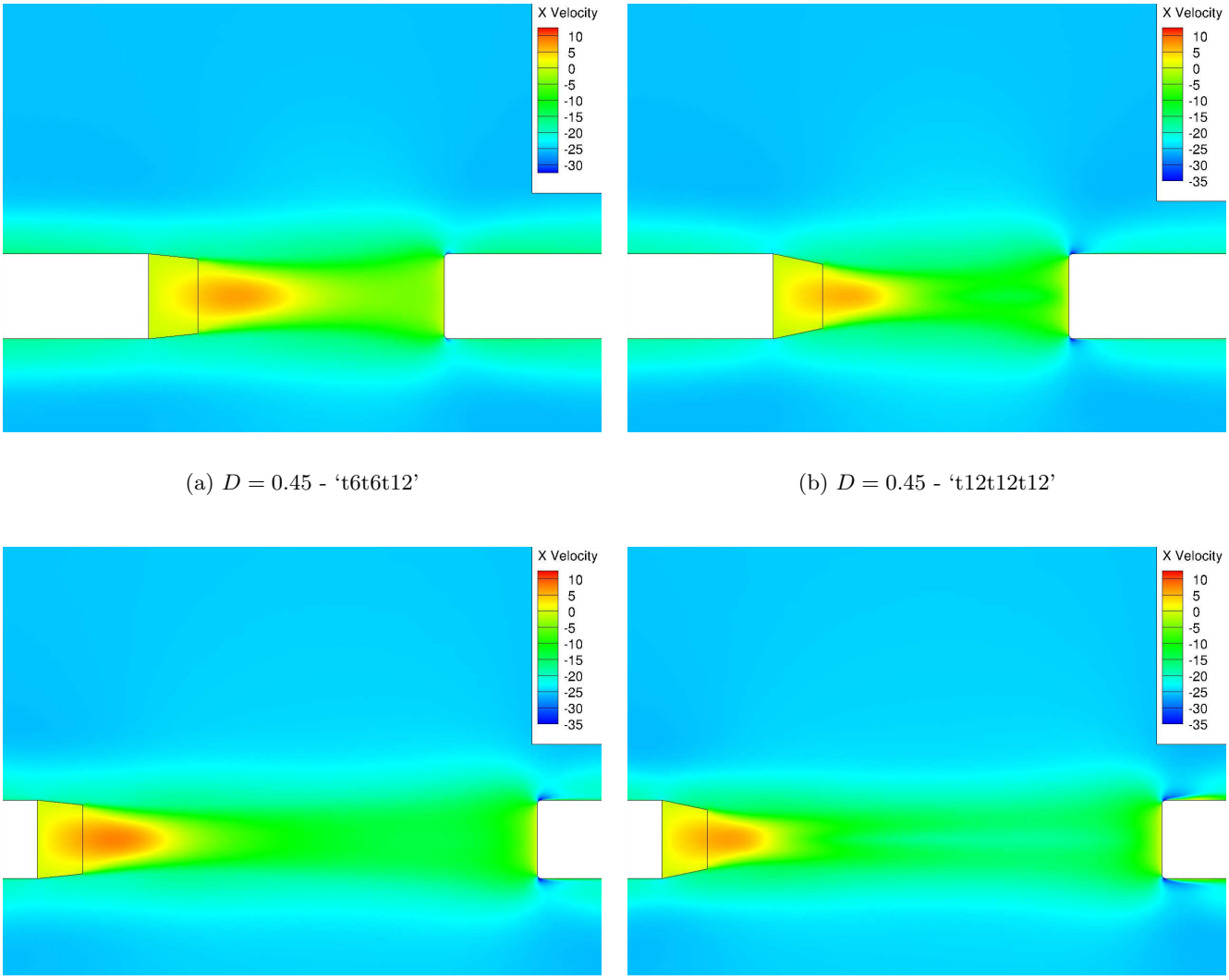

(a) $D = 0.45$ - 't6t6t12'

(b) $D = 0.45$ - 't12t12t12'

(c) $D = 0.91$ - 't6t6t12'

(d) $D = 0.91$ - 't12t12t12'

Figure 4.43: Top view of the contour of the x-velocity around the base of the middle vehicle and the front of the trailing vehicle for different inter-vehicle distances and tail configurations. The plane is located halfway the vehicle's height at $z = 2.3175$.

4.3.3 Effect of yaw angle

The addition of tails makes the bluff bodies more streamlined and will therefore affect the behaviour in cross wind conditions. In subsection 4.2.3 and subsection 4.1.3, it was seen that the cross wind decreased the savings in a platoon for the more streamlined bodies (with a radius of 0.27 m or higher), while it increased the platoon savings for the less streamlined bodies (with a radius of 0.135 m). It is seen that, also for the all tailed platoon configurations, the cross wind decreases the drag reductions for the vehicles with a large radius, this can be seen in Figure 4.44. The ΔC_D stands for the decrease or increase in drag that the vehicles experience in the platoon formation. For the vehicles with the lowest radius, the results are more complex.

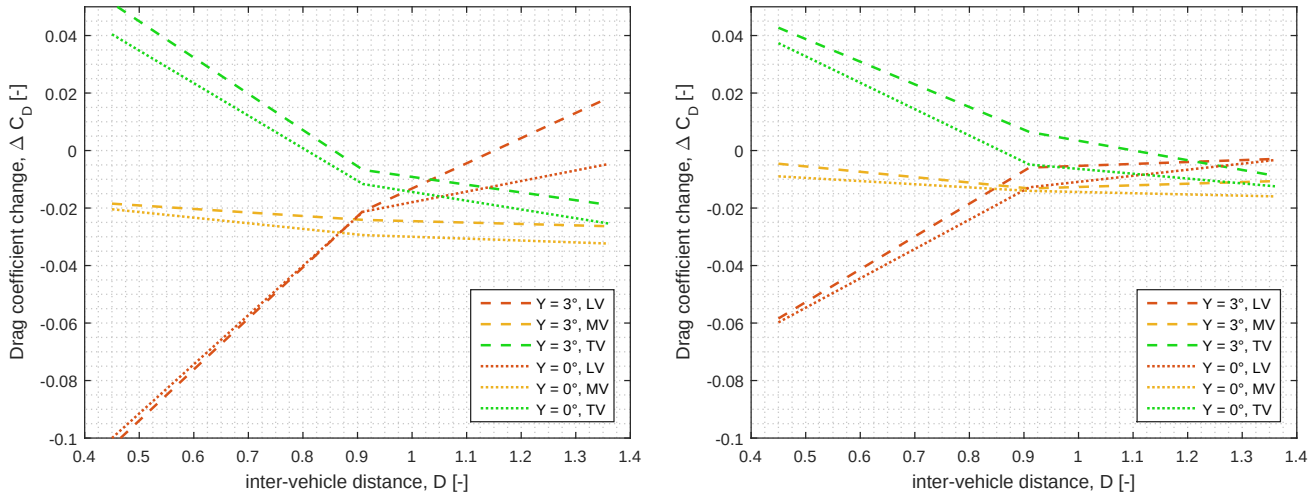

(a) 't0t0t12' (b) 't12t12t12'

Figure 4.44: Effect of the yaw angle on the drag reductions of the different vehicles in a platoon. The frontal edge radius is 0.27 m. The reference drag coefficient was the value from the corresponding geometry in isolation.

For the vehicles with the lowest radius, the complexity of the results increases. This can be due to the fact that the RANS simulations have difficulties to cope with the complex flow separation and reattachment. The drag reductions can be seen in Figure 4.45. Some differences occur between the 't6t6t12' and the 't12t12t12' configuration. In the 't12t12t12' configuration, both the middle and the trailing vehicle do not experience a significant different in drag reductions due to the cross wind. The trailing vehicle however, experiences a much lower drag reduction when a yaw angle is applied. When looking at the 't6t6t12' configuration, the behaviour of the lead vehicle remains the same. The middle and trailing vehicle experience higher drag reductions in cross wind conditions for specific inter-vehicle distances.

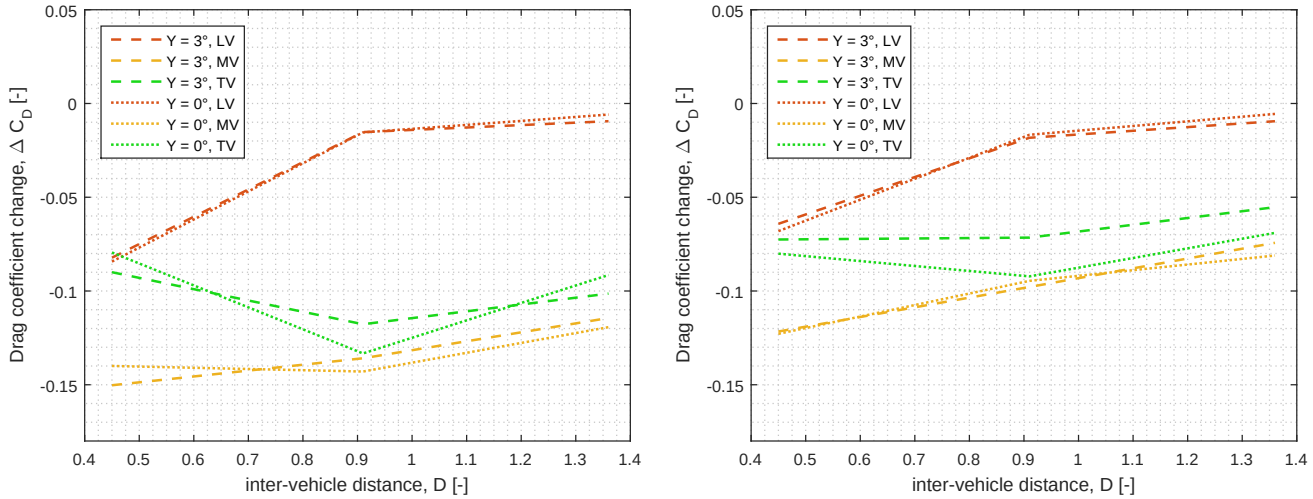

(a) 't6t6t12'

(b) 't12t12t12'

Figure 4.45: Effect of the yaw angle on the drag reductions of the different vehicles in a platoon. The frontal edge radius is 0.135 m. The reference drag coefficient was the value from the corresponding geometry in isolation.

The different contributions to the drag of the trailing vehicle in the two configurations can be seen in Figure 4.46. It is noticed that the drag reductions of the front part are decreased when cross wind conditions are applied. This effect is more pronounced for the inter-vehicle distance of 0.91. This causes the drag reductions to decrease for the case with cross wind.

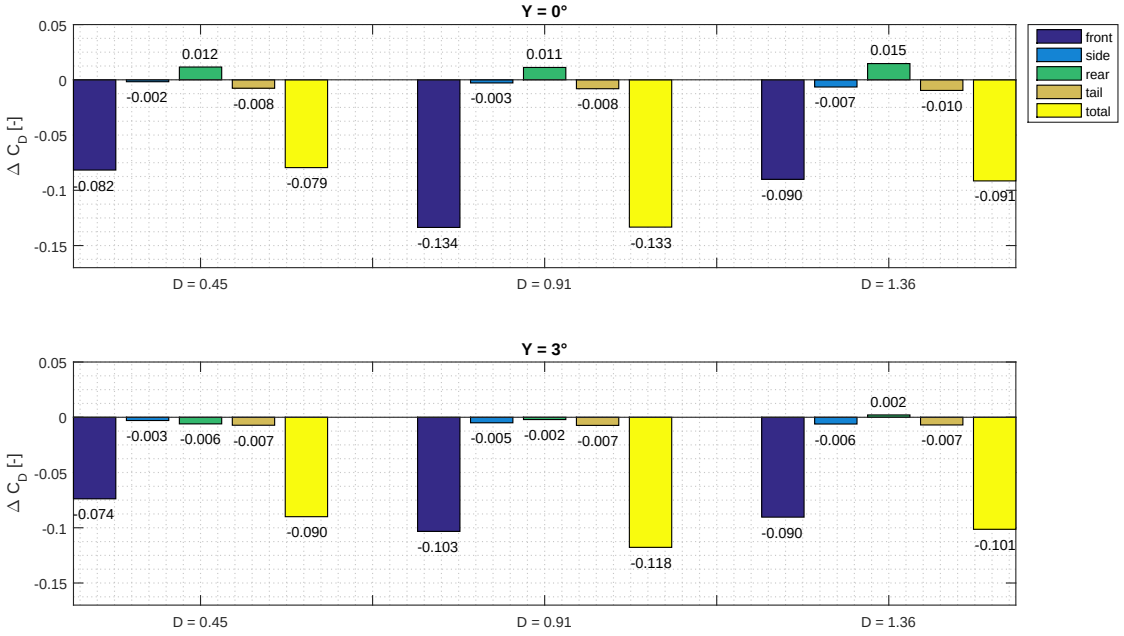

(a) 't6t6t12'

Figure 4.46: Effect of the yaw angle on the drag reductions of the trailing vehicle, with a frontal edge radius of 0.135 m, in a platoon.

It was already discussed in section 4.1 that the lead vehicle redirects the flow such that the following vehicles experience significantly lower side forces. This effect becomes slightly less pronounced when the tails are deflected more inwards. The side forces of the middle and trailing vehicle increase when the tail angle of the leading vehicle is increased. This can be seen in Figure 4.47. The trailing vehicle experiences the lowest side force. The side force of the leading vehicle increases slightly when the inter-vehicle distance is decreased. This can be due to the influence of the middle vehicle on the flow around the lead vehicle. This effect is however rather small.

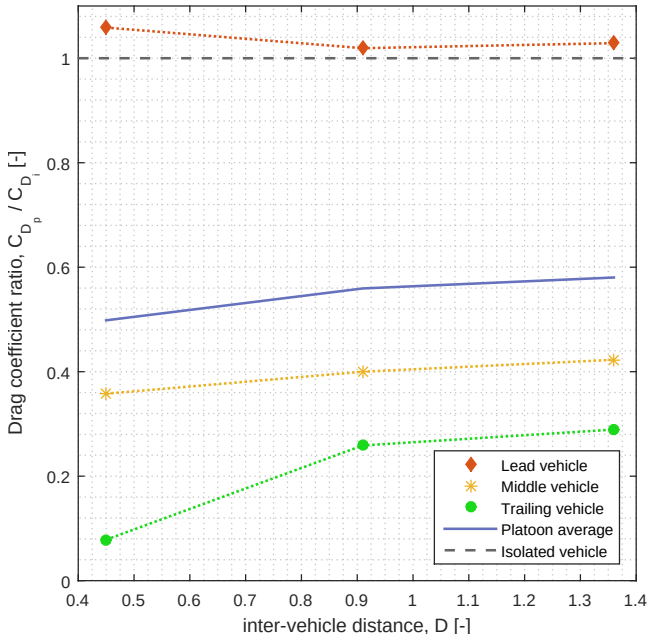

(a) 't0t0t12' configuration

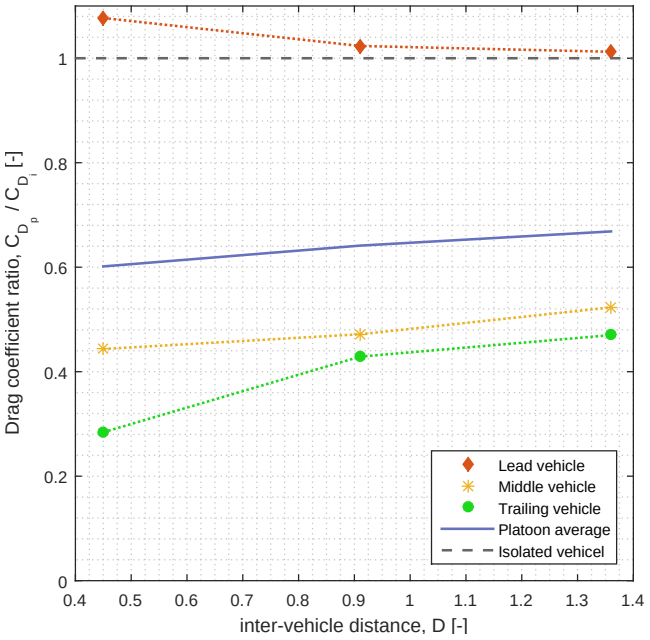

(b) 't6t6t12' configuration

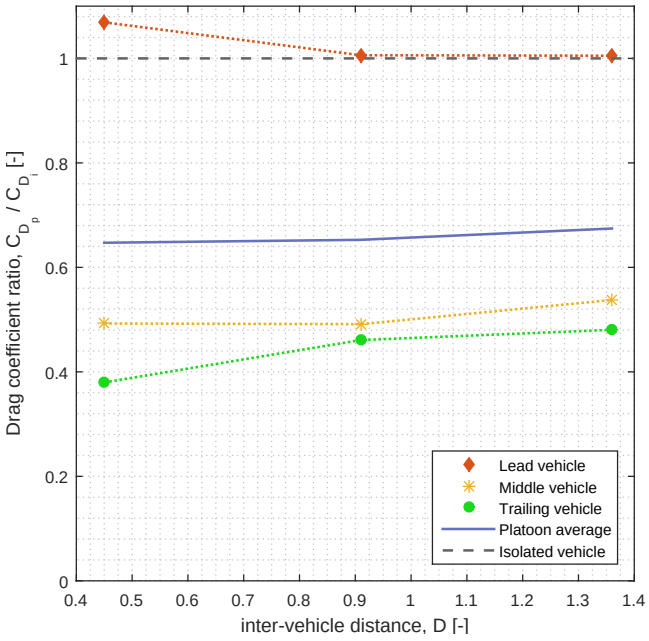

(c) 't12t12t12' configuration

Figure 4.47: Effect of the inter-vehicle distance on the side force coefficient of the vehicles in different platoons. The frontal edge radius is 0.27 m.

4.3.4 Absolute drag values

All the effects of platooning are illustrated by showing the drag and side forces relative to those in isolation. This way, the effect of the different configurations on the effectiveness of a platoon is studied. However, a comparison can still be made with absolute values in order to check whether a less streamlined configuration suddenly outperforms a more streamlined configuration if both are placed in a platoon. The absolute drag coefficients as a function of the inter-vehicle distance and the frontal edge radius are shown in Figure 4.48 for the 't6t6t12' configuration and in Figure 4.49 for the 't12t12t12' configuration. It can be seen that the vehicles with the larger frontal edge radius still outperform the vehicles with a lower radius. The trend of the lead vehicle drag shows the least variation with the inter-vehicle distance as the front part of this vehicle is not affected by the platoon formation. The platoon average drag coefficient becomes less dependent on the inter-vehicle distance when the frontal edge radius is increased. All the drag coefficient results for the 'ttt' configurations can be seen in Tables A.5–A.8 in Appendix A.

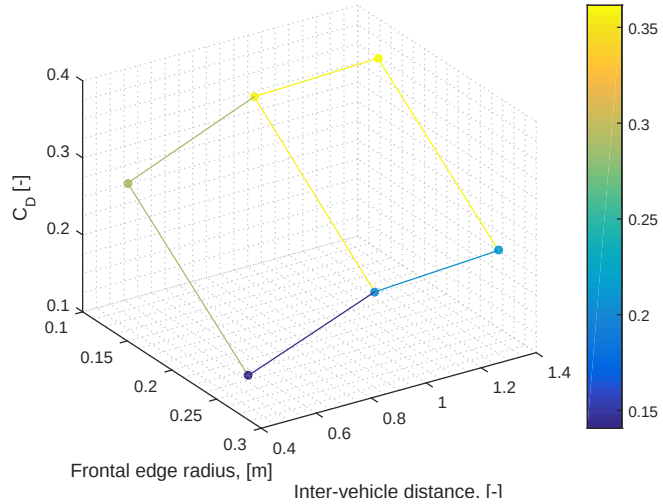

(a) Lead vehicle

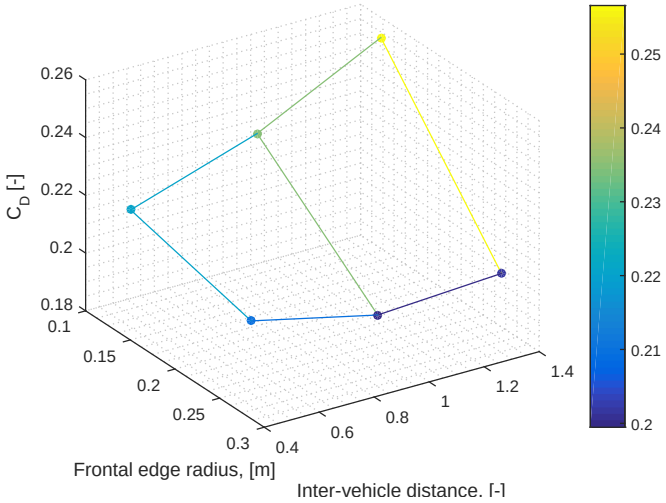

(b) Middle vehicle

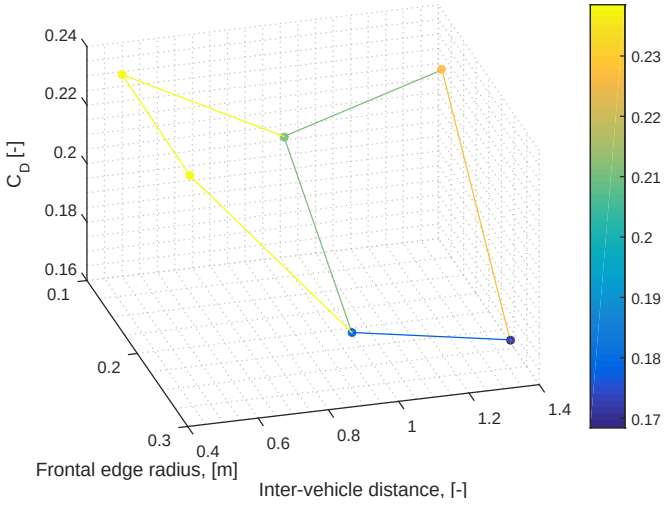

(c) Trailing vehicle

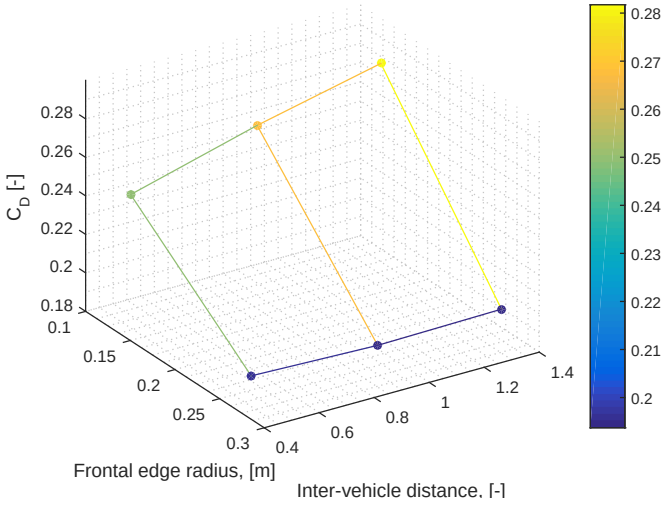

(d) Platoon average

Figure 4.48: Drag coefficients for all vehicles and the platoon average of the 't6t6t12' configuration for different inter-vehicle distances and frontal edge radii. The yaw angle is 3°.

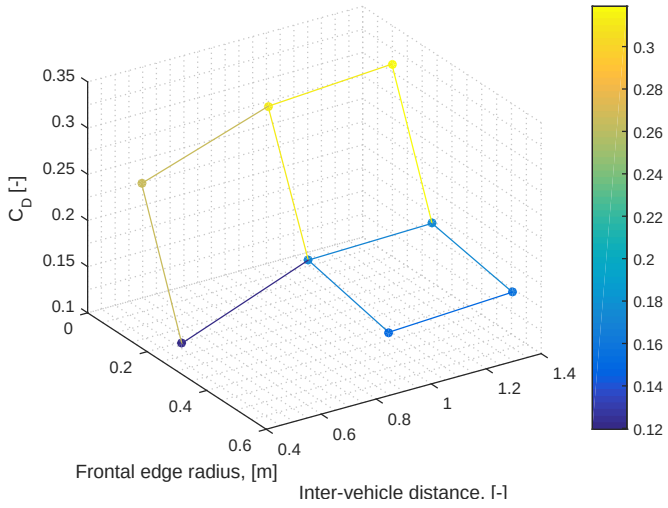

(a) Lead vehicle

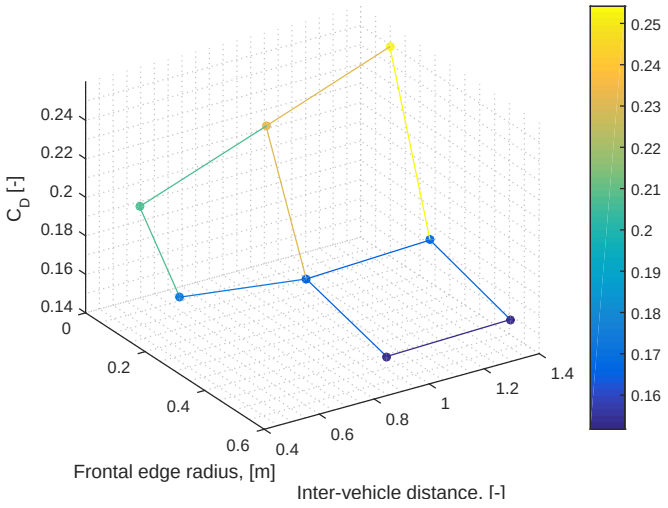

(b) Middle vehicle

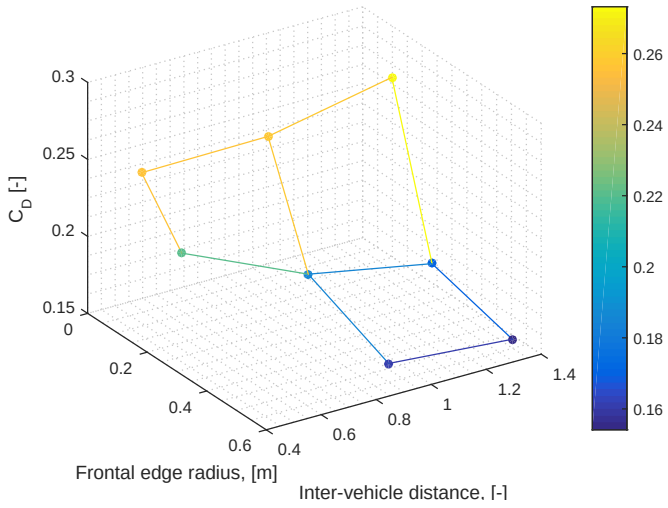

(c) Trailing vehicle

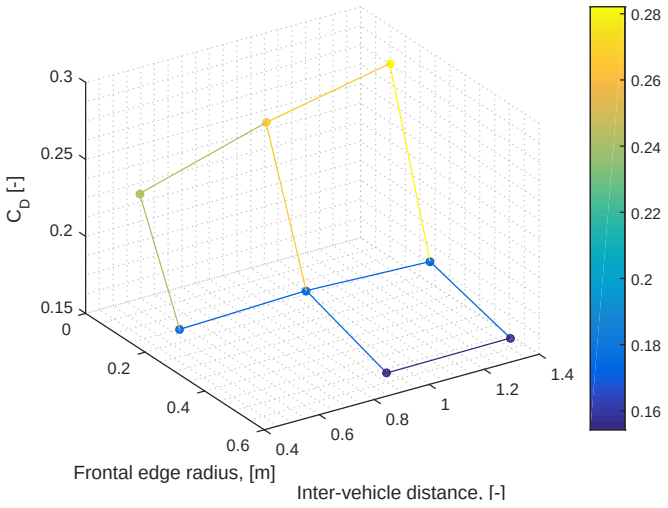

(d) Platoon average

Figure 4.49: Drag coefficients for all vehicles and the platoon average of the 't12t12t12' configuration for different inter-vehicle distances and frontal edge radii. The yaw angle is 3°.

4.3.5 Summary of the 'ttt' configurations

The addition of various tails to the platoon formation did not affect the trends of the drag reductions of the platoon drastically. Although, several interesting effects take place when varying the tail angles. The drag in isolation of the vehicles decreases due to the addition of tails, therefore their absolute drag reductions also decrease. The relative drag decrease of the lead vehicle remains unaffected by the variation of the tail angle. The change of a vehicle's tail angle has a specific effect on the following vehicle. The effect of deflecting the tail of a vehicle strongly depends on the inter-vehicle distance and on the tail angle itself.

It can be stated that deflecting a tail inward has two main effects on the following vehicle. Firstly, increasing the tail angle increases the stagnation pressure on the frontal surface while, at the same time, it reduces the negative pressure peak on the edges and thus reduces the thrust force on the frontal edges as seen before in section 4.1. Secondly, increasing the tail angle deflects the streamlines more inward and reduces the size of the wake. This causes the dynamic pressure, experienced by the following vehicles, to increase with respect to the 'nnn' configuration. Changing the tail angle thus has the same global effect on the vehicles as changing the inter-vehicle distance, they both decrease the influence of the wake on the following vehicle. Whether the combination of these effects increases or decreases the drag reductions in the platoon depends on the inter-vehicle distance and the tail angle.

For the vehicles with a frontal edge radius of 0.27 m, the total drag of the trailing vehicle is first increased when the tail angle is increased from 0° to 6°, but it is decreased when increasing the tail angle from 6° to 12°. The drag changes of the front part of the vehicle were not affected significantly when deflecting the tail from 0° to 6°. Deflecting it from 6° to 12° reduced the drag coefficient of the front part. The drag behaviour for the vehicles with a frontal edge radius of 0.135 m is more complex. While the total drag reductions were always decreased for an increasing tail angle, the change in drag reductions of the front part was not monotonic. For the inter-vehicle distance of $0.45 - 0.91$, the front drag reductions increased when the tail is deflected from 0° to 6°, but they decrease when the tail is deflected from 6° to 12°. For the largest inter-vehicle distance the front drag reductions always decrease for the vehicles with a frontal edge radius of 0.135 m. If the combination of the inter-vehicle distance and the tail angle is low, the front drag reductions are increased by the deflection of the tails. If the combination is high, the front drag reductions decrease when the tails are deflected inwards. When the tail angle is kept constant, the drag reductions are increased when the inter-vehicle distance is increased from 0.45 to 0.91. Increasing the distance to 1.36 makes the drag reductions decrease again, except for the platoons without a tail angle.

It was shown that the lead vehicle redirects the flow such that the middle and trailing vehicle experience a significantly lower side force. This effect was less pronounced when the tail angle of the lead and middle vehicle was increased. Now that all platoon configurations are discussed. chapter 5 will compare the different platoons for every individual vehicle as well as for the platoon average values.

Chapter 5

Platoon Comparison

In Chapter 4 the differences between the three vehicles are discussed for every platoon. This chapter will focus on the difference in performance between the different platoon configurations for every individual vehicle as well as for the platoon average. Using these results, the optimal platoon configuration can be found and the decrease in drag can be linked to fuel savings. First, sections 5.1–5.4 compare the different platoon configurations for every individual vehicle. The trailing vehicle is discussed before the middle vehicle since the middle vehicle experiences the same effects as the trailing and lead vehicle, but combined. At last, section 5.5 shows the optimal platoon configuration. The optimal platoon can be defined in two ways. The platoon that has the highest drag reduction, i.e. $C_D\%$ and ΔC_D, due to the platoon formation and the platoon with the lowest absolute platoon averaged drag values.

5.1 Leading vehicle

When looking at the results for all leading vehicles in Figure 5.1(a), it can be regarded that the vehicles with the more rounded frontal edge radii benefit more from the platoon configuration compared to their own drag coefficient. This can be explained by the fact that, for the more streamlined vehicles, the pressure drag due to the wake resembles a larger portion of the total drag than for the configurations with the lower front curvature radius. If one looks at the absolute drag reductions in Figure 5.1(b), the clear distinction between the different frontal edge radii is absent . For the smallest inter-vehicle distance, the main difference in drag reductions come from the addition and deflection of a tail. This is logical since the platoon formation only affects the rear part of the leading vehicle. Vehicles with less deflected tails or no tails show the largest decrease in drag coefficient. Increasing the inter-vehicle distance makes the differences between the configurations less pronounced. It must be noted that the result for the largest inter-vehicle distance is ignored in the case of the 't0t0t12' configuration. This shows a drag coefficient that is much larger than for a vehicle in isolation. This is caused by numerical errors, since the drag coefficient should go to unity for increasing inter-vehicle

distance.

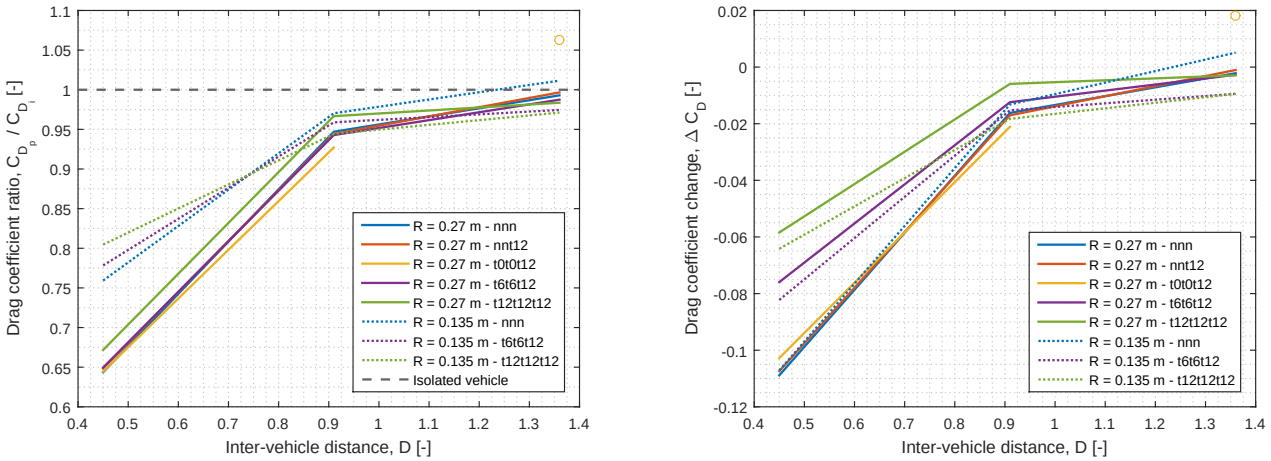

(a) Drag coefficient ratio

(b) Drag coefficient change

Figure 5.1: Effect of the platoon configuration on the drag coefficient reductions of the lead vehicle with a yaw angle of 3°. The circle is the data point for the 't0t0t12' configuration.

Figure 5.2 shows the absolute drag coefficient of all lead vehicles. It is clear that for all configurations, the drag coefficient is lowest for the lowest inter-vehicle distance. For a given distance, the drag decreases when the vehicles are more streamlined, i.e. large frontal edge radius or more deflected tail. Changing the frontal edge radius of the lead vehicle seems to be much more significant in reducing the drag than the addition and angle of a tail. Since the lead vehicle in a platoon is only affected by a following vehicle, the only advantage it gains comes from the increases base pressure. Therefore, the drag of the lead vehicle is affected more by the platoon if the largest contribution to the drag originates from the rear surface. Therefore the frontal edges of the leading vehicle should be increased as much as possible. This will both increase the absolute performance of the lead vehicle and the drag reductions due to the platoon.

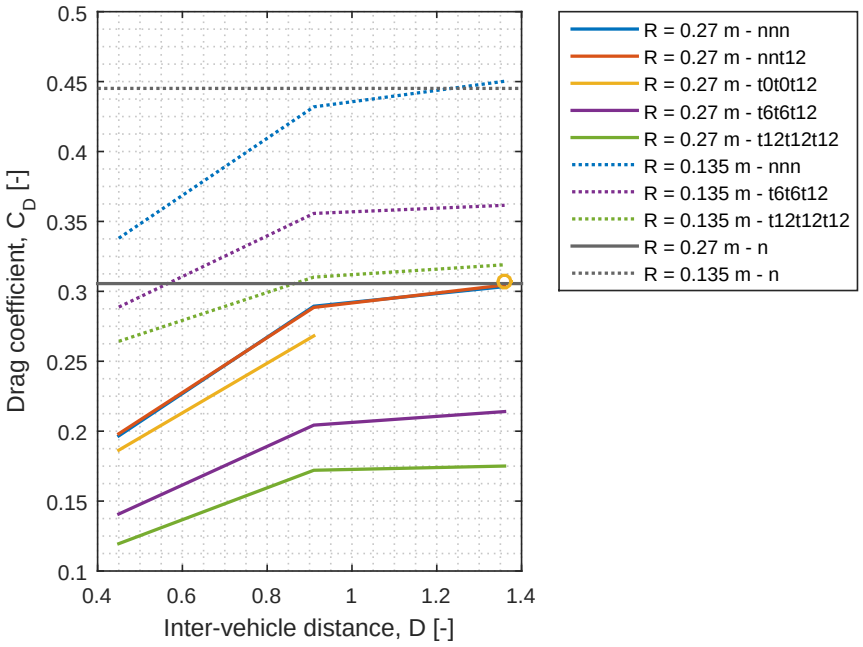

Figure 5.2: Drag coefficient of the lead vehicle in all platoon configurations with a yaw angle of 3°. The circle is the data point for the 't0t0t12' configuration.

5.2 Trailing vehicle

In Figure 5.3, it can be seen that at the closest inter-vehicle distance the trailing vehicle experiences an increase in drag due to platooning when the frontal edge radius is 0.27 m. This is due to the fact that the forward force on the frontal edges represents a large part of the entire front drag. This forward force is largely decreased due to the inward deflected streamlines coming from the vehicle in front. The tail angle of the trailing vehicle remains fixed for most of the platoon configurations, so the effects that are seen due to a tail angle variation are only due to the changes in tail angle of the vehicles in front. The most important result here is that, if the trailing vehicle has a smaller frontal edge radius, its drag coefficient becomes more sensitive to the change in tail angle of the middle vehicle. For an inter-vehicle distance of 0.91, the difference between the 't6t6t12' and the 't12t12t12' configuration is 14% or 0.0455 when the frontal edge radius is 0.135 m. This difference is only 3.6% or 0.0071 when the radius is 0.27 m. When the tail of the middle vehicle is deflected more inwards, the drag reduction of the trailing vehicle decreases. Again the vehicles with the least streamlined geometry (no/less deflected tails and lower frontal edge radius) show the highest decrease in drag due to the platoon.

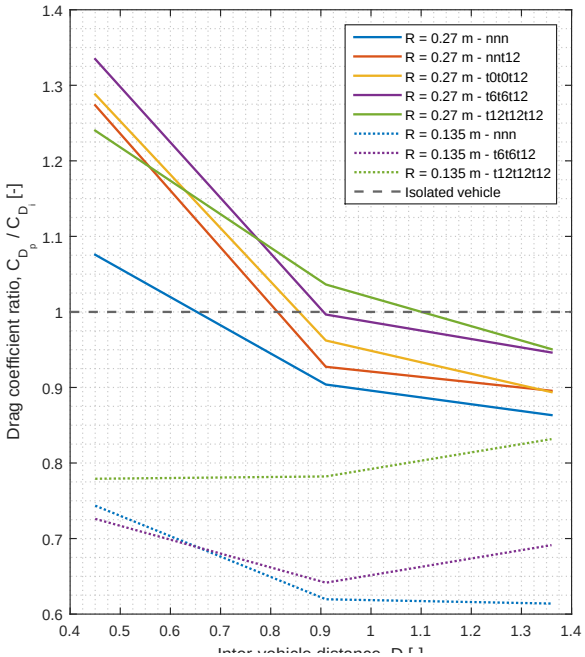

(a) Drag coefficient ratio

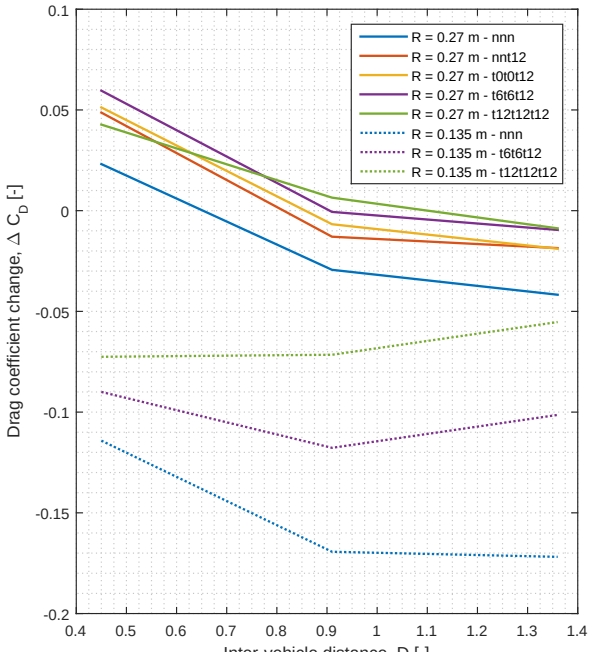

(b) Drag coefficient change

Figure 5.3: Effect of the platoon configuration on the drag coefficient reductions of the trailing vehicle.

The absolute drag coefficient in Figure 5.4 indicates that adding a tail on the middle vehicle is disadvantageous for the drag of the trailing vehicle. For an inter-vehicle distance of 0.91 and a frontal edge radius of 0.27m, the drag coefficient increases from 0.1650 to 0.1844 when adding a tail to the middle vehicle and deflecting it to an angle of 12°. The streamlines are deflected due to the tail of the middle vehicle. These streamlines decreases the beneficial effect of the platoon on the trailing vehicle. Again, this effect proves to be more significant for the vehicles with a small frontal edge radius.

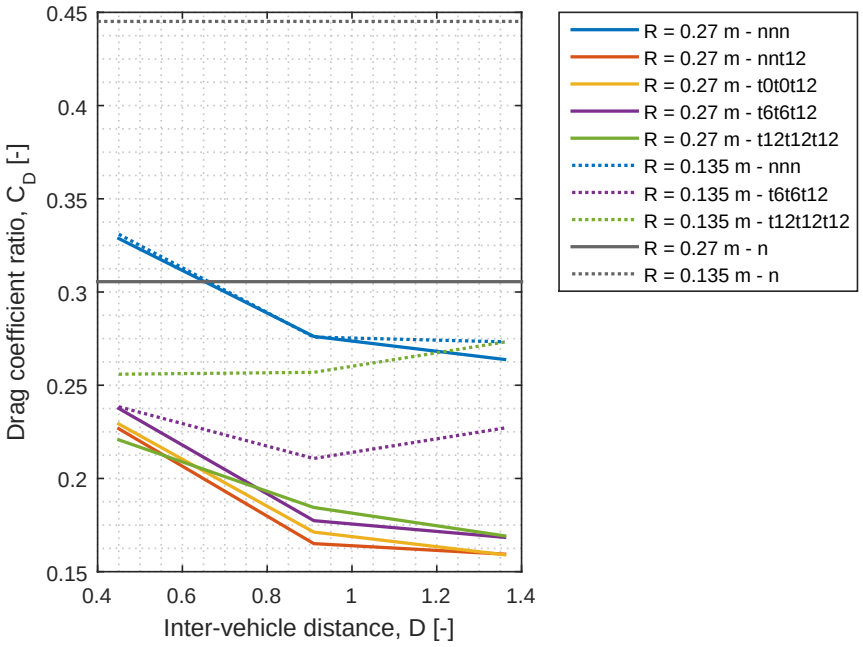

Figure 5.4: Drag coefficient of the trailing vehicles in all platoon configurations.

5.3 Middle vehicle

Looking at Figure 5.5, it is seen that for the middle vehicles with a frontal edge radius of 0.27 m, the drag decreases with increasing inter-vehicle distance. If the radius is 0.135 m, the drag increases with increasing inter-vehicle distance. This is due to the fact that in the configuration with the larger radius, the front part of the vehicles can experience an increase in drag due to the decreased suction force in the wake of a leading vehicle. Due to this effect, the potential drag reductions for the middle and trailing vehicles are significantly reduced for the configurations with a radius of 0.27 m or larger. It is also noticed that making the vehicle more streamlined by adding a tail or increasing the frontal edge radius decreases the drag reductions.

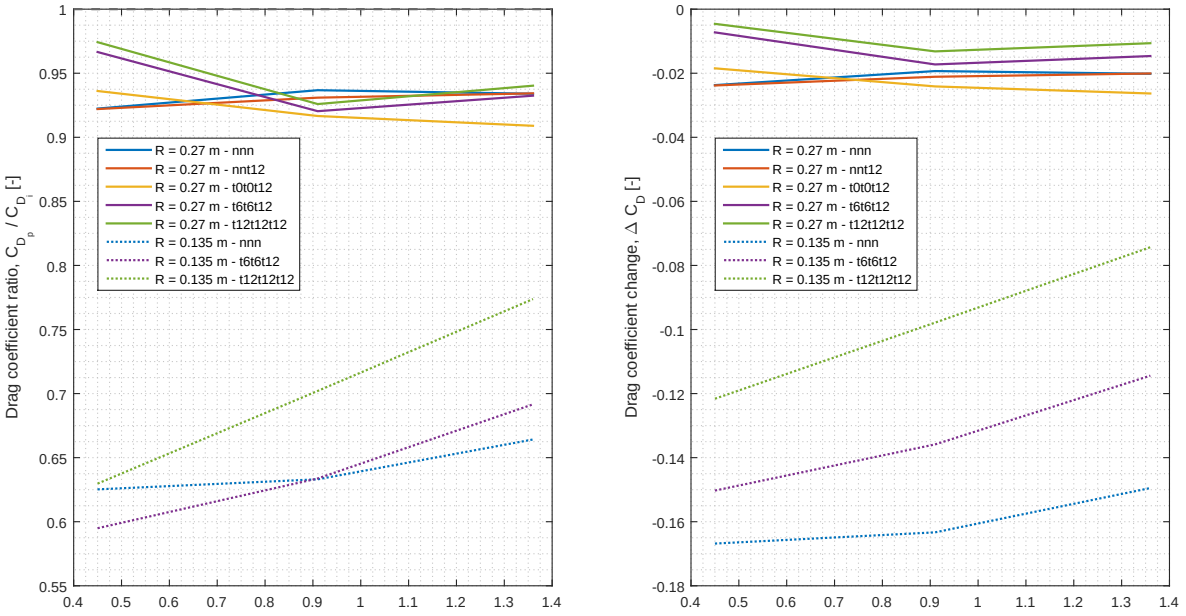

(a) Drag coefficient ratio

(b) Drag coefficient change

Figure 5.5: Effect of the platoon configuration on the drag coefficient reductions of the middle vehicle.

Figure 5.6 shows the drag coefficient of the middle vehicle in all platoon configurations. The middle vehicle experiences the most complex changes in the flow field since it is surrounded by vehicles. It is seen that some of the configurations with a lower radius outperform configurations with a higher radius unlike for the lead vehicle where the higher radius always leads to the lowest drag. This is due to the fact that the vehicles with the lowest frontal edge radius benefit a lot from the wake of the lead vehicle, while vehicles with a larger radius might experience a drag increase due to the lead vehicle's presence. It is always beneficial for the middle vehicle to add a tail to the vehicle or to increase the angle of this tail. Although this reduces the drag of the middle vehicle, this will increase the drag on the trailing vehicle. Since the tail configuration of the lead and the middle vehicle are the same in every platoon, it can be concluded that the negative influence of adding a tail on the lead vehicle is less than the decrease in drag by adding a tail to the middle vehicle itself. It also seems that adding tails to the platoon configuration decreases the sensitivity of the drag coefficient to changes of the inter-vehicle distance. For the configuration without any tails it is thus slightly better to have a smaller frontal edge radius.

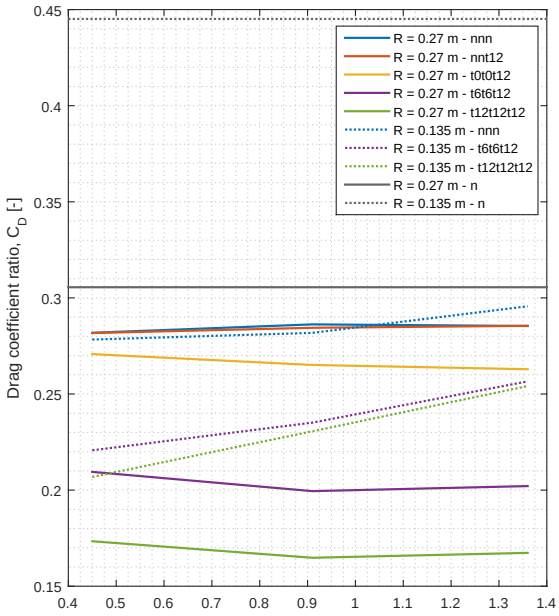

Figure 5.6: Drag coefficient of the middle vehicles in all platoon configurations.

5.4 Platoon average

Combining all of the above results, the platoon averaged drag coefficient is shown in Figure 5.7. Again it is seen that the drag reductions decrease significantly as the geometry of the vehicles becomes more streamlined, i.e. larger frontal edge radius and more deflected tails.

When looking at the absolute drag coefficients, the same trends as shown before are again present. The more streamlined the vehicles are, the lower the platoon averaged drag coefficient is. The platoon that experiences the largest drag reduction due to the platoon formation is also the platoon with the largest absolute drag increase.

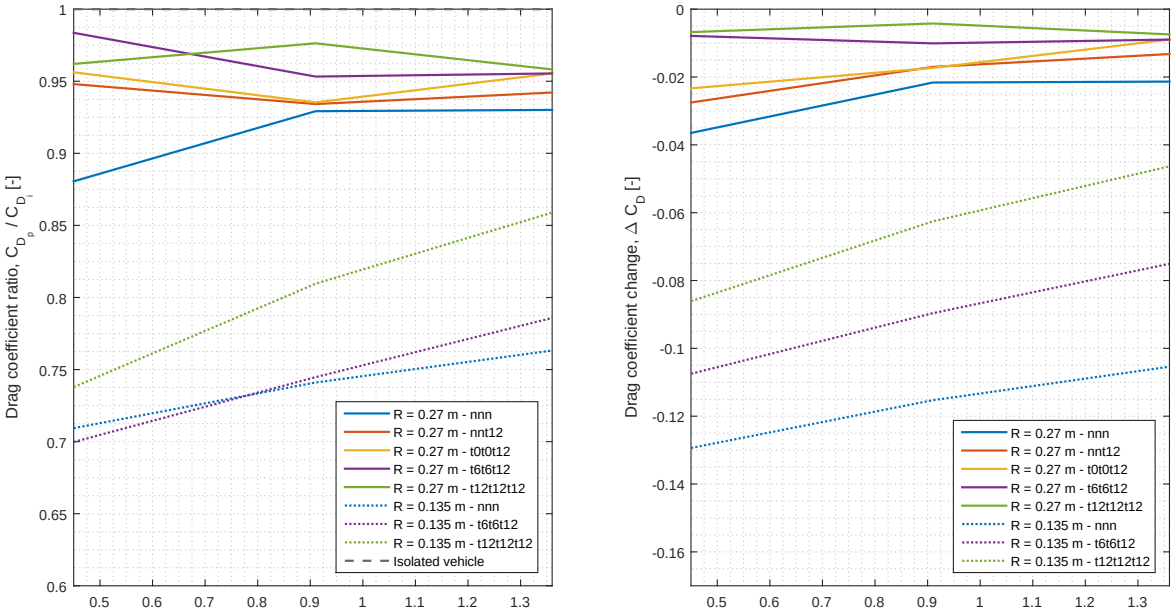

(a) Drag coefficient ratio

(b) Drag coefficient change

Figure 5.7: Effect of the platoon configuration on the platoon averaged drag coefficient reductions.

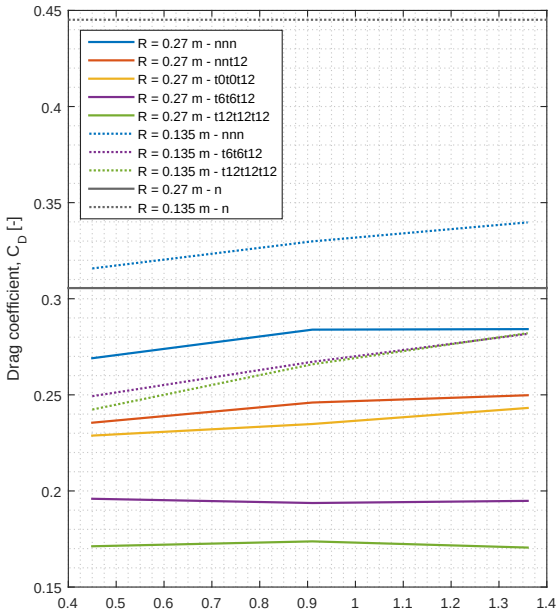

Figure 5.8: Platoon averaged drag coefficient of all configurations.

5.5 Optimal platoon

The configuration that benefits the most from the platoon formation is not necessarily the same as the the formation that experiences the lowest drag force. Considering only the reductions of drag due to the platooning, it can be stated that the 'nnn' configuration with a low frontal edge radius is optimal for every vehicle, except for the leading vehicle. This is logical since the vehicle that performs the worst can benefit the most from the advantages of a platoon formation. This platoon has a platoon average drag coefficient reduction of 0.1223 for the lowest inter-vehicle distance. This corresponds to a fuel saving of 1.71 L/100km per vehicle, according to an calculation sheet [1]. This value of course depends on the total drag of a vehicle in isolation. The drag coefficients of the used models are much smaller than the drag coefficients of a real truck. If the drag reduction in percentages, 71%, of this platoon is used to calculate the drag count of a real heavy-duty vehicle, the resultant drag decrease would be 1775 drag counts, based on a drag coefficient of 0.75 [42]. This would lead to a fuel saving of 2.48 L/100km per vehicle. Of course, this value is only an estimation but it gives an indication on how much fuel could be saved.

The platoon configuration that has the lowest absolute drag coefficient is the platoon where all vehicles are equipped with tails of 12°. This indicates that while platooning offers great advantages in drag reduction of heavy-duty vehicles, the individual shape of the vehicle is still of great importance if one wants to decrease the drag of a vehicle. Although, care should be taken when comparing geometries of vehicles that are slightly better, since the geometry that is outperformed in isolation might gain an advantage when the vehicles are placed in a platoon formation.

In real situations, the vehicles of a platoon might not have the same frontal edge radius like in this study. This study however points out that the vehicle with the most streamlined front part (largest radius) should be placed in the lead position. Vehicles with a less streamlined front part need to be placed after the lead vehicle. It is also beneficial to the platoon that the vehicle with the highest tail angle should be placed in trailing position.

[1] This calculation sheet was provied by Gandert Van Raemdonck from WABCO Automotive

Chapter 6

Conclusion & Recommendations

In this chapter, the conclusions of the different analyses will be presented along with conclusions about the used methodology. In order to improve the current work or to build further on this study, some recommendations are stated.

6.1 Conclusions

Isolated vehicle

In order to analyse a platoon of bluff bodies, the isolated GETS model was first simulated, to serve as baseline results and to show the effects of a varying frontal edge radius, tail and yaw angle on a vehicle in isolation. It was shown that the frontal edge radius influences the flow behaviour largely. The amount of thrust force generated by the low pressure region on these edges greatly determines the drag of the vehicle as well as the relative drag contribution of the front part. For the radii of 0.54 m and 0.27 m, the large thrust force decreased the drag of the front part of the vehicle significantly such that the drag contribution of the front part was lower than 15% of the total drag while the pressure drag at the rear delivered around 70% of the drag. halving the frontal edge radius to 0.135 m, caused the drag contributions of the front and rear part of the vehicle to be almost equal, about 45% of the total drag. The total drag also increased largely when the edge radius was lowered. This was mainly due to the flow separation occurring on the frontal edges.

The addition of tails proved to significantly increase the base pressure of the vehicles and decreasing the size of the wake. Adding an inward deflected tail increased the base pressure and therefore reduced the drag until the drag contribution of the rear surface was almost zero or even slightly negative for some cases, i.e. a thrust force. Adding a cross wind component to the incoming flow results in an increase in drag and a resulting side force. Making the geometries more streamlined by adding tails or by increasing the frontal edge radius made

the drag less sensitive to yaw angles. The side force on the vehicles was slightly increased by increasing the frontal edge radius, but the addition of tails decreased this side force significantly. The vehicles in cross wind acted like airfoils and redirected the flow in the near wake towards the windward side.

Effect of inter-vehicle distance

The inter-vehicle distance had a large influence on the drag of the individual vehicles. At a very short distance, the lead vehicle experienced a very large drag reduction because the low pressure in the wake of the lead vehicle was increased by the presence of the high pressure region in front of the middle vehicle. This lead to a large reduction in pressure drag origination from the rear surface of the model. When the distance is increased, the drag goes asymptotically to the value in isolation. The trailing vehicle showed the opposite behaviour. When the inter-vehicle was decreased, the drag of the trailing vehicle increased up to a certain distance between 0.23 and 0.45, after which it decreased again. The up-going trend of the drag of the trailing vehicle was explained by the fact that the streamlines were deflected inward after the middle vehicle and they experienced a deceleration due to the concave trajectory of the flow arriving at the frontal surfaces of the trailing vehicle. This lead to a decreased thrust force on the frontal edges of the trailing vehicle. The decrease in thrust force was larger than the decrease in drag due to the lower stagnation pressure on the frontal surface of the trailing vehicle. This lead to the drag increase with decreasing inter-vehicle distance. For the lowest inter-vehicle distance, the trailing vehicle was positioned inside the near-wake of the middle vehicle and the drag decreased again. The decrease in stagnation pressure became more dominant than the decrease in thrust force at the frontal edges. The middle vehicle experience a combination of the effects on the lead and trailing vehicle, its drag remains fairly constant except for the closest distance where the negative effect on the frontal part starts to decrease. These trends are similar for all platoons, the amount of drag increase or decrease however was determined by the geometric variables and the cross wind condition.

Effect of frontal edge radius

The drag reductions of the different vehicles in the platoon was mainly determined by the frontal edge radius. The relative drag reductions on the leading vehicle were higher when the frontal edge radius was larger, since then the pressure drag at the rear represents a larger portion of the total drag. The drag decrease in drag counts however only slightly changed. The effect of the frontal edges on the trailing vehicle was much more pronounced. Decreasing the frontal edge radius decreased the importance of the thrust force on the edges on the total front drag. For the large radii, the trailing vehicle experienced a drag that increased up to a value above that in isolation when the inter-vehicle distance was decreased. For the lowest inter-vehicle distance of 0.23 it was decreasing again. A trailing vehicle with the smallest frontal edge radius, 0.135 m, experienced a drag reduction. The combined effects of the lead and trailing vehicle caused the drag reductions of the middle vehicle to increase with a lower frontal edge radius.

Effect of tails

While adding a tail to the trailing vehicle did not change the drag behaviour of the vehicles drastically, several interesting effects were noticed when tails were applied on the front and middle vehicle with varying tail angle. A tail on a specific vehicle, mainly influences the vehicle driving behind the tail. It was found that for an increasing tail angle, the stagnation pressure on the frontal surface increases, which would lead to a drag increase. Besides this, the loss in thrust force on the frontal edges is reduced, this would lead to a drag decrease. Which of these two effects is larger depends on the inter-vehicle distance, the tail angle and the frontal edge radius. Next to these effects on the front drag of a following vehicle, deflecting a tail also reduced the drag reductions caused by the slower incoming flow field, i.e. the lower dynamic pressure. Deflecting a tail on the lead vehicle inward has the same effect on the middle vehicle as increasing the inter-vehicle distance, it decreases the influence of the lead vehicle's wake on the middle vehicle. When the frontal edge radius was 0.27 m, increasing the tail angle of a vehicle in front always increased the drag reduction at the front part of the following vehicles. The pressure decrease on the frontal edges due to the deflected tails is thus dominant over the pressure increase on the stagnation surface. Combining this with the effect of the lower dynamic pressure after a vehicle lead to the result that the total drag reduction of a following vehicle was decreased when the tail was deflected from 0° to 6°, but it was increased when deflection the tail from 6° to 12°. Decreasing the frontal edge radius to 0.135 m gave different results. The total drag was increased when the tails were deflected more inward, while the front drag was now only decreased when the combination of the inter-vehicle distance tail deflection was small (0° to 6°).

Effect of cross wind conditions

The effect of cross wind on the drag reduction in the platoon depended on the frontal edge radius. For a small frontal edge radius, the drag reductions due to platooning increased, while they decreased for a larger frontal edge radius. This was due to the fact that the drag reductions at the rear part became more effective with a non-zero yaw angle and those at the front became less effective. For vehicles with a large frontal edge radius, the change in drag at the front were dominant, while for the other vehicles this was reversed. Overall, the drag reductions obtained in a platoon were not much affected by the applied cross wind conditions. It is shown that the lead vehicle of a platoon redirects the flow such that the middle and trailing vehicle experience a significantly lower side force. The side force of the lead vehicle itself is not changed significantly. When inward deflected tails are applied to the lead and middle vehicle, the side force reduction on the following vehicles is diminished but still significant.

The final results showed that the platoon with the worst performing vehicles in isolation, the 'nnn' configuration with $R = 0.135$ m, experienced the largest drag reduction, namely 29%, corresponding to 1223 drag counts. If this is extrapolated to a vehicle with an initial drag coefficient as high as a real heavy-duty vehicle, this could lead to a fuel saving of 2.48 $\frac{L}{100km}$. Considering the absolute drag coefficients, the platoon with the best performing vehicles was

still the optimal platoon with the lowest drag coefficient, namely the 't12t12t12' platoon with the largest frontal edge radius. This aerodynamic analysis investigated the effect of the drag reduction devices in a platoon of bluff bodies subjected to cross wind conditions. It was shown that the frontal edge radius can determine whether the following vehicles experience a drag reduction or a drag increase. Tails reduced the drag of the individual vehicles but did also decrease the drag reductions experienced in the platoon. The drag reductions were still present under cross wind conditions. The small research gap that was present due to the discrepancies between studies was filled by explaining why trailing vehicles in some platoons experienced a drag increase, while other platoons, they experienced a drag decrease.

6.2 Recommendations

Although this conclusion concludes this study, the research on platoon aerodynamics is far from finished. Based on the performed work and on the obtained results, recommendations can be stated.

Simulation set-up

The accuracy of the used solver is of course limited. Especially the unsteadiness in the wake of the vehicle and its influence on the other vehicles is not simulated. Therefore, the decision can be made for further investigations to increase the computational time by using DES or LES. Then, the turbulent structures can be (partially) solved and the unsteadiness of the flow can be taken into account. This study used wind tunnel experiments on a single GETS model to validate the CFD simulations. Although the obtained results were similar to results of platoons with other vehicle models. The results of the different platoons should be validated with wind tunnel experiments on a platoon of GETS models.

Vehicle model and platoon configurations

The truck model that is used had several disadvantages. The main disadvantage is the fact that the drag of the model is a lot smaller than for real heavy-duty vehicles. This influences the absolute drag reductions and thus the predicted fuel savings. The drag coefficient decrease in percentages on the other hand is less influenced by the total drag of the vehicle but more by the drag contribution of the different vehicle parts. It can thus be recommended to use a more detailed model of a heavy-duty vehicle or to perform one simulation on a highly detailed geometry and then use this result to build a simplified model that has the same relative drag contributions of the different parts of the vehicle. For this study, this could lead to a certain frontal edge radius that is more representative for the currently operating heavy-duty vehicles. The simplified GETS model can be extended with a gap between the tractor and trailer, since this gap largely influences the drag and the relative drag contributions.

In the used platoon configurations, the tails on the vehicles were different for the different platoon positions. The frontal edge radius is kept the same for all vehicles. The variation of this radius with the platoon position would be very interesting to investigate. It was shown in this study that the lead vehicle drag reductions were increased when its frontal edge radius was increased. But if both vehicles have different tails and different frontal edge radii, it is still unclear which vehicle should be best placed in front. This study could be combined with an optimisation algorithm that defines the best platoon for a given set of different vehicles. Besides changing the frontal edge radius, the entire shape of the forebody can be altered. In the near future, regulations will be adapted in order to allow trucks to have an increased forebody length. This could lead to trucks with a certain nose shape, similar to the American heavy-duty vehicles.

Extra research topics

The influence of the wake size on the critical inter-vehicle distance where the drag of a following vehicle starts to decrease again for smaller inter-vehicle distances is only touched on slightly in this study. A follow-up study can focus on this phenomenon. Several platoons with different sized vehicles could be tested in order to find the critical inter-vehicle distance as a function of the vehicle size and wake size. The difference in inter-vehicle distance should therefore be smaller than for this study.

The applied tails in this study had such a length that the horizontal extension of the vehicle was always 1.5 m. However, when a certain tail would be deflected inward during the operation of the vehicle, its horizontal length would be decreased and its influence on the flow would be less. Other investigation can focus on the implementation of tails that are varied during the operation of the vehicle.

A topic that is not studied in this thesis is the effect of the reduced mass flow through the engine when driving in a platoon. If the mass flow through the engine is decreased significantly, this could reduce the performance of the engine or increase the need for a cooling system to be activated. This could potentially reduce the fuel savings.

Bibliography

[1] "United Nations Framework Convention on Climate Change." [Online]. Available: http://unfccc.int/meetings/paris{_}nov{_}2015/meeting/8926.php

[2] A. Kuhlman, "Peak Oil, info & strategies." [Online]. Available: http://www.oildecline.com/

[3] R. Muncrief and B. Sharpe, "Overview of the heavy-duty vehicle market and CO2 emissions in the European Union," 2015.

[4] R. Pankajakshan, B. Mitchell, and D. L. Whitfield, "Full-scale simulations of drag reduction devices for class 8 trucks," *Lecture Notes in Applied and Computational Mechanics*, vol. 41, pp. 339–348, 2009.

[5] K. Sreenivas, B. Mitchell, S. Nichols, D. Hyams, and D. Whitfield, "Computational simulation of the GCM tractor-trailer configuration," *Lecture Notes in Applied and Computational Mechanics*, vol. 41, pp. 325–338, 2009.

[6] Harwell and Didcot, "Good Practice Guide: Truck Aerodynamic Styling," Department for Transport, Tech. Rep., 2001.

[7] C. Bonnet and H. Fritz, "Fuel Consumption Reduction Experienced by two Promote-Chauffeur Trucks in Electronic Towbar Operation," *Traffic*, vol. 8, pp. 1–8, 2000.

[8] S. Tsugawa, S. Kato, and K. Aoki, "An automated truck platoon for energy saving," *IEEE International Conference on Intelligent Robots and Systems*, pp. 4109–4114, 2011.

[9] P. Hong, B. Marcu, F. Browand, and A. Tucker, "Drag Forces Experienced by Two , Full-Scale Vehicles at Close Spacing at Close Spacing," *Transportation*, no. February, 1998.

[10] J. Eckhardt, "European Truck Platooning Challenge 2016," 2016. [Online]. Available: www.eutruckplatooning.com

[11] S. Ashley, "Truck platoon demo reveals 15% bump in fuel economy," *SAE International*, 2013.

[12] "ISSUU - tno_truckplatooning_whitepaper by Eisma Media Groep bv."

[13] R. M. Wood, "A Discussion of a Heavy Truck Advanced Aerodynamic Trailer System," 2006.

[14] J. M. Ortega, T. Dunn, R. McCallen, and K. Salari, "Computational Simulation of a Heavy Vehicle Trailer Wake," in *The Aerodynamics of Heavy Vehicles: Trucks, Buses, and Trains*, F. Pfeiffer and P. Wriggers, Eds., 2002.

[15] G. Van Raemdonck, "Design of Low Drag Bluff Road Vehicles," Ph.D. dissertation, TU Delft, 2012.

[16] P. Das, M. Tsubokura, T. Matsuuki, N. Oshima, and K. Kitoh, "Large Eddy Simulation of the flow-field around a full-scale heavy-duty truck," *Procedia Engineering*, vol. 56, pp. 521–530, 2013. [Online]. Available: http://dx.doi.org/10.1016/j.proeng.2013.03.155

[17] K. Cooper, "Commercial Vehicle Aerodynamic Drag Reduction: Historical Perspective as a Guide," in *The Aerodynamics of Heavy Vehicles: Trucks, Buses, and Trains*, F. Pfeiffer and P. Wriggers, Eds., 2002.

[18] I. Hucho, "Aerodynamics of Road Vehicles," *Annual Review of Fluid Mechanics*, vol. 25, pp. 485–537, 1993.

[19] M. Hammache and F. Browand, "On the Aerodynamics of Tractor-Trailers," in *The Aerodynamics of Heavy Vehicles: Trucks, Buses, and Trains*, F. Pfeiffer and P. Wriggers, Eds., 2002.

[20] C. L. News, "Canada Considering Legalization of Payload Boat Tails," 2015. [Online]. Available: http://cdllife.com/2012/top-trucking-news/canada-considering-legalization-of-payload-boat-tails/

[21] R. C. Mccallen, K. Salari, J. M. Ortega, and C. J. Roy, "DOE s Effort to Reduce Truck Aerodynamic Drag Joint Experiments and Computations Lead to Smart Design," no. July, pp. 1–16, 2004.

[22] A. Davila, "Report on Fuel Consumption," Tech. Rep., 2013. [Online]. Available: http://www.sartre-project.eu/en/publications/Documents/SARTRE{_}4{_}003{_}PU.pdf

[23] R. M. Pagliarella, "On the Aerodynamic Performance of Automotive Vehicle Platoons Featuring Pre and Post-Critical Leading Forms," Ph.D. dissertation, 2012.

[24] G. K. Rajamani, "CFD Analysis of Air Flow Interactions in Vehicle Platoons," *Manufacturing Engineering*, no. August, 2006.

[25] S. Watkins and G. Vino, "The effect of vehicle spacing on the aerodynamics of a representative car shape," *Journal of Wind Engineering and Industrial Aerodynamics*, vol. 96, pp. 1232–1239, 2008.

[26] M. Zabat, N. Stabile, S. Farascaroli, and F. Browand, "The Aerodynamic Performance Of Platoons: A Final Report," *California Partners for Advanced Transit and Highways (PATH)*, 1995. [Online]. Available: http://escholarship.org/uc/item/8ph187fw{#}page-1

[27] J. Smith, R. Mihelic, B. Gifford, and M. Ellis, "Aerodynamic Impact of Tractor-Trailer in Drafting Configuration," pp. 619–625, 2014. [Online]. Available: http://www.sae.org/technical/papers/2014-01-2436

[28] S. P. Doppenberg, "Drag Influence of Tails in a Platoon of Bluff Bodies," Master's thesis, Delft University of Technology, 2015.

[29] B. Marcu and F. Browand, "Aerodynamic Forces Experienced by a 3-Vehicle Platoon in a Crosswind," *Vehicle Aerodynamics and Wind Noise*, no. 724, 1999.

[30] G. Van Raemdonck and M. Van Tooren, "Time-Averaged Phenomenological Investigation of a Wake behind a Bluff Body," *BBAA VI International Colloquium on: Bluff Bodies Aerodynamics & Applications*, pp. 20–24, 2008. [Online]. Available: http://bbaa6.mecc.polimi.it/uploads/validati/Tbaf09.pdf

[31] D. Pointer, T. Sofu, J. Chang, and D. Weber, "Applicability of commercial CFD tools for assessment of heavy vehicle aerodynamic characteristics," in *The Aerodynamics of Heavy Vehicles II: Trucks, Buses, and Trains*, F. Pfeiffer and P. Wriggers, Eds., vol. 41. Springer, 2007, pp. 349–361.

[32] S. B. Pope, *Turbulent Flows*. Cambridge University Press, 2013.

[33] F. M. White, *Viscous Fluid Flow*. McGraw-Hill, 2006.

[34] SAE International, "Surface Vehicle Recommended Practice," 2013.

[35] B. R. McAuliffe, L. Belluz, and M. Belzile, "Measurement of the On-Road Turbulence Environment Experienced by Heavy Duty Vehicles," *SAE International Journal of Commercial Vehicles*, vol. 7, no. 2, pp. 685–702, 2014. [Online]. Available: http://papers.sae.org/2014-01-2451/

[36] T. Favre, "Aerodynamics simulations of ground vehicles in unsteady crosswind," Ph.D. dissertation, KTH School of Engineering Sciences, 2011.

[37] Fluent, "ANSYS Fluent User ' s Guide," vol. 15317, no. November, p. 2498, 2011. [Online]. Available: http://cdlab2.fluid.tuwien.ac.at/LEHRE/TURB/Fluent.Inc/v140/flu{_}ug.pdf

[38] M. Lanfrit, "Best practice guidelines for handling Automotive External Aerodynamics with Fluent," vol. 2, pp. 1–14, 2005.

[39] "Bußgeldkatalog - Bußgeld Abstand." [Online]. Available: http://bussgeldkatalog.kfz-auskunft.de/abstand.html

[40] B. Scheepers, J. Ploeg, and R. Wouters, "Towards Implementation Of Truck Platooning On Public Roads."

[41] C. J. Baker, "Ground Vehicle in High Cross Winds Part I: Steady Aerodynamic Forces," *Journal of Fluids and Structures*, vol. 5, pp. 69–90, 1991.

[42] G. Leduc, *Longer and Heavier Vehicles: An overview of technical aspects*, 2009.

Appendix A

Absolute drag values of all vehicles

Table A.1 shows all the exact values of the total drag coefficients of the simulated models in isolation.

Table A.1: Drag coefficients of all simulated vehicles in isolation.

	$Y = 0°$			$Y = 3°$		
	$R = 0.135$	$R = 0.27$ m	$R = 0.54$ m	$R = 0.135$ m	$R = 0.27$ m	$R = 0.54$ m
no tail	0.4208	0.3005	0.2881	0.4451	0.3055	0.2918
$t = 0°$	0.4062	0.2852	0.2691	0.4245	0.2893	0.2721
$t = 6°$	0.3590	0.2131	0.1949	0.3710	0.2167	0.1986
$t = 12°$	0.3215	0.1756	0.1566	0.3251	0.1780	0.1582

Table A.2 and Table A.3 show all the resulting drag coefficients of the vehicles in the 'nnn' configuration. Per vehicle, the values are ranged from lowest inter-vehicle distance to highest. It is clear that while, less streamlined vehicles have significantly more benefit from driving in a platoon, the more streamlined vehicles still experience the least amount of drag.

Table A.2: Drag coefficients of all simulated vehicles in the 'nnn' configuration.

	$Y = 0°$		
	$R = 0.135$ m	$R = 0.27$ m	$R = 0.54$ m
Leading vehicle	0.27 - 0.32 - 0.41 - 0.43	0.13 - 0.19 - 0.28 - 0.30	n/a - 0.18 - 0.27 - 0.29
Middle vehicle	0.19 - 0.26 - 0.27 - 0.28	0.20 - 0.27 - 0.27 - 0.27	n/a - 0.26 - 0.26 - 0.25
Trailing vehicle	0.28 - 0.31 - 0.27 - 0.26	0.30 - 0.31 - 0.26 - 0.25	n/a - 0.30 - 0.25 - 0.24
Platoon average	0.25 - 0.30 - 0.32 - 0.33	0.21 - 0.26 - 0.27 - 0.27	n/a - 0.25 - 0.26 - 0.26

Table A.3: Drag coefficients of all simulated vehicles in the 'nnn' configuration.

	$Y = 3°$		
	$R = 0.135$ m	$R = 0.27$ m	$R = 0.54$ m
Leading vehicle	0.27 - 0.34 - 0.43 - 0.45	0.12 - 0.20 - 0.29 - 0.30	n/a - 0.19 - 0.28 - 0.29
Middle vehicle	0.20 - 0.28 - 0.28 - 0.29	0.23 - 0.28 - 0.29 - 0.28	n/a - 0.27 - 0.27 - 0.27
Trailing vehicle	0.34 - 0.33 - 0.28 - 0.27	0.36 - 0.33 - 0.28 - 0.26	n/a - 0.32 - 0.26 - 0.25
Platoon average	0.27 - 0.32 - 0.33 - 0.34	0.24 - 0.27 - 0.28 - 0.28	n/a - 0.26 - 0.27 - 0.27

Table A.4 shows all the resulting drag coefficients of the vehicles in the 'nnt12' configuration.

Table A.4: Drag coefficients of all simulated vehicles in the 'nnt12' configuration.

	$Y = 0°$		$Y = 3°$	
	$R = 0.27$ [m]	$R = 0.54$ [m]	$R = 0.27$ [m]	$R = 0.54$ [m]
Leading vehicle	0.19 - 0.28 - 0.30	0.18 - 0.27 - 0.28	0.20 - 0.29 - 0.30	0.19 - 0.28 - 0.29
Middle vehicle	0.27 - 0.27 - 0.27	0.26 - 0.26 - 0.25	0.28 - 0.28 - 0.29	0.27 - 0.27 - 0.27
Trailing vehicle	0.21 - 0.16 - 0.15	0.21 - 0.15 - 0.14	0.23 - 0.17 - 0.16	0.22 - 0.16 - 0.14
Platoon average	0.23 - 0.24 - 0.24	0.22 - 0.23 - 0.23	0.24 - 0.25 - 0.25	0.22 - 0.23 - 0.23

All the results for the 'ttt' configurations can be seen in Tables A.5–A.8. Per vehicle, the values are ranged from lowest inter-vehicle distance to highest. It is clear that while, less streamlined vehicles have significantly more benefit from driving in a platoon, the more streamlined vehicles still experience the least amount of drag.

Table A.5: Drag coefficients of all simulated vehicles in the 't0t0t12' configuration. The frontal edge radius is 0.27 m.

	$Y = 0°$	$Y = 3°$
Leading vehicle	0.19 - 0.26 - 0.28	0.19 - 0.27 - 0.31
Middle vehicle	0.26 - 0.26 - 0.25	0.27 - 0.27 - 0.26
Trailing vehicle	0.22 - 0.16 - 0.15	0.23 - 0.17 - 0.16
Platoon average	0.22 - 0.23 - 0.23	0.23 - 0.23 - 0.24

Table A.6: Drag coefficients of all simulated vehicles in the 't6t6t12' configuration.

	$Y = 0°$		$Y = 3°$	
	$R = 0.135$ m	$R = 0.27$ m	$R = 0.135$ m	$R = 0.27$ m
Leading vehicle	0.27 - 0.34 - 0.35	0.14 - 0.20 - 0.21	0.29 - 0.36 - 0.36	0.14 - 0.20 - 0.21
Middle vehicle	0.22 - 0.22 - 0.24	0.21 - 0.20 - 0.19	0.22 - 0.24 - 0.26	0.21 - 0.21 - 0.20
Trailing vehicle	0.24 - 0.19 - 0.23	0.23 - 0.18 - 0.17	0.24 - 0.21 - 0.23	0.24 - 0.18 - 0.17
Platoon average	0.25 - 0.25 - 0.27	0.19 - 0.19 - 0.19	0.25 - 0.27 - 0.28	0.20 - 0.19 - 0.19

Table A.7: Drag coefficients of all simulated vehicles in the 't12t12t12' configuration for $Y = 0°$.

	$Y = 0°$		
	$R = 0.135$ m	$R = 0.27$ m	$R = 0.54$ m
Leading vehicle	0.25 - 0.30 - 0.32	0.12 - 0.16 - 0.17	0.10 - 0.15 - 0.16
Middle vehicle	0.20 - 0.23 - 0.24	0.17 - 0.16 - 0.16	0.15 - 0.15 - 0.15
Trailing vehicle	0.24 - 0.23 - 0.25	0.21 - 0.17 - 0.16	0.20 - 0.16 - 0.15
Platoon average	0.23 - 0.25 - 0.27	0.17 - 0.17 - 0.17	0.15 - 0.15 - 0.15

Table A.8: Drag coefficients of all simulated vehicles in the 't2t12t12' configuration for $Y = 3°$.

	$Y = 3°$		
	$R = 0.135$ m	$R = 0.27$ m	$R = 0.54$ m
Leading vehicle	0.26 - 0.31 - 0.32	0.12 - 0.17 - 0.18	n/a - 0.15 - 0.16
Middle vehicle	0.21 - 0.23 - 0.25	0.17 - 0.16 - 0.17	n/a - 0.15 - 0.15
Trailing vehicle	0.26 - 0.26 - 0.27	0.22 - 0.18 - 0.17	n/a - 0.16 - 0.15
Platoon average	0.24 - 0.27 - 0.28	0.17 - 0.17 - 0.17	n/a - 0.15 - 0.15